

Supporting Information

A H-Bond Strategy to Develop Acid-Resistant Photoswitchable Rhodamine Spirolactams for Super-Resolution Single-Molecule Localization Microscopy

Qingkai Qi,^a Weijie Chi,^b Yuanyuan Li,^c Qinglong Qiao,^a Jie Chen,^a Lu Miao,^a Yi Zhang,^a Jin Li,^a Wei Ji,^c Tao Xu,^{*c} Xiaogang Liu,^{*b} Juyoung Yoon,^{*d} and Zhaochao Xu^{*a}

^aCAS Key Laboratory of Separation Science for Analytical Chemistry, Dalian Institute of Chemical Physics, Chinese Academy of Sciences, Dalian 116023, China.

^bSingapore University of Technology and Design, 8 Somapah Road, Singapore 487372, Singapore.

^cNational Laboratory of Biomacromolecules, Institute of Biophysics, Chinese Academy of Sciences, Beijing 100101, China.

^dDepartment of Chemistry and Nano Science, Ewha Womans University, Seoul 120-750, Korea.

* Email: zcxu@dicp.ac.cn; xiaogang_liu@sutd.edu.sg; xutao@ibp.ac.cn; jyoon@ewha.ac.kr

Table of Contents

1. Data-Mining of 3D molecular structures of rhodamine spirolactams	3
2 General Information for synthesis and characterizations	6
2.1 Materials	6
2.2 Instruments	6
2.3 Computational methods	7
2.4 Determination of quantum yields	7
2.5 Synthesis and characterizations	7
2.6 Time-dependent UV-vis absorption and PL spectra, and their dynamic studies of P1-P8 in CH ₂ Cl ₂ /CH ₃ OH (9/1, v/v) before and after the addition of CF ₃ COOH.	22
2.7 Crystal data and intensity collection parameters	24
2.8 Optimized molecular structures of P1-P6 in water	25
2.9 Ring-opening tendency in acidic environments	25
2.10 Energy barriers during ring-opening reactions	29
2.11 UV-vis absorption and PL spectra of P9 and P10 in different pH PBS buffer solution.	33
2.12 Switching properties of rhodamine spirolactams determined by laser flash photolysis.	33
2.13 CLSM images of MCF-7 cells stained with P12 and P13 and taken at different culture time	35
2.14 Time-dependent change of the peak absorbance of the open isomer of P1 and P7 in CH ₂ Cl ₂ solution under and then after 254 nm UV irradiations were removed.	36
2.15 Calculated UV-vis absorption spectrum and frontier molecular orbitals of P17 in aqueous solution.	36
2.16 Single molecule properties of P17 at optimal laser power density	37
2.17 Comparative analyses of various aspects of our best perform rhodamine spirolactams (P17 and P7) with common P1 and the Alexa 647. Single molecule properties of P17 at optimal laser power density	37
2.18 Pearson Correlation Coefficients for CLSM images of MCF-7 cells stained with LTG and P12 or P13	38
3. ¹HNMR, ¹³CNMR and MS spectra of the compounds	39
4. References.....	65

1. Data-Mining of 3D molecular structures of rhodamine spirolactams

To gain deep insights on the ring-opening process of rhodamine spirolactams, we conducted extensive data-mining in the Cambridge Crystallographic Data Center (CCDC) to discover the 3D molecular structures of spirolactams, both before and after the ring-opening process of these dyes. From our results, most rhodamine structures (199 hits) adopt a closed-ring lactam configuration (Table S1), but 21 hits exhibit an open-ring zwitterion configuration (owing to coordination with metal ions or interactions with co-solvent molecules; Table S2).

By comparing the structural differences between closed-ring and open-ring structures, we notice that the ring-opening process of rhodamine spirolactams involves not only the bond breaking at the meso-position, but also the rotation of the lactam group (-CONR) with respect to the phenyl moiety.

We denoted the dihedral angle between the lactam group and the phenyl ring in rhodamine spirolactams as θ (Figure S1). In the closed-ring structures, the distribution of θ centers at 0.16° with a small standard deviation of 2.88° (Figure S1a). In contrast, in the open-ring structures, the average value of θ shifts to 92.28° and its standard deviation increases to 17.30° (Figure S1b). These significant changes in θ values suggest that the ring-opening process in spirolactams is also accompanied with a large rotation of the lactam group.

We thus speculated that incorporating a substitute to hinder the rotation of the lactam group might prevent its ring-opening process, thus lowering the pK_a for turning on fluorescence and endowing rhodamine spirolactams with higher acid-resistance.

Table S1. Reference codes and dihedral angle θ returned from the structural search of closed-ring rhodamine spirolactams in CCDC.^a

S.N.	Refcode	θ (°)	S.N.	Refcode	θ (°)	S.N.	Refcode	θ (°)	S.N.	Refcode	θ (°)
1	APILUI	-0.473	51	FOVVO	1.556	101	MOLWAN	1.751	151	TUFBU	-2.927
2	APINEU	0.823	52	FOWQIS	-0.238	102	MUCGOI	1.725	152	TUFCA	4.909
3	APINEU	-1.346	53	GABVIR	1.397	103	MUCGOI	0.798	153	TUGPO	-0.178
4	ATIJOE	2.013	54	GAHGUU	-1.916	104	MUPQUL	2.737	154	TUQKO	-0.997
5	EMALEL	2.159	55	GAJKUA	0.549	105	MURROI	-8.294	155	TUQLIB	-0.622

6	MOLWAN01	2.962	56	GISSUX	-0.918	106	MURROI	-6.549	156	URAPEK	-2.812
7	OVEWET	0.755	57	GODCAE	1.395	107	NESFUN	-1.955	157	URAPEK	0.265
8	OVEWIX	-0.504	58	GONYAL	-2.551	108	OFUVOC	3.952	158	URAPEK	0
9	ADIFOK	0.256	59	GONYIT	2.213	109	OHAJAK	-4.397	159	URAPEK	-1.079
10	ADIFUQ	2.377	60	GONYIT	1.753	110	OHUMOV	1.224	160	VARJOP	-2.382
11	ADIGAX	-1.684	61	GORJAA	-0.506	111	OHURAM	4.179	161	VOYQAD	-1.511
12	AFUSEA	1.221	62	GUCJEU	5.253	112	OMIMII	0.084	162	VOYQEH	0.422
13	AGUZUZ	1.016	63	GUMTUF	2.305	113	OPEHEX	3.024	163	VUBYAU	-1.573
14	ALUFUJ	-1.57	64	GUMVAN	2.269	114	OPEHIB	0.34	164	VUBYAU01	2.818
15	ANIJOY	2.381	65	HAVCEO	-3.996	115	OPEVEM	1.81	165	VULRIF	1.325
16	AQAFEE	1.907	66	HAVCEO	-5.573	116	OPEVEM	-3.674	166	WACTOM	-2.251
17	AQAFII	4.801	67	HAVCIS	-4.742	117	OSUFIS	1.068	167	WAFBOX	4.207
18	AQAFOO	0	68	HOBCIL	2.136	118	PELDAN	-3.256	168	WOGJIN	4.09
19	AQAFUU	-0.999	69	HOBCIL01	-2.523	119	POFZUH	0.137	169	WUMSEE	0.583
20	AQAGAB	-0.878	70	HUDLEZ	1.164	120	POJKUV	3.313	170	WUNNID	-0.705
21	AQAGAB	2.247	71	HUDLID	-2.269	121	PURYOS	-1.507	171	XAFNUP	2.465
22	AVIBIQ	3.405	72	HUFYEO	2.98	122	PURYOS	2.47	172	XIBTUZ	-0.749
23	BAZGUG	5.369	73	HULVIU	4.61	123	QAMQEC	-6.005	173	XIKNOW	-1.429
24	BONSII	-2.178	74	IPEHUH	0.086	124	QAMQEC01	4.307	174	ZAQJUY	2.059
25	BONSII	3.834	75	IQILIE	7.921	125	QAMQEC02	4.041	175	ZARJAF	-0.853
26	CINQEX	-0.329	76	IQILIE	7.264	126	QAQLIF	4.021	176	ZIGPUC	-0.687
27	CINQEX	0.376	77	ITESIK	-4.048	127	QASGIC	3.769	177	ZOCNOW	-0.818
28	CISYIO	-2.099	78	ITOPUD	-1.292	128	QIYLER	0.73	178	ZOCNOW	-2.125
29	CUNYUH	2.451	79	JODREA	2.765	129	QIYLIV	-1.862	179	ZUNPEF	-5.963
30	CUNYUH	2.565	80	JODREA01	2.765	130	QIYLOB	0.643	180	ZUNPEF	-5.633
31	CUNYUH	-3.416	81	JULJIL	0.934	131	QUDQOX	1.627	181	ZUVYAS	1.756
32	CUXNOA	1.42	82	JUXLAR	-2.711	132	QUKFEI	0.358	182	ZUVYEW	-0.344
33	DABTUX	2.059	83	KUCVUB	-2.518	133	QUYCOE	5.927	183	ZUVYIA	1.303
34	DAQYEB	-1.964	84	KUJYAR	-3.484	134	QUYCOE	-5.989	184	ZUVYOG	-0.517
35	DAQYIF	-0.136	85	KUZCAL	-0.563	135	REQFUQ	-3.597	185	FEYMED01	0.052
36	DAZFOB	1.332	86	LAGFUX	1.201	136	REQFUQ	2.988	186	ICAFOK	-2.686
37	DEZTUY	1.045	87	LAGFUX	-1.327	137	SAXDUS	-5.103	187	IXUNAS	-6.048
38	DILJEO	-0.72	88	LALNIX	2.526	138	SICSOO	0.491	188	MICGAH01	-6.196
39	DISPUS	0.844	89	LAQWOQ	-1.862	139	SOYRUV	-5.743	189	OYAXET	2.83
40	EFECID	-0.408	90	LUJTUG	0	140	SOYRUV	-5.608	190	OYAXET	1.73
41	EGEZOH	1.565	91	LUJYIA	-0.323	141	SOYSAC	2.28	191	OYAXIX	3.698
42	EKORUT	2.667	92	LUMHOR	1.405	142	SOYSEG	-3.23	192	OZEHUY	5.33
43	ELEWEZ	0.754	93	LUMHOR	2.4	143	SOYSIK	-0.137	193	PAMLEX	0.581
44	ELIXII	-0.253	94	LUMHOR01	1.467	144	SUGYAW	-0.981	194	UDACOU	-1.125

45	EMIPEX	-1.132	95	LUZREE	-0.249	145	TAJZIQ	-1.057	195	FAQLAN	3.416
46	EMONIF	0.369	96	MICGAH	-6.196	146	TIBZUB	3.081	196	MARBOZ	-4.834
47	EMUQUZ	-4.77	97	MIXNAK	-2.111	147	TIXHEP	0.519	197	NAMWOQ	4.98
48	EVEJAR	-0.79	98	MODWIM	5.093	148	TIXHEP	-0.122	198	QARGOI	-1.024
49	FEYMED	-0.471	99	MOJSIO	-1.416	149	TOCNEG	1.618	199	VARDAW	4.862
50	FIDZUP	-0.034	100	MOJSOU	0.938	150	TOCNIK	-2.246			

^a More than 1 hit are returned for crystal structures that contain >1 asymmetrical molecules in a unit cell.

Table S2. Reference codes and dihedral angle θ returned from the structural search of open-ring rhodamine spirolactams in CCDC.^a

S.N.	Refcode	θ (°)	S.N.	Refcode	θ (°)	S.N.	Refcode	θ (°)
1	ADIGEB	-113.657	8	GONYEP	96.491	15	VARJUV	59.396
2	BACZUD	-110.312	9	GUQMOV	-75.399	16	WAFBUD	-71.798
3	FOSBAR	-105.843	10	JULMOU	120.848	17	WAFCAK	-99.454
4	FOSBAR	-103.41	11	KIBZOL	-64.941	18	WAFCEO	-86.069
5	FOSBEV	-84.981	12	KIBZOL	-103.864	19	YILSET	-93.776
6	FOSBEV	103.423	13	SAXFAA	96.587	20	ZUVXUL	102.71
7	GONYEP	95.194	14	UYANIS	60.943	21	ZUVXUL	-88.918

^a More than 1 hit are returned for crystal structures that contain >1 asymmetrical molecules in a unit cell.

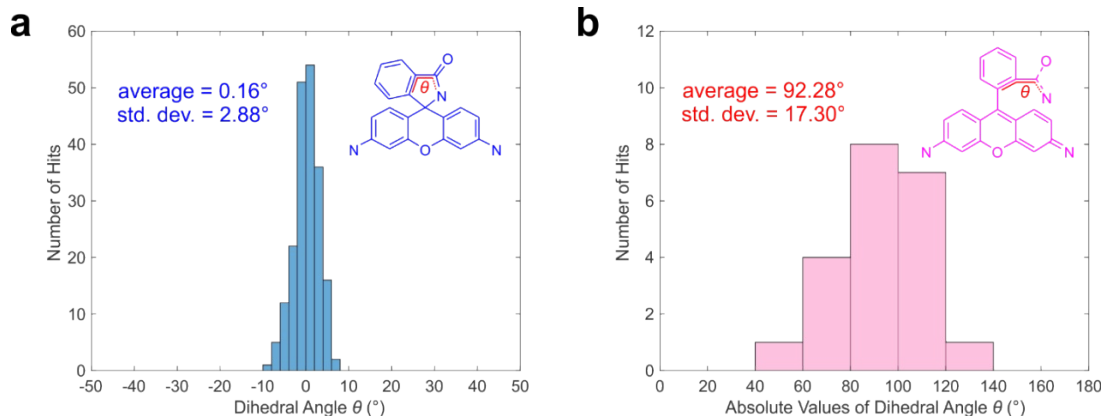


Figure S1. Histograms of the dihedral angle θ in the crystal structures of (a) ring-closed and (b) ring-opened rhodamine spirolactams; the insets show the search moieties during the data-mining in the Cambridge Crystallographic Data Centre (CCDC).

2 General Information for synthesis and characterizations

2.1 Materials

3-nitrophthalic anhydride, 4-nitrophthalic anhydride, zinc chloride, N, N-diethyl-3-aminophenol, rhodamine B (RhB), butylamine, methyl iodide, acetonitrile, potassium carbonate, palladium/C catalyst, acetyl chloride, tolylsulfonyl chloride, aniline, 4-ethynylaniline, phosphorus oxychloride, 1,2-dichloroethane and trimethylamine were purchased from Energy Chemical and used as received. 3-iodopropionic acid, 4-bromo-1,8-naphthalic anhydride, 17-amino-3,6,9,12,15-pentaoxaheptadecanol, 2,5,8,11,14,17-hexaoxonadecan-19-amine, 2-morpholinoethanamine, 4-(aminomethyl)pyridine and N-hydroxysuccinimide (NHS) were purchased from Aladdin and used as received without further purification. 3-nitro-RhB, 4-nitro-RhB and 5-nitro-RhB were all synthesized according to previous literature reports.¹ The solvent and all the other chemicals were purchased from Aladdin and used as received without further purification. H₂O (18.2 MΩ cm⁻¹) was purified with a millipore Integral 3 system. The MCF-7 cells and *bacillus subtilis* were purchased from American type culture collection (ATCC).

2.2 Instruments

¹H NMR spectra were recorded on a 400 MHz BrukerAvance, using CDCl₃ or DMSO-d₆ as solvent and tetramethylsilane (TMS) as an internal standard ($\delta = 0.00$ ppm). ¹³C NMR spectra were recorded on a 101 MHz BrukerAvance, using CDCl₃ as a solvent and CDCl₃ as an internal standard ($\delta = 77.00$ ppm). Mass spectrometry data were obtained with a HP1100LC/MSD mass spectrometer and a LC/Q-TOF MS spectrometer. UV-vis absorption spectra were collected on an Agilent Cary 60. Fluorescence measurements were performed on an Agilent CARY Eclipse fluorescence spectrophotometer. Lifetimes of open forms of rhodamine spirolactams were measured on an Edinburgh Instrument LP920 - Laser flash photolysis spectrometer equipped with a 266 nm and a 355 nm laser. Confocal laser scanning microscopy (CLSM) images were performed by using ANDORTM live cell imaging system. Super-resolution images were performed by using Nikon N-STORM 5.0 Super-Resolution Microscope System with a motorized inverted microscope ECLIPSE Ti2-E, a 100 x / NA 1.49 oil immersion TIRF objective lens (CFI HP), LU-NV series laser unit (laser combination: 405 nm / 561 nm), and an ORCA-Flash 4.0 sCMOS camera (Hamamatsu Photonics K.K.).

2.3 Computational methods

Density functional theory (DFT) and time-dependent (TD)-DFT calculations were performed using *Gaussian 16*.² Geometry optimizations of various conformations of **P1-P6** employed the M062X functional,³ in combination with the TZVP basis set. Solvent effects were considered using the SMD model.⁴ Frequency checks were carried out after each geometry optimization to ensure that the minima on the potential energy surfaces (PES) were found. During the geometry optimizations of the lactams and zwitterions of **P1-P6** and in search for the associated transition states, the butyl group attached to the amide groups in **P1-P6** was replaced by a methyl group to reduce computational load.

2.4 Determination of quantum yields

Fluorescence quantum yields (ϕ_F) of **P1-P8** in CH₂Cl₂/ CH₃OH (9/1, v/v) after the addition of 2.3 μ L CF₃COOH for 2 hours were measured by using RhB as the reference ($\phi_F = 0.69$ in dilute ethanol solution with excitation wavelength of 365 nm) and were calculated according to the following equation:

$$\eta_s = \eta_r \left(\frac{A_r}{A_s} \right) \left(\frac{I_s}{I_r} \right) \left(\frac{n_r^2}{n_s^2} \right)$$

where (η_r) and (η_s) are the fluorescence quantum yields of the standard and the sample, respectively. A_r and A_s are the absorbance of the standard and the measured sample at the excitation wavelength, respectively. I_r and I_s are the integrated emission intensities of the standard and the sample, respectively. n_r and n_s are the refractive indices of the corresponding solvents of the solutions, respectively.

2.5 Synthesis and characterizations

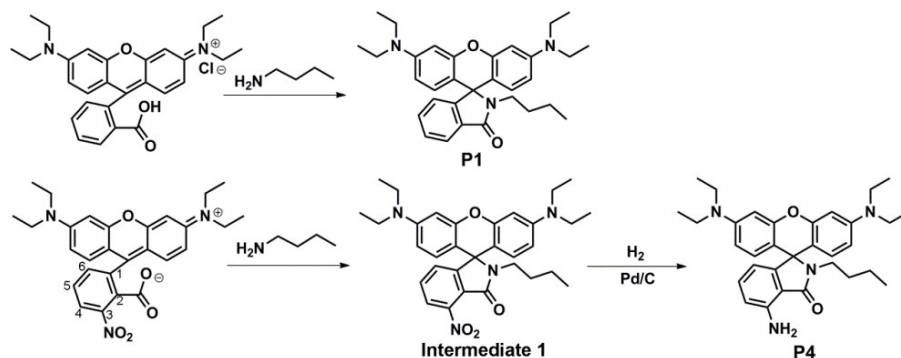
Synthesis of P1: **P1** was synthesized as shown in Scheme S1 according to previous literature reports.⁵

P1: ¹H NMR (400 MHz, CDCl₃) δ 7.89 (dd, $J = 5.9, 2.7$ Hz, 1H), 7.49 – 7.38 (m, 2H), 7.07 (dd, $J = 5.7, 2.6$ Hz, 1H), 6.44 (d, $J = 8.8$ Hz, 2H), 6.38 (d, $J = 2.5$ Hz, 2H), 6.27 (dd, $J = 8.9, 2.5$ Hz, 2H), 3.34 (q, $J = 7.0$ Hz, 8H), 3.11 (t, $J = 6.9$ Hz, 2H), 1.16 (t, $J = 7.0$ Hz, 12H), 1.13 – 1.04 (m, 4H), 0.68 (t, $J = 6.7$ Hz, 3H). LC-MS (ESI): m/z: calcd: 497.3042; found: 498.3128 [M+H]⁺.

Synthesis of P4: **P4** was synthesized according to Scheme S1. The synthesis of intermediate 1 was similar to that of **P1**. The mixture of 3-nitro-RhB (2.4 g, 5 mmol) and n-butylamine (1.4 g, 20 mmol) was refluxed in ethanol (50 mL) for 8 h. Then, the solvent was removed by rotary evaporation. The crude product was purified with column chromatography (silica gel, petroleum ether/ethyl acetate, 8:1 v/v) to give intermediate **1** as a yellow solid (2.6 g, 95%). Then, the obtained powders of intermediate **1** (2.1 g, 4 mmol) were dissolved in 50 mL methanol/CH₂Cl₂ (3:1 v/v) mixed solvent and reduced with 0.21 g 10% Pd/C under hydrogen atmosphere. The reaction mixture was filtered, and then the filtrate was evaporated to give **P4** as a white powder (2 g, 98%).

Intermediate **1**: ¹H NMR (400 MHz, CDCl₃) δ 7.69 (dd, *J* = 7.9, 0.6 Hz, 1H), 7.50 (t, *J* = 7.8 Hz, 1H), 7.28 (d, *J* = 0.6 Hz, 1H), 6.48 (d, *J* = 8.9 Hz, 2H), 6.39 (d, *J* = 2.5 Hz, 2H), 6.30 (dd, *J* = 8.9, 2.6 Hz, 2H), 3.35 (q, *J* = 7.1 Hz, 8H), 3.13 – 3.07 (m, 2H), 1.22 – 1.05 (m, 16H), 0.69 (t, *J* = 7.1 Hz, 3H). ¹³C NMR (101 MHz, CDCl₃) δ 162.74, 156.19, 153.28, 149.00, 145.78, 132.50, 128.66, 127.83, 122.99, 122.44, 108.15, 104.29, 97.86, 64.44, 44.37, 40.66, 29.97, 20.35, 13.49, 12.53. LC-MS (ESI): *m/z*: calcd: 542.2893; found: 543.2967 [M+H]⁺.

P4: ¹H NMR (400 MHz, CDCl₃) δ 7.14 (t, *J* = 7.6 Hz, 1H), 6.56 (t, *J* = 8.2 Hz, 3H), 6.41 – 6.25 (m, 5H), 3.34 (dd, *J* = 13.4, 6.5 Hz, 8H), 3.05 (s, 2H), 1.24 – 1.04 (m, 16H), 0.68 (t, *J* = 7.1 Hz, 3H). ¹³C NMR (101 MHz, CDCl₃) δ 169.59, 154.86, 153.08, 148.63, 144.95, 133.24, 129.03, 114.15, 113.31, 112.11, 108.04, 106.77, 97.69, 64.59, 44.33, 39.70, 30.64, 20.32, 13.57, 12.57 ppm. LC-MS (ESI): *m/z*: calcd: 512.3151; found: 513.3220 [M+H]⁺.



Scheme S1. The chemical structures and synthetic approaches for **P1** and **P4**.

Synthesis of P2 and P3: **P2** and **P3** were synthesized according to Scheme S2. The mixture of 4-nitro-RhB and 5-nitro-RhB (0.49 g, 1 mmol), and n-butylamine (0.29 g, 4 mmol) was refluxed in ethanol (10 mL) for 8 h. Then, the solvent was removed by rotary evaporation. The crude product was purified with column chromatography (silica gel, petroleum ether/ethyl acetate, 8:1 v/v) to separate intermediate **2** (0.26 g, 48%) and intermediate **3** (0.25 g, 47%) respectively. Then, both the intermediate **2** or **3** (0.16 g, 0.3 mmol) were dissolved in 5 mL methanol/CH₂Cl₂ (3:1 v/v) mixed solvent and reduced with 16 mg 10% Pd/C under hydrogen atmosphere for 2 h respectively. The reaction mixture was filtered, and then the filtrate was evaporated respectively to give **P2** (0.15 g, 98%) and **P3** (0.15 g, 98%) as white powders.

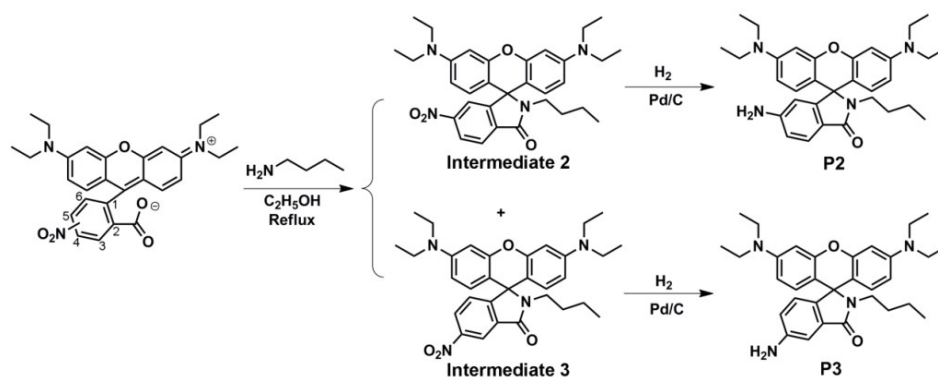
Intermediate **2**: ¹H NMR (400 MHz, CDCl₃) δ 8.30 (dd, *J* = 8.3, 1.7 Hz, 1H), 8.04 (d, *J* = 8.3 Hz, 1H), 7.90 (d, *J* = 1.5 Hz, 1H), 6.40 (t, *J* = 5.6 Hz, 4H), 6.28 (dd, *J* = 8.9, 2.4 Hz, 2H), 3.35 (q, *J* = 7.0 Hz, 8H), 3.14 (t, *J* = 7.1 Hz, 2H), 1.18 (t, *J* = 7.0 Hz, 12H), 1.15 – 1.06 (m, 4H), 0.70 (t, *J* = 6.8 Hz, 3H). ¹³C NMR (101 MHz, CDCl₃) δ 165.73, 154.75, 153.26, 150.74, 148.99, 136.52, 128.47, 123.81, 123.61, 119.40, 108.13, 103.73, 97.91, 65.35, 44.39, 40.60, 30.04, 20.29, 13.53, 12.52. LC-MS (ESI): *m/z*: calcd: 542.2893; found: 543.2962 [M+H]⁺.

Intermediate **3**: ¹H NMR (400 MHz, CDCl₃) δ 8.73 (d, *J* = 2.0 Hz, 1H), 8.28 (dd, *J* = 8.3, 2.1 Hz, 1H), 7.22 (d, *J* = 8.3 Hz, 1H), 6.40 (dd, *J* = 5.6, 3.2 Hz, 4H), 6.28 (dd, *J* = 8.9, 2.5 Hz, 2H), 3.35 (q, *J* = 7.0 Hz, 8H), 3.14 (t, *J* = 7.2 Hz, 2H), 1.17 (t, *J* = 7.0 Hz, 12H), 1.15-1.07 (m, 4H), 0.70 (t, *J* = 6.9 Hz, 3H). ¹³C NMR (101 MHz, CDCl₃) δ 165.65, 159.00, 153.17, 149.02, 148.15, 132.76, 128.56, 127.20, 124.87, 118.60, 108.10, 103.89, 97.81, 65.21, 44.37, 40.50, 30.13, 20.29, 13.54, 12.51. LC-MS (ESI): *m/z*: calcd: 542.2893; found: 543.2972 [M+H]⁺.

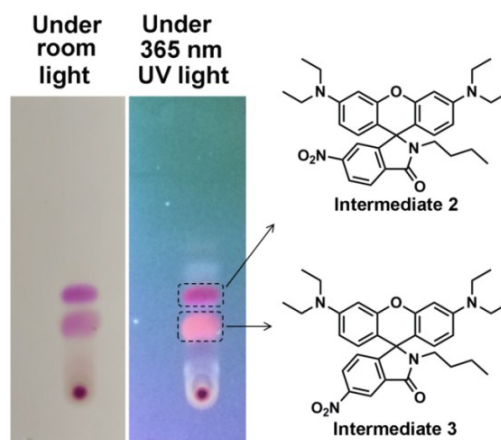
P2: ¹H NMR (400 MHz, CDCl₃) δ 7.66 (d, *J* = 7.9 Hz, 1H), 6.65 (d, *J* = 7.6 Hz, 1H), 6.53 (d, *J* = 8.7 Hz, 2H), 6.37 (s, 2H), 6.28 (d, *J* = 10.3 Hz, 3H), 3.83 (s, 2H), 3.34 (q, *J* = 7.0 Hz, 8H), 3.06 (t, *J* = 6.8 Hz, 2H), 1.17 (t, *J* = 6.5 Hz, 12H), 1.12 – 1.04 (m, 4H), 0.67 (t, *J* = 6.5 Hz, 3H). ¹³C NMR (101 MHz, CDCl₃) δ 168.38, 156.07, 153.11, 150.30, 148.58, 129.16, 124.03, 121.91, 114.77, 108.78, 107.99, 106.73, 97.59, 64.18, 44.34, 39.97, 30.63, 20.29, 13.60, 12.57. LC-MS (ESI): *m/z*: calcd: 512.3151; found: 513.3237 [M+H]⁺.

P3: ¹H NMR (400 MHz, CDCl₃) δ 7.16 (d, *J* = 2.0 Hz, 1H), 6.85 (d, *J* = 8.1 Hz, 1H), 6.74 (dd, *J* = 8.1, 2.1 Hz, 1H), 6.48 (d, *J* = 8.8 Hz, 2H), 6.36 (d, *J* = 2.4 Hz, 2H), 6.27 (dd, *J* = 8.8, 2.5 Hz,

2H), 3.83 (s, 2H), 3.34 (q, $J = 7.0$ Hz, 8H), 3.05 (t, $J = 6.8$ Hz, 2H), 1.16 (t, $J = 7.0$ Hz, 12H), 1.10 – 1.04 (m, 4H), 0.66 (t, $J = 6.5$ Hz, 3H). ^{13}C NMR (101 MHz, CDCl_3) δ 168.05, 153.31, 148.56, 146.45, 144.12, 132.98, 129.04, 124.34, 119.44, 107.99, 107.79, 106.70, 97.65, 64.39, 44.34, 40.11, 30.33, 20.29, 13.57, 12.56. LC-MS (ESI): m/z : calcd: 512.3151; found: 513.3178 $[\text{M}+\text{H}]^+$.



Scheme S2. The chemical structures and synthetic approaches for **P2** and **P3**.



Note: The mixture of 4-nitro-RhB and 5-nitro-RhB, as initial raw materials, cannot be separated by the TLC plate and gel silica column chromatography. However, the intermediate **2** and **3** with lower polarity can be easily separated on the TLC plate and purified by the gel silica column chromatography.

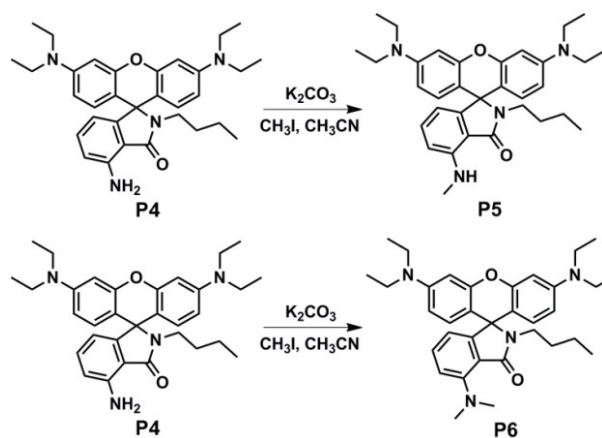
Synthesis of P5: **P5** was synthesized according to Scheme S3. The mixture of **P4** (0.25 g, 0.5 mmol), CH_3I (0.28 g, 2 mmol) and K_2CO_3 (0.34 g, 2.5 mmol) was refluxed in CH_3CN (8 mL) for 10 h. After cooling to room temperature, the filtrate was collected by filtration from the reaction

mixture. Then, the solvent was removed by rotary evaporation. The crude product was purified with column chromatography (silica gel, petroleum ether/ethyl acetate, 10:1 v/v) to give **P5** as a white powder (0.17 g, 65%).

P5: ^1H NMR (400 MHz, CDCl_3) δ 7.23 (t, $J = 7.9$ Hz, 1H), 6.75 (d, $J = 4.9$ Hz, 1H), 6.57 (t, $J = 9.3$ Hz, 2H), 6.49 (d, $J = 8.1$ Hz, 1H), 6.41 – 6.22 (m, 5H), 3.33 (q, $J = 7.0$ Hz, 8H), 3.04 (s, 2H), 2.97 (d, $J = 4.9$ Hz, 3H), 1.16 (t, $J = 6.9$ Hz, 12H), 1.07 (s, 4H), 0.67 (t, $J = 6.5$ Hz, 3H). ^{13}C NMR (101 MHz, CDCl_3) δ 170.15, 154.93, 153.09, 148.60, 147.23, 133.78, 129.01, 113.08, 110.19, 108.01, 107.53, 106.74, 97.67, 44.33, 39.63, 30.69, 29.42, 20.30, 13.60, 12.57. LC-MS (ESI): m/z : calcd: 526.3308; found: 527.3523 $[\text{M}+\text{H}]^+$.

Synthesis of P6: **P6** were synthesized similar as **P5**. The mixture of **P4** (0.25 g, 0.5 mmol), CH_3I (0.71 g, 5 mmol) and K_2CO_3 (0.34 g, 2.5 mmol) was refluxed in CH_3CN (8 mL) for 10 h. After cooling to room temperature, the filtrate was collected by filtration from the reaction mixture. Then, the solvent was removed by rotary evaporation. The crude product was purified with column chromatography (silica gel, petroleum ether/ethyl acetate, 15:1 v/v) to give **P6** as a white powder (0.20 g, 75%).

P6: ^1H NMR (400 MHz, CDCl_3) δ 7.23 (d, $J = 7.8$ Hz, 1H), 6.81 (d, $J = 8.0$ Hz, 1H), 6.57 – 6.49 (m, 3H), 6.40 (d, $J = 2.5$ Hz, 1H), 6.37 (d, $J = 2.5$ Hz, 1H), 6.33 (dd, $J = 8.9, 2.5$ Hz, 1H), 6.30 – 6.26 (m, 1H), 3.34 (q, $J = 7.0$ Hz, 8H), 3.10 (s, 6H), 3.07 (t, $J = 7.4$ Hz, 2H), 1.15 (t, $J = 6.9$ Hz, 12H), 1.13 – 1.05 (m, 4H), 0.67 (t, $J = 7.0$ Hz, 3H). ^{13}C NMR (101 MHz, CDCl_3) δ 167.54, 157.00, 153.13, 153.09, 152.99, 149.75, 148.54, 132.72, 128.90, 115.40, 115.11, 108.41, 108.03, 98.35, 97.69, 46.69, 44.43, 44.33, 40.34, 37.38, 30.49, 20.40, 13.64, 12.57, 11.34. LC-MS (ESI): m/z : calcd: 540.3464; found: 541.3159 $[\text{M}+\text{H}]^+$.



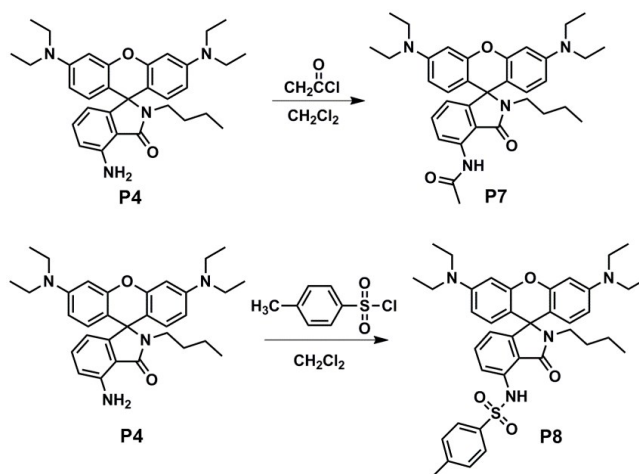
Scheme S3. The chemical structures and synthetic approaches for **P5** and **P6**.

Synthesis of P7: **P7** were synthesized according to Scheme S4. **P4** (0.25 g, 0.5 mmol) and acetylchloride (58 mg, 0.75 mmol) were mixed in CH₂Cl₂ (5 mL) and stirred for 2 h. Then, the solvent was removed by rotary evaporation. The crude product was purified with column chromatography (silica gel, petroleum ether/ethyl acetate, 8:1 v/v) to give **P7** as a white powder (0.26 g, 95%).

P7: ¹H NMR (400 MHz, CDCl₃) δ 10.60 (s, 1H), 8.43 (d, *J* = 8.2 Hz, 1H), 7.39 (t, *J* = 7.9 Hz, 1H), 6.74 (d, *J* = 7.6 Hz, 1H), 6.46 (d, *J* = 8.8 Hz, 2H), 6.38 (d, *J* = 2.6 Hz, 2H), 6.28 (dd, *J* = 8.9, 2.6 Hz, 2H), 3.34 (q, *J* = 7.0 Hz, 8H), 3.06 (t, *J* = 7.0 Hz, 2H), 2.29 (s, 3H), 1.17 (t, *J* = 7.0 Hz, 12H), 1.12 – 1.02 (m, 4H), 0.69 (t, *J* = 6.7 Hz, 3H). ¹³C NMR (101 MHz, CDCl₃) δ 169.30, 168.85, 158.27, 153.50, 153.27, 148.83, 136.75, 133.81, 128.78, 117.95, 117.52, 116.43, 108.07, 105.32, 101.26, 99.97, 97.72, 65.17, 44.36, 39.98, 30.41, 24.97, 20.35, 13.55, 12.55. LC-MS (ESI): *m/z*: calcd: 554.3257; found: 555.3382 [M+H]⁺.

Synthesis of P8: **P8** were synthesized according to Scheme S4. **P4** (0.25 g, 0.5 mmol) and tolylsulfonyl chloride (95 mg, 0.5 mmol) were mixed in CH₂Cl₂ (5 mL) and stirred for 3 h. Then, the solvent was removed by rotary evaporation. The crude product was purified with column chromatography (silica gel, petroleum ether/ethyl acetate, 6:1 v/v) to give **P8** as a yellow powder (0.30 g, 91%).

P8: ^1H NMR (400 MHz, CDCl_3) δ 9.88 (s, 1H), 7.83 (d, $J = 8.3$ Hz, 2H), 7.51 (d, $J = 8.1$ Hz, 1H), 7.32 – 7.25 (m, 3H), 6.67 (d, $J = 7.5$ Hz, 1H), 6.35 (d, $J = 1.9$ Hz, 2H), 6.28 – 6.14 (m, 4H), 3.33 (q, $J = 7.1$ Hz, 8H), 2.99 (t, $J = 7.0$ Hz, 2H), 2.41 (s, 3H), 1.16 (t, $J = 7.0$ Hz, 12H), 1.07 – 0.96 (m, 4H), 0.67 (t, $J = 6.8$ Hz, 3H). ^{13}C NMR (101 MHz, CDCl_3) δ 167.92, 153.86, 153.14, 148.78, 143.49, 136.52, 135.47, 133.45, 129.43, 128.58, 127.52, 118.59, 118.03, 117.21, 107.90, 105.02, 97.67, 65.03, 44.34, 39.76, 30.25, 21.55, 20.19, 13.54, 12.50. LC-MS (ESI): m/z : calcd: 666.3240; found: 667.3211 $[\text{M}+\text{H}]^+$.



Scheme S4. The chemical structures and synthetic approaches for **P7** and **P8**.

Synthesis of P9: **P9** was synthesized according to Scheme S5. The mixture of RhB (0.24 g, 0.5 mmol) and 17-amino-3,6,9,12,15-pentaoxaheptadecanol (0.14 g, 0.5 mmol) was refluxed in ethanol (8 mL) for 8 h. Then, the solvent was removed by rotary evaporation. The crude product was purified with column chromatography (silica gel, ethyl acetate/methanol, 10:1 v/v) to give **P9** as a colorless viscous liquid (0.28 g, 80%).

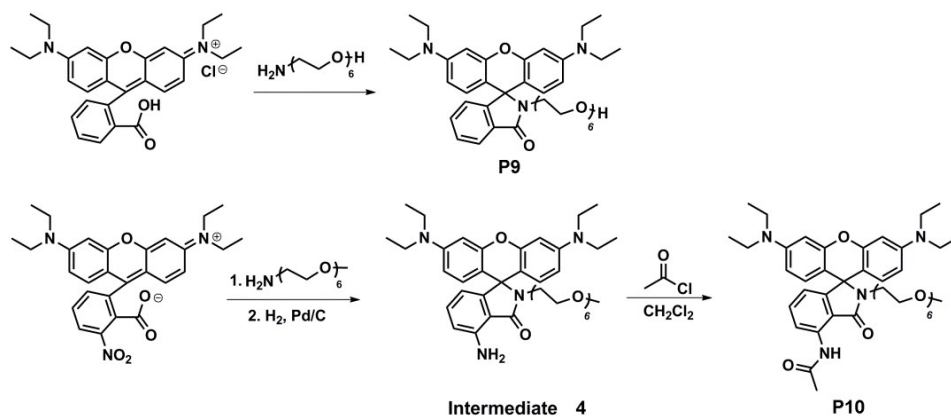
P9: ^1H NMR (400 MHz, CDCl_3) δ 7.88 (dd, $J = 5.6, 3.0$ Hz, 1H), 7.42 (dd, $J = 5.5, 3.1$ Hz, 2H), 7.06 (dd, $J = 5.4, 3.1$ Hz, 1H), 6.42 (d, $J = 8.8$ Hz, 2H), 6.37 (d, $J = 2.3$ Hz, 2H), 6.26 (dd, $J = 8.9, 2.4$ Hz, 2H), 3.73 – 3.69 (m, 2H), 3.68 – 3.55 (m, 14H), 3.51 – 3.46 (m, 2H), 3.42 – 3.28 (m, 12H), 3.16 (t, $J = 7.2$ Hz, 2H), 1.16 (t, $J = 7.0$ Hz, 12H). ^{13}C NMR (101 MHz, CDCl_3) δ 168.21, 153.73, 153.20, 148.71, 132.32, 130.93, 128.78, 127.89, 123.73, 122.69, 108.01, 105.44, 97.73,

72.45, 70.50, 70.47, 70.46, 70.45, 70.43, 70.32, 70.26, 69.88, 67.77, 64.80, 61.64, 44.31, 39.19, 12.56. LC-MS (ESI): m/z: calcd: 705.3989; found: 706.4084 [M+H]⁺.

Synthesis of P10: P10 was synthesized according to Scheme S5. The mixture of 3-nitro-RhB (0.24 g, 0.5 mmol) and 2,5,8,11,14,17-Hexaoxonadecan-19-amine (0.14 g, 0.5 mmol) was refluxed in ethanol (8 mL) for 8 h. Then, the solvent was removed by rotary evaporation. The crude product was dissolved in methanol (5 mL) and reduced with 20 mg 10% Pd/C under hydrogen atmosphere. The reaction mixture was filtered, and then the solvent of filtrate was removed by rotary evaporation. The crude product was purified with column chromatography (silica gel, ethyl acetate/methanol, 20:1 v/v) to give intermediate 4 as a sticky liquid (0.33 g, 90%). Intermediate 4 (0.22 g, 0.3 mmol) and acetylchloride (35 mg, 0.45 mmol) were mixed in CH₂Cl₂ (5 mL) and stirred for 2 h. Then, the solvent was removed by rotary evaporation. The crude product was purified with column chromatography (silica gel, ethyl acetate/methanol, 20:1 v/v) to give P10 as a sticky liquid (0.22 g, 95%).

Intermediate 4: ¹H NMR (400 MHz, CDCl₃) δ 7.11 (t, *J* = 7.7 Hz, 1H), 6.54 (t, *J* = 8.9 Hz, 3H), 6.35 (d, *J* = 2.4 Hz, 2H), 6.32 – 6.23 (m, 3H), 5.37 (s, 2H), 3.67 – 3.51 (m, 16H), 3.51 – 3.46 (m, 2H), 3.41 – 3.25 (m, 15H), 3.13 (t, *J* = 7.2 Hz, 2H), 1.15 (t, *J* = 7.0 Hz, 12H). ¹³C NMR (101 MHz, CDCl₃) δ 169.55, 154.76, 152.76, 148.38, 144.91, 133.28, 128.65, 113.20, 113.08, 111.69, 107.79, 106.04, 97.44, 71.66, 70.32, 70.27, 70.24, 70.24, 70.22, 70.11, 69.70, 67.85, 64.26, 58.74, 44.09, 38.56, 12.38. LC-MS (ESI): m/z: calcd: 734.4255; found: 735.4290 [M+H]⁺.

P10: ¹H NMR (400 MHz, CDCl₃) δ 10.47 (s, 1H), 8.39 (d, *J* = 8.2 Hz, 1H), 7.34 (t, *J* = 7.9 Hz, 1H), 6.68 (d, *J* = 7.6 Hz, 1H), 6.41 (d, *J* = 8.8 Hz, 2H), 6.33 (d, *J* = 2.4 Hz, 2H), 6.24 (dd, *J* = 8.9, 2.4 Hz, 2H), 3.60 – 3.48 (m, 16H), 3.47 – 3.42 (m, 2H), 3.35 – 3.25 (m, 15H), 3.08 (t, *J* = 7.1 Hz, 2H), 2.25 (s, 3H), 1.13 (t, *J* = 7.0 Hz, 13H). ¹³C NMR (101 MHz, CDCl₃) δ 169.06, 168.82, 153.52, 152.97, 148.66, 136.57, 133.85, 128.43, 117.79, 117.38, 115.71, 107.90, 104.58, 97.56, 71.69, 70.34, 70.30, 70.11, 69.82, 67.62, 64.95, 58.78, 44.15, 38.83, 24.73, 12.38. LC-MS (ESI): m/z: calcd: 776.4360; found: 777.4435 [M+H]⁺.



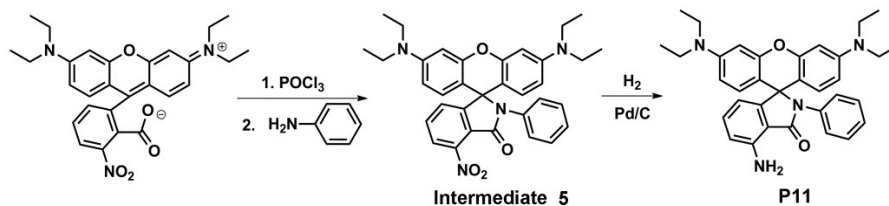
Scheme S5. The chemical structures and synthetic approaches for **P9-P10**.

Synthesis of P11: **P11** were synthesized according to Scheme S6. The mixture of 3-nitro-RhB (0.19 g, 0.4 mmol) and POCl_3 (0.61 g, 4 mmol) was refluxed in 1,2-dichloroethane (15 mL) for 2 h, after which the solvent was removed to give dark violet-red oil. The crude acid chloride was dissolved in CH_2Cl_2 (15 mL), then trimethylamine (0.3 mL) and aniline (37.2 mg, 0.4 mmol) were dropwise added into the mixture solution. The reaction mixture was stirred at room temperature for 24 h. Then, the solvent was removed and the crude residue was purified with column chromatography (silica gel, petroleum ether/ethyl acetate, 4:1 v/v) to give intermediate **5** as a yellow powder (0.15 g, 65%). Then, the powders of intermediate **5** (0.11 g, 0.2 mmol) were dissolved in 5 mL methanol/ CH_2Cl_2 (3:1 v/v) mixed solvent and reduced with 11 mg 10% Pd/C under hydrogen atmosphere. The reaction mixture was filtered, and then the filtrate was evaporated to give **P11** as a white powder (0.10 g, 98%).

Intermediate **5**: $^1\text{H NMR}$ (400 MHz, CDCl_3) δ 7.73 (d, $J = 7.8$ Hz, 1H), 7.58 (t, $J = 7.8$ Hz, 1H), 7.36 (d, $J = 7.1$ Hz, 1H), 7.15 – 7.06 (m, 3H), 6.85 – 6.77 (m, 2H), 6.67 (d, $J = 8.8$ Hz, 2H), 6.34 (dd, $J = 8.9, 2.5$ Hz, 2H), 6.26 (d, $J = 2.5$ Hz, 2H), 3.33 (q, $J = 7.1$ Hz, 8H), 1.15 (t, $J = 7.0$ Hz, 12H). $^{13}\text{C NMR}$ (101 MHz, CDCl_3) δ 162.30, 155.68, 153.08, 148.98, 146.17, 135.82, 133.19, 128.60, 128.52, 128.09, 127.15, 127.00, 122.61, 122.43, 108.18, 104.64, 97.81, 66.86, 44.31, 12.51. LC-MS (ESI): m/z: calcd: 562.2580; found: 563.2624 $[\text{M}+\text{H}]^+$.

P11: $^1\text{H NMR}$ (400 MHz, CDCl_3) δ 7.25 – 7.18 (m, 1H), 7.15 – 7.04 (m, 3H), 6.84 – 6.74 (m, 4H), 6.60 (d, $J = 8.0$ Hz, 1H), 6.40 (d, $J = 7.4$ Hz, 1H), 6.31 (d, $J = 2.6$ Hz, 2H), 6.23 (d, $J = 2.5$

Hz, 2H), 5.40 (s, 2H), 3.31 (q, $J = 7.2$ Hz, 8H), 1.14 (t, $J = 7.0$ Hz, 12H). ^{13}C NMR (101 MHz, CDCl_3) δ 169.31, 154.58, 152.87, 148.64, 145.58, 136.57, 133.99, 128.88, 128.42, 127.19, 126.36, 113.46, 113.36, 112.21, 108.06, 107.10, 97.71, 67.14, 44.28, 12.57. LC-MS (ESI): m/z : calcd: 532.2838; found: 533.2830 $[\text{M}+\text{H}]^+$.



Scheme S6. The chemical structure and synthetic approach for **P11**.

Synthesis of P12: **P12** was synthesized as shown in Scheme S7 according to previous literature reports.⁶

P12: ^1H NMR (400 MHz, CDCl_3) δ 7.93 – 7.87 (m, 1H), 7.47 – 7.39 (m, 2H), 7.14 – 7.04 (m, 1H), 6.44 (d, $J = 8.8$ Hz, 2H), 6.37 (d, $J = 2.4$ Hz, 2H), 6.26 (dd, $J = 8.9, 2.5$ Hz, 2H), 3.65 – 3.51 (t, $J = 4.0$ Hz, 4H), 3.33 (q, $J = 7.0$ Hz, 8H), 3.29 – 3.18 (m, 2H), 2.25 (s, 4H), 2.10 (t, $J = 7.4$ Hz, 2H), 1.16 (t, $J = 7.0$ Hz, 12H). ^{13}C NMR (101 MHz, CDCl_3) δ 167.85, 153.42, 153.27, 148.63, 132.20, 131.29, 129.01, 127.90, 123.69, 122.60, 107.94, 105.62, 97.60, 66.88, 64.71, 56.01, 53.17, 44.32, 36.90, 12.51.

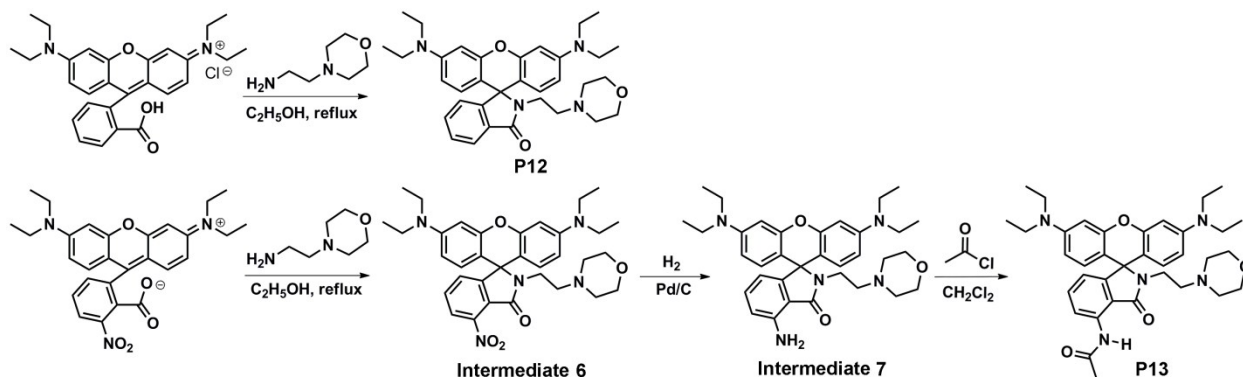
Synthesis of P13: **P13** was synthesized according to Scheme S7. The mixture of 3-nitro-RhB (200.0 mg, 0.42 mmol), 2-morpholinoethanamine (91.0 mg, 1.25 mmol), and ethanol (5 mL) was refluxed for 10 h. Then, the solvent was removed by rotary evaporation. The crude product was purified with column chromatography (silica gel, petroleum ether/ethyl acetate, 4:1 v/v) to give intermediate **6** as a yellow powder (1.03 g, 95%). Then, the obtained powders (1 g, 1.67 mmol) were dissolved in 5 mL methanol/ CH_2Cl_2 (3:1, v/v) mixed solvent and reduced with 0.1 g 10% Pd/C under hydrogen atmosphere. The reaction mixture was filtered, and then the filtrate was evaporated to give intermediate **7** as a white powder (1.84 g, 98%). Intermediate **7** (1.14 g, 2 mmol) and acetylchloride (58 mg, 0.75 mmol) were mixed in CH_2Cl_2 (5 mL) and stirred for 2 h. Then, the solvent was removed by rotary evaporation. The crude product was purified with

column chromatography (silica gel, petroleum ether/ethyl acetate, 8:1 v/v) to give **P13** as a white powder (0.26 g, 95%).

Intermediate 6: ^1H NMR (400 MHz, CDCl_3) δ 7.71 (dd, $J = 7.9, 0.7$ Hz, 1H), 7.52 (t, $J = 7.8$ Hz, 1H), 7.29 (dd, $J = 7.7, 0.7$ Hz, 1H), 6.48 (d, $J = 8.9$ Hz, 2H), 6.38 (d, $J = 2.6$ Hz, 2H), 6.30 (d, $J = 2.6$ Hz, 1H), 6.28 (d, $J = 2.6$ Hz, 1H), 3.60 – 3.52 (m, 4H), 3.35 (q, $J = 7.1$ Hz, 8H), 3.29 – 3.23 (m, 2H), 2.24 (s, 4H), 2.17 – 2.09 (m, 2H), 1.17 (t, $J = 7.0$ Hz, 12H). ^{13}C NMR (101 MHz, CDCl_3) δ 162.75, 156.10, 153.25, 148.96, 145.72, 132.70, 128.74, 127.94, 122.74, 122.55, 108.09, 103.83, 97.73, 66.90, 64.37, 55.71, 53.22, 44.38, 37.42, 12.51. LC-MS (ESI): m/z : calcd: 599.3108; found: 600.3187 $[\text{M}+\text{H}]^+$.

Intermediate 7: ^1H NMR (400 MHz, CDCl_3) δ 7.15 (t, $J = 7.7$ Hz, 1H), 6.56 (dd, $J = 8.3, 5.8$ Hz, 3H), 6.34 (t, $J = 5.3$ Hz, 3H), 6.28 (dd, $J = 8.9, 2.6$ Hz, 2H), 5.30 (s, 2H), 3.63 – 3.52 (m, 4H), 3.33 (q, $J = 7.0$ Hz, 8H), 3.24 – 3.15 (m, 2H), 2.24 (s, 4H), 2.11 – 2.04 (m, 2H), 1.16 (t, $J = 7.0$ Hz, 12H). ^{13}C NMR (101 MHz, CDCl_3) δ 169.45, 154.71, 153.07, 148.58, 144.93, 133.41, 129.08, 113.91, 113.36, 112.15, 107.97, 106.32, 97.55, 66.89, 64.52, 56.33, 53.22, 44.32, 36.55, 12.54. LC-MS (ESI): m/z : calcd: 569.3366; found: 570.3457 $[\text{M}+\text{H}]^+$.

P13: ^1H NMR (400 MHz, CDCl_3) δ 10.52 (s, 1H), 8.45 (d, $J = 8.2$ Hz, 1H), 7.40 (t, $J = 7.9$ Hz, 1H), 6.75 (d, $J = 7.6$ Hz, 1H), 6.47 (d, $J = 8.8$ Hz, 2H), 6.37 (d, $J = 2.5$ Hz, 2H), 6.28 (dd, $J = 8.9, 2.5$ Hz, 2H), 3.62 – 3.51 (m, 4H), 3.34 (q, $J = 7.0$ Hz, 8H), 3.25 – 3.16 (m, 2H), 2.29 (s, 3H), 2.23 (s, 4H), 2.10 – 2.03 (m, 2H), 1.16 (t, $J = 7.0$ Hz, 12H). ^{13}C NMR (101 MHz, CDCl_3) δ 169.30, 168.76, 153.38, 153.30, 148.85, 136.77, 133.97, 128.87, 118.03, 117.62, 116.29, 108.08, 105.01, 97.67, 66.87, 65.14, 56.07, 53.22, 44.37, 36.82, 29.67, 24.97, 12.53. LC-MS (ESI): m/z : calcd: 611.3472; found: 612.3507 $[\text{M}+\text{H}]^+$.



Scheme S7. The chemical structures and synthetic approaches for **P12** and **P13**.

Synthesis of P14: **P14** was synthesized according to Scheme S8. A suspension of 5-bromine anhydride naphthalene (2.76 g, 10 mmol), 4-ethynylaniline (1.17 g, 10mmol), Pd(PPh₃)₂Cl₂ (36.8 mg, 0.03 mmol), and CuI (7.62 mg, 0.04 mmol) in a mixture of THF (30 mL) and Et₃N (20 mL) was degassed with nitrogen for three times at room temperature. The mixture was stirred at reflux for 10 h, and then the solvents were removed under reduced pressure. The residue was purified by column chromatography (silica gel, dichloromethane/petroleum ether, 4:1 v/v) to afford intermediate **8** as an orange solid (2.97 g, 95%). Then, the mixture of 3-nitro-RhB (2.92 g, 6 mmol) and POCl₃ (5.6 mL, 60 mmol) was refluxed in 1,2-dichloroethane (150 mL) for 2 h, after which the solvent was removed to give dark violet-red oil. The crude acid chloride was dissolved in CH₂Cl₂ (100 mL), then trimethylamine (3 mL) and intermediate **8** (1.88 g, 6 mmol) were dropwise added into the mixture solution. The reaction mixture was stirred at room temperature for 24 h. Then, the solvent was removed and the crude residue was purified with column chromatography (silica gel, dichloromethane/ethyl acetate, 30:1 v/v) to give **P14** as a yellow powder (2.44 g, 52%).

Intermediate **8**: ¹H NMR (400 MHz, DMSO) δ 8.81 (d, *J* = 7.8 Hz, 1H), 8.57 (d, *J* = 7.3 Hz, 1H), 8.44 (d, *J* = 7.7 Hz, 1H), 8.06 – 7.93 (m, 2H), 7.46 (d, *J* = 8.4 Hz, 2H), 6.64 (d, *J* = 8.6 Hz, 2H), 5.90 (s, 2H). ¹³C NMR (101 MHz, DMSO) δ 161.14, 160.78, 151.41, 134.16, 133.71, 133.33, 132.39, 131.04, 130.36, 130.13, 129.38, 128.69, 120.01, 117.71, 114.12, 106.96, 104.08, 99.99, 84.94. LC-MS (ESI): *m/z*: calcd: 313.0739; found: 314.0812 [M+H]⁺.

P14: ¹H NMR (400 MHz, CDCl₃) δ 8.75 (d, *J* = 8.4 Hz, 1H), 8.65 (d, *J* = 7.1 Hz, 1H), 8.55 (d, *J* = 7.7 Hz, 1H), 7.92 (d, *J* = 7.6 Hz, 1H), 7.90 – 7.82 (m, 1H), 7.75 (d, *J* = 7.7 Hz, 1H), 7.61 (t, *J* = 7.8 Hz, 1H), 7.46 (d, *J* = 8.6 Hz, 2H), 7.36 (d, *J* = 7.6 Hz, 1H), 7.11 (d, *J* = 8.6 Hz, 2H), 6.68 (d, *J* = 8.5 Hz, 2H), 6.40 – 6.24 (m, 4H), 3.34 (dd, *J* = 14.0, 6.8 Hz, 8H), 1.17 (t, *J* = 7.0 Hz, 12H). ¹³C NMR (101 MHz, CDCl₃) δ 162.61, 160.40, 160.12, 155.81, 152.86, 149.11, 146.15, 137.83, 133.85, 133.78, 133.65, 132.56, 132.34, 131.68, 130.88, 130.18, 129.25, 128.33, 128.03, 127.85, 125.99, 122.74, 121.48, 119.52, 119.04, 117.77, 108.34, 104.38, 100.50, 97.83, 86.03, 66.95, 44.33, 12.52. LC-MS (ESI): *m/z*: calcd: 782.2740; found: 783.2810 [M+H]⁺.

Synthesis of P15: **P15** was synthesized according to Scheme S8. The mixture of **P14** (1.56 g, 2 mmol), SnCl₂•2H₂O (1.80 g, 8 mmol), and concentrated hydrochloric acid (9 mL) was refluxed in ethanol (50 mL) for 8 h. Then, the solvents were removed under reduced pressure. The residue was purified by column chromatography (silica gel, ethyl acetate/petroleum ether, 1:3 v/v) as eluent to afford **P15** as a yellow solid (1.27 g, 85%).

P15: ¹H NMR (400 MHz, CDCl₃) δ 8.75 (d, *J* = 8.3 Hz, 1H), 8.64 (d, *J* = 7.2 Hz, 1H), 8.54 (d, *J* = 7.7 Hz, 1H), 7.90 (d, *J* = 7.7 Hz, 1H), 7.85 (t, *J* = 7.8 Hz, 1H), 7.44 (d, *J* = 8.5 Hz, 2H), 7.22 (t, *J* = 7.7 Hz, 1H), 7.13 (d, *J* = 8.6 Hz, 2H), 6.76 (d, *J* = 8.5 Hz, 2H), 6.60 (d, *J* = 8.0 Hz, 1H), 6.37 (d, *J* = 7.4 Hz, 1H), 6.35 – 6.24 (m, 4H), 5.44 (s, 2H), 3.32 (q, *J* = 7.0 Hz, 8H), 1.16 (t, *J* = 7.0 Hz, 12H). ¹³C NMR (101 MHz, CDCl₃) δ 169.69, 160.45, 160.16, 154.88, 152.57, 148.73, 145.74, 138.85, 134.52, 133.91, 133.73, 132.58, 132.28, 131.66, 130.76, 130.19, 129.48, 128.53, 127.77, 125.45, 119.00, 118.41, 117.57, 113.36, 112.35, 111.95, 108.16, 106.83, 101.06, 97.69, 85.74, 67.17, 44.26, 12.57. LC-MS (ESI): *m/z*: calcd: 752.2999; found: 753.3073 [M+H]⁺.

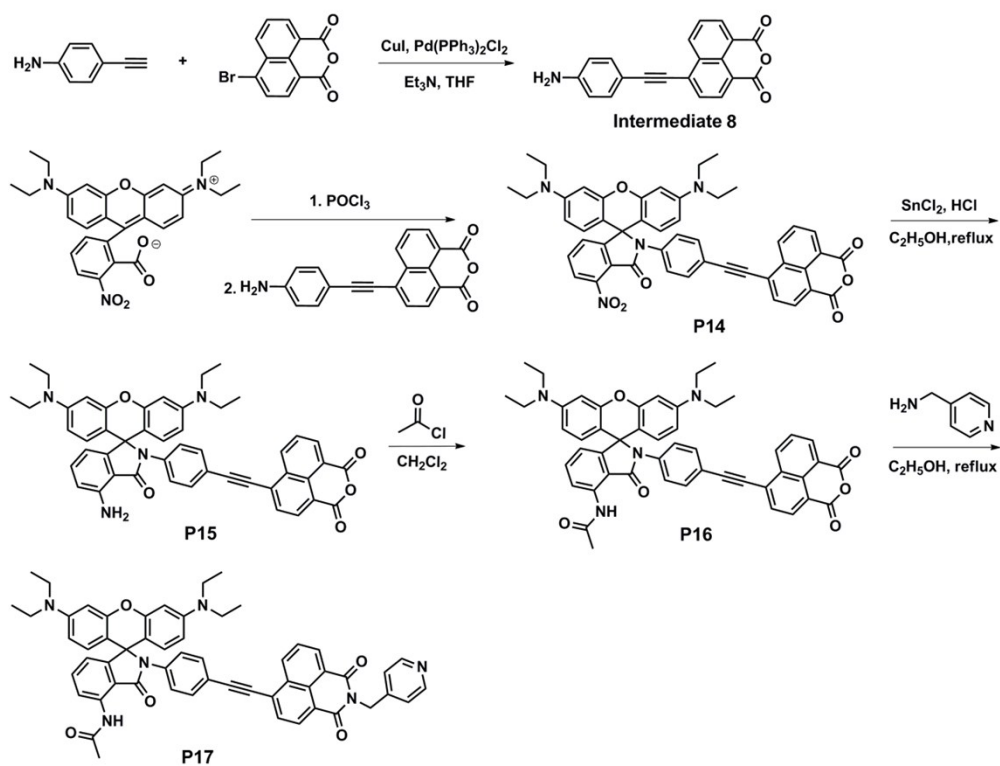
Synthesis of P16: **P16** was synthesized according to Scheme S8. **P15** (0.75 g, 1 mmol) and acetylchloride (0.12 g, 1.5 mmol) were mixed in CH₂Cl₂ (10 mL) and stirred for 2 h. Then, the solvent was removed by rotary evaporation. The crude product was purified with column chromatography (silica gel, ethyl acetate/petroleum ether, 1:3 v/v) to give **P16** as a yellow powder (0.76 g, 96%).

P16: ¹H NMR (400 MHz, CDCl₃) δ 10.58 (s, 1H), 8.75 (d, *J* = 8.2 Hz, 1H), 8.65 (d, *J* = 7.2 Hz, 1H), 8.55 (d, *J* = 7.7 Hz, 1H), 8.51 (d, *J* = 8.2 Hz, 1H), 7.92 (d, *J* = 7.7 Hz, 1H), 7.90 – 7.82 (m, 1H), 7.56 – 7.43 (m, 3H), 7.00 (d, *J* = 8.5 Hz, 2H), 6.81 (d, *J* = 7.6 Hz, 1H), 6.67 (d, *J* = 8.8 Hz, 2H), 6.37 – 6.26 (m, 4H), 3.33 (q, *J* = 7.0 Hz, 8H), 2.31 (s, 3H), 1.17 (t, *J* = 7.0 Hz, 12H). ¹³C NMR (101 MHz, CDCl₃) δ 169.31, 168.94, 160.38, 160.11, 153.44, 152.94, 148.99, 137.79, 137.43, 134.99, 133.82, 133.77, 132.55, 132.43, 131.70, 130.91, 130.20, 129.24, 128.48, 127.84, 126.34, 119.68, 119.10, 118.08, 117.81, 115.18, 108.26, 105.41, 100.48, 97.77, 86.08, 67.99, 44.32, 24.98, 12.55. LC-MS (ESI): *m/z*: calcd: 794.3104; found: 795.3177 [M+H]⁺.

Synthesis of P17: **P17** was synthesized according to Scheme S8. The mixture of **P16** (0.40 g, 0.5 mmol), 4-(aminomethyl)pyridine (0.15 mL, 1.5 mmol), and ethanol (10 mL) was refluxed for 8 h. Then, the solvent was removed by rotary evaporation. The crude product was purified with

column chromatography (silica gel, dichloromethane/methanol, 20:1 v/v) to give **P17** as a yellow powder (0.42 g, 96%).

P17: ^1H NMR (400 MHz, CDCl_3) δ 10.59 (s, 1H), 8.66 (dd, $J = 16.5, 7.7$ Hz, 2H), 8.52 (d, $J = 9.9$ Hz, 4H), 7.89 (d, $J = 7.5$ Hz, 1H), 7.81 (t, $J = 7.7$ Hz, 1H), 7.48 (dd, $J = 13.1, 8.0$ Hz, 3H), 7.37 (d, $J = 4.3$ Hz, 2H), 6.98 (d, $J = 8.1$ Hz, 2H), 6.81 (d, $J = 7.4$ Hz, 1H), 6.67 (d, $J = 8.7$ Hz, 2H), 6.42 – 6.23 (m, 4H), 5.36 (s, 2H), 3.33 (q, $J = 7.0$ Hz, 8H), 2.30 (s, 3H), 1.16 (t, $J = 6.6$ Hz, 12H). ^{13}C NMR (101 MHz, CDCl_3) δ 169.29, 168.89, 163.89, 163.61, 153.41, 152.95, 149.99, 148.97, 145.77, 137.50, 137.41, 134.93, 132.83, 132.34, 132.04, 131.60, 130.83, 130.67, 128.48, 128.12, 127.48, 126.40, 123.21, 122.49, 121.48, 120.04, 118.08, 117.78, 115.25, 108.23, 105.40, 99.36, 97.76, 86.49, 67.99, 44.30, 42.64, 24.97, 12.54. LC-MS (ESI): m/z : calcd: 884.3686; found: 885.3804 $[\text{M}+\text{H}]^+$.

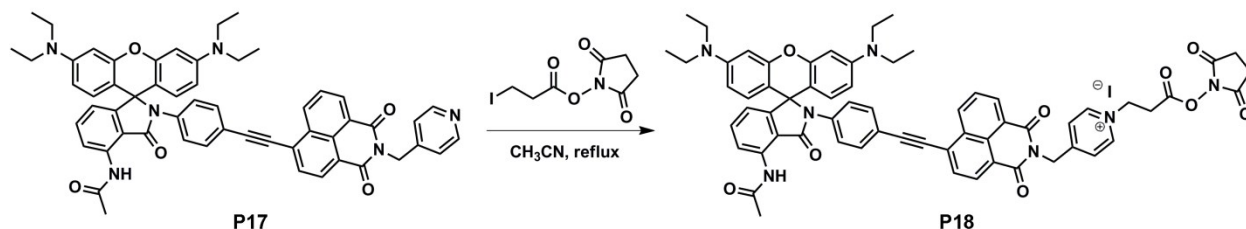


Scheme S8. The chemical structures and synthetic approaches for **P14**-**P17**.

Synthesis of P18: **P18** was synthesized according to Scheme S9. **P17** (0.26 g, 0.3 mmol) and 2,5-dioxopyrrolidin-1-yl 3-iodopropanoate⁷ (0.1 g, 0.35 mmol) were dissolved in 10 mL

acetonitrile and refluxed 24 hours. The acetonitrile was removed under reduced pressure. A brown solid was obtained which was crushed into powder and stirred in ethyl acetate overnight and filtered to afford **P18** as a brown solid (0.26 g, 74%).

P18: ^1H NMR (400 MHz, DMSO) δ 10.41 (s, 1H), 9.02 (d, $J = 5.8$ Hz, 2H), 8.83 (d, $J = 8.0$ Hz, 1H), 8.58 (d, $J = 7.0$ Hz, 1H), 8.49 (d, $J = 7.5$ Hz, 1H), 8.34 (d, $J = 8.0$ Hz, 1H), 8.24 (d, $J = 5.8$ Hz, 2H), 8.07 (d, $J = 7.4$ Hz, 1H), 8.04 – 7.94 (m, 1H), 7.66 (d, $J = 8.1$ Hz, 2H), 7.60 – 7.49 (m, 1H), 7.09 (d, $J = 7.6$ Hz, 2H), 6.73 (d, $J = 6.8$ Hz, 2H), 6.62 – 6.12 (m, 4H), 5.50 (s, 2H), 4.92 (t, 2H), 3.63 (t, 2H), 3.35 (q, $J = 7.0$ Hz, 8H), 2.80 (s, 4H), 2.25 (s, 3H), 1.08 (t, $J = 6.1$ Hz, 12H). ^{13}C NMR (101 MHz, DMSO) δ 169.99, 168.86, 168.05, 166.49, 163.52, 163.23, 157.90, 151.96, 145.00, 137.69, 137.05, 135.13, 132.44, 132.38, 131.53, 130.98, 130.93, 130.25, 128.36, 127.94, 126.44, 125.39, 122.76, 122.12, 119.02, 117.65, 117.38, 114.52, 113.45, 98.45, 86.69, 66.59, 54.76, 42.98, 31.27, 25.45, 24.63, 12.17. LC-MS (ESI): m/z : calcd: 1054.4134; found: 1054.4212 $[\text{M}]^+$.



Scheme S9. The chemical structure and synthetic approach for **P18**.

2.6 Time-dependent UV-vis absorption and PL spectra, and their dynamic studies of P1-P8 in CH₂Cl₂/ CH₃OH (9/1, v/v) before and after the addition of CF₃COOH

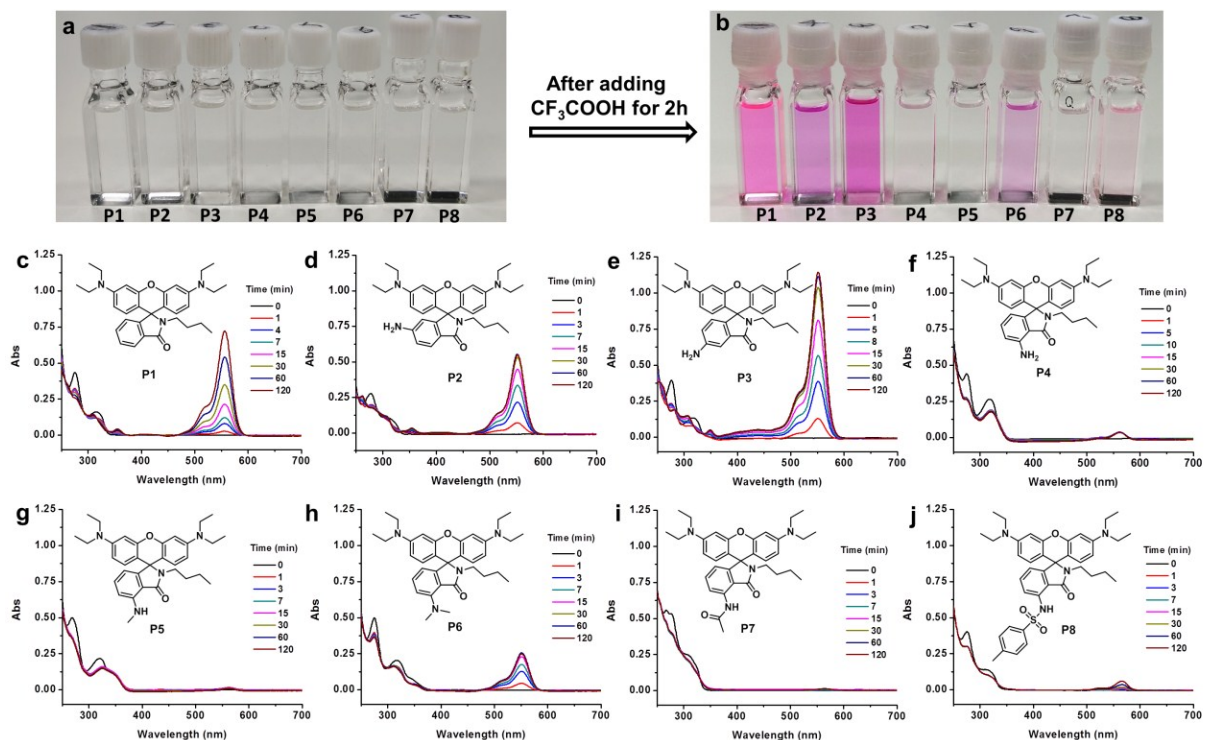


Figure S2. Photographs of **P1-P8** (10^{-5} M) in CH₂Cl₂/CH₃OH (9/1, v/v) (a) before and (b) after the addition of 2.3 μ L CF₃COOH (1000 equivalent) under ambient light. (c-j) Time-dependent UV-vis absorption spectra of **P1-P8** (10^{-5} M) in CH₂Cl₂/CH₃OH (9/1, v/v), before and after the addition of CF₃COOH. Corresponding insets: chemical structures of **P1-P8**.

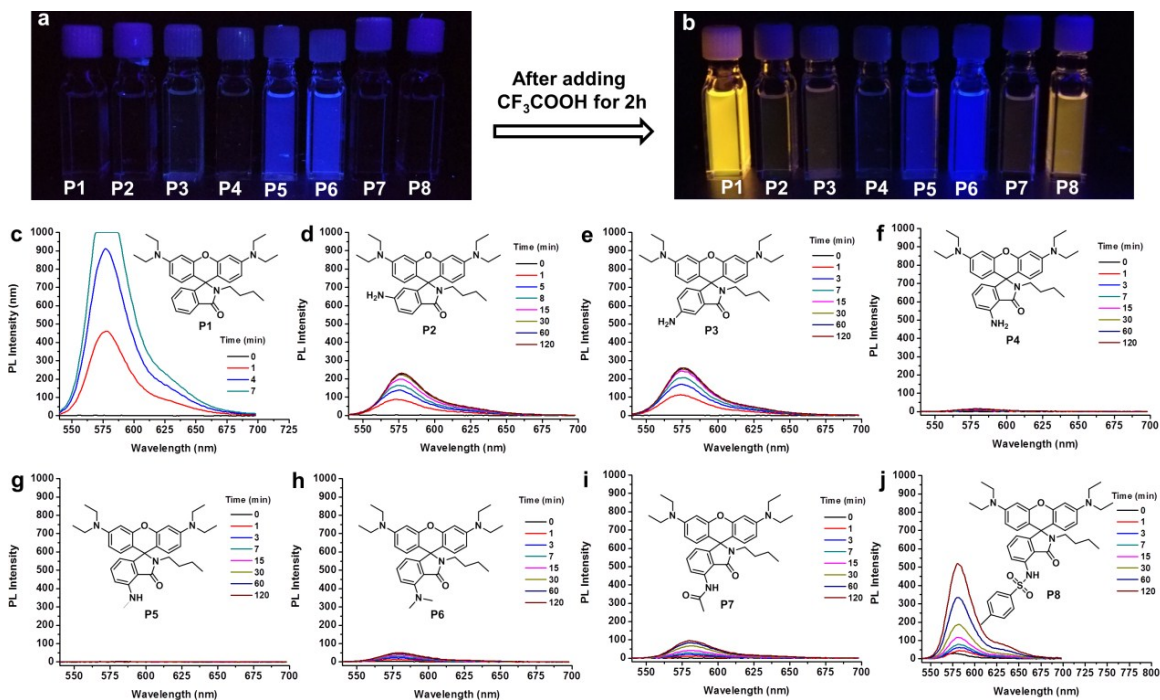


Figure S3. Photographs of **P1-P8** (10^{-5} M) in $\text{CH}_2\text{Cl}_2/\text{CH}_3\text{OH}$ (9/1, v/v) in a dark room with 365 nm UV radiations, (a) before and (b) after the addition of 2.3 μL CF_3COOH (1000 equivalent). (c-j) Time-dependent PL spectra of **P1-P8** (10^{-5} M) in $\text{CH}_2\text{Cl}_2/\text{CH}_3\text{OH}$ (9/1, v/v) before and after the addition of 2.3 μL CF_3COOH . Excitation wavelength: 520 nm. Corresponding insets: chemical structures of **P1-P8**.

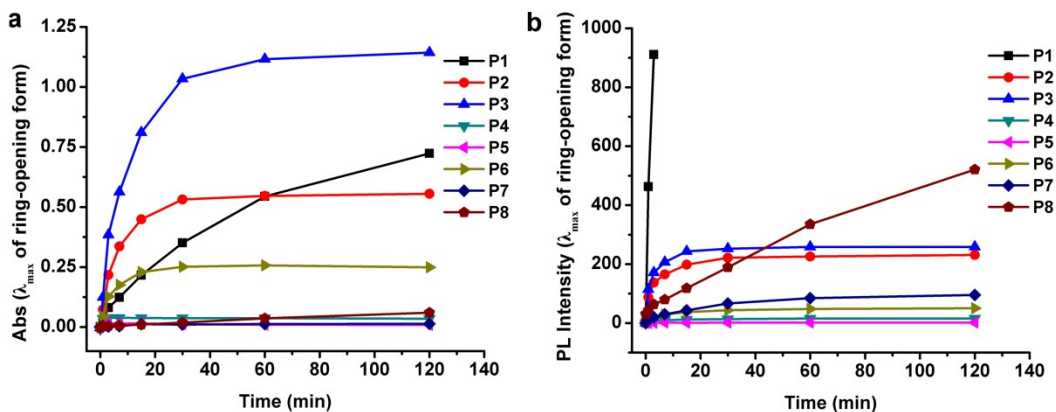


Figure S4. a) UV-vis absorption and b) PL dynamic studies of **P1-P8** (10^{-5} M) in $\text{CH}_2\text{Cl}_2/\text{CH}_3\text{OH}$ (9/1, v/v) after the addition of CF_3COOH (2.3 μL , 1000 eq).

2.7 Crystal data and intensity collection parameters

Table S3. Summary of crystal data and intensity collection parameters of **P4**, **P6**, **P7** and **P8**.

	P4	P6	P7	P8
Empirical formula	C ₃₂ H ₄₀ N ₄ O ₂	C ₃₄ H ₄₄ N ₄ O ₂	C ₃₄ H ₄₂ N ₄ O ₃	C ₃₉ H ₄₆ N ₄ O ₄ S
Formula weight	512.68	540.73	554.71	666.86
Crystal system	Triclinic	Triclinic	Monoclinic	Triclinic
Space group	<i>P1</i>	<i>P</i> $\bar{1}$	<i>Cc</i>	<i>P</i> $\bar{1}$
<i>a</i> , Å	10.1957(4)	11.0084(7)	21.0138(12)	11.7633(8)
<i>b</i> , Å	12.2494(5)	12.0389(7)	10.9924(7)	12.4781(9)
<i>c</i> , Å	23.2226(10)	12.2322(8)	26.6620(16)	13.0623(9)
α , deg	92.193(3)	79.257(5)	90.00	106.839(6)
β , deg	93.573(3)	66.321(6)	97.694(5)	100.035(6)
γ , deg	106.021(3)	78.199(5)	90.00	93.786(6)
Volume, Å ³	2777.56(19)	1443.40(17)	6103.3(6)	1793.2(2)
<i>Z</i>	4	2	8	2
<i>D</i> _x , g/cm ³	1.226	1.244	1.207	1.235
<i>M</i> μ /mm ⁻¹	0.077	0.078	0.078	0.136
<i>F</i> ₀₀₀	1104	584	2384	712
Temp, (K)	193(2)	130(6)	128(2)	126(2)
<i>M</i> (Mo <i>K</i> α), mm ⁻¹	0.079	0.083	0.434	0.710
2 θ range, deg	5.74-58.87	5.73-58.77	6.43-52.83	5.89-58.61
Reflections collected	26499	11619	8465	8324
Independent reflections	18223	6788	8465	8324
<i>R</i> (int)	0.0413	0.0309	0.0594	-
Data/restraints/parameters	18223/3/1389	6788/7/376	8465/4/757	8324/3/463
<i>R</i> ₁ , <i>wR</i> ₂ [obs <i>I</i> > 2 σ (<i>I</i>)]	0.0727, 0.1827	0.0665, 0.1684	0.0799, 0.1927	0.0800, 0.2216
<i>R</i> ₁ , <i>wR</i> ₂ (all data)	0.0842, 0.1926	0.1224, 0.1948	0.0857, 0.1963	0.1034, 0.2367
Residual peak/hole e. Å ⁻³	0.42/-0.36	0.30/-0.50	0.40/-0.38	0.59/-0.55
Goodness-of-fit on <i>F</i> ²	1.064	0.969	1.132	1.114
CCDC number	1582847	1901370	1901371	1901372

2.8 Optimized molecular structures of P1-P6 in water

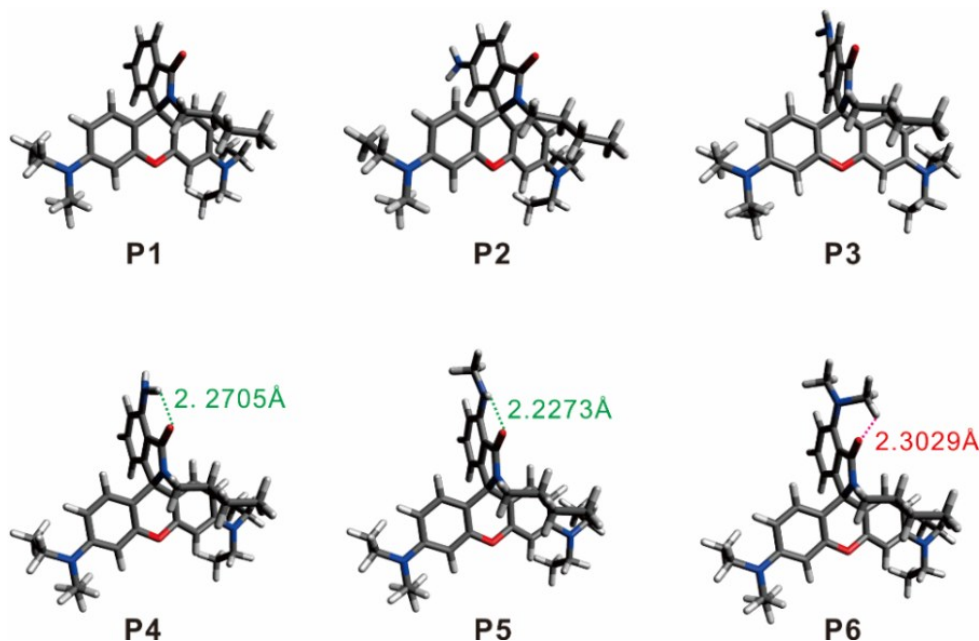


Figure S5. Optimized molecular structures of **P1-P6** in water. Notes: **P4** and **P5** possess strong NH...O hydrogen bondings (highlighted in green), while **P6** possess weak CH...O interaction (highlighted in red).

Notes: We have optimized the molecular structures of the lactams of **P1-P6** in water (Figure S5). Among **P1-P6**, only **P4** and **P5** possess a strong hydrogen bond with the amide group (highlighted in green). We also noted that weak CH...O interactions were present at the amide group of **P6** (highlighted in red).

2.9 Ring-opening tendency in acidic environments

During our computational modeling, we first investigated the ring-opening tendency of spiro lactams *in acidic environments*. To this end, we have calculated the Gibbs free energies of eight representative protonation states of **P1-P6** (Figure S6). Among these eight states, four of them possess emissive open-ring structures (highlighted in pink) and the rest four display non-emissive closed-ring structures (highlighted in grey).

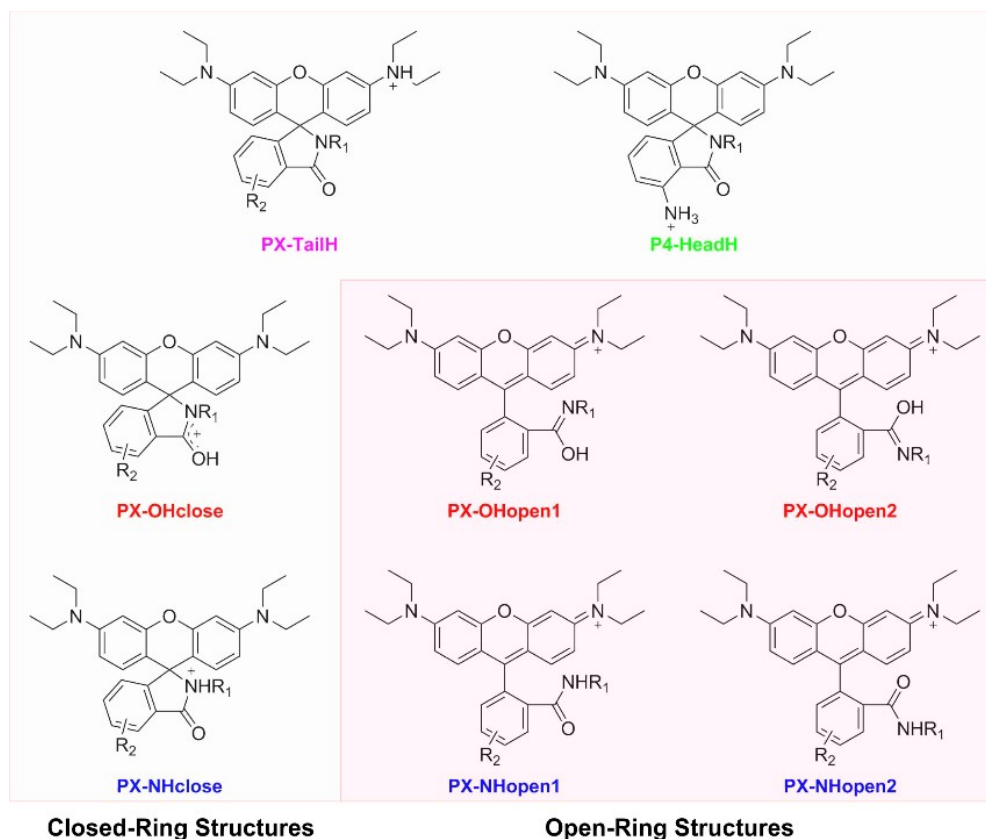


Figure S6. Molecular structures of eight representative protonation states of **P1-P6**. Note that **X = 1-6**, and $R_1 = -C_4H_9$; the molecular structures of **PX-HeadH** is represented on by **P4-HeadH** only, as **P1-P6** possesses distinct R_2 substituents.

We then selected the most stable closed-ring structures and the most stable open-ring structures and computed the difference in the Gibbs free energy (δ) between these two structures. We defined this difference δ as the ring-opening tendency in acidic environments (Equation S1). From the thermodynamic point of view, a large δ corresponds to a strong driving force for ring-opening reactions in rhodamine spirolactams to proceed.

$$\delta = \min \{G_{closed - ring\ structures}\} - \min \{G_{open - ring\ structures}\} \quad \text{Equation S1}$$

From our DFT results (Table S4; Figures S7-S12), we computed the ring-opening tendency of **P1-P6** (Figure 2e). We noticed that **P4** and **P5** exhibited a significantly lower ring-opening tendency than **P1-P3** and **P6** did.

Table S4. Relative Gibbs free energy (eV) in the representative protonation states, and the ring-opening tendency δ (eV) of **P1-P6**.^{a,b,c}

Compound	TailH	HeadH	OHclosed	OHopen1	OHopen2	NHclosed	NHopen1	NHopen2	δ
P1	0		0.36	0.54	0.59	0.71	-0.08	-0.15	0.15
P2	0	0.09	0.24	0.55	0.62	0.53	-0.07	-0.14	0.14
P3	0	0.01	0.35	0.49	0.57	0.72	-0.15	-0.19	0.19
P4	0	0.11	0.35	0.64	0.72	0.63	-0.02	0	0.02
P5	0	-0.01	0.27	0.61	0.71	0.57	-0.03	0.01	0.02
P6	0		0.37	0.61	0.68	0.61	-0.06	-0.08	0.08

^a **PXTailH** is set as a reference in the calculations of relative Gibbs free energy of **PX**, where **X = 1-6**.

^b The Gibbs free energy of **P1HeadH** was not computed because the R₂ substituent in **P1** (i.e., H) does not have a valid protonation state.

^c The Gibbs free energy of **P6HeadH** was not considered. This is because **P6** was designed as a “control” compound without any intramolecular hydrogen bonding in the spiroamides. However, **P6HeadH** possesses such a hydrogen bond, and thus violates our assumption.

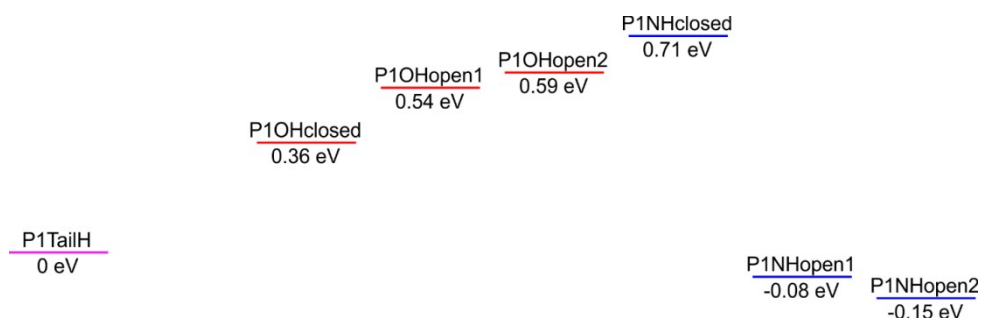


Figure S7. Relative Gibbs free energy of representative protonation state of **P1** in acidic environments. Note that we did not consider **P1HeadH** because the R₂ substituent in **P1** (i.e. H) does not have a protonation state.

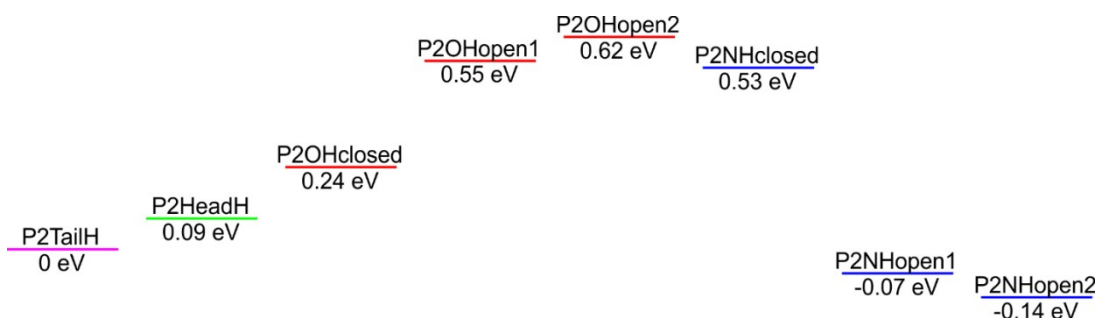


Figure S8. Relative Gibbs free energy of representative protonation state of **P2** in acidic environments.

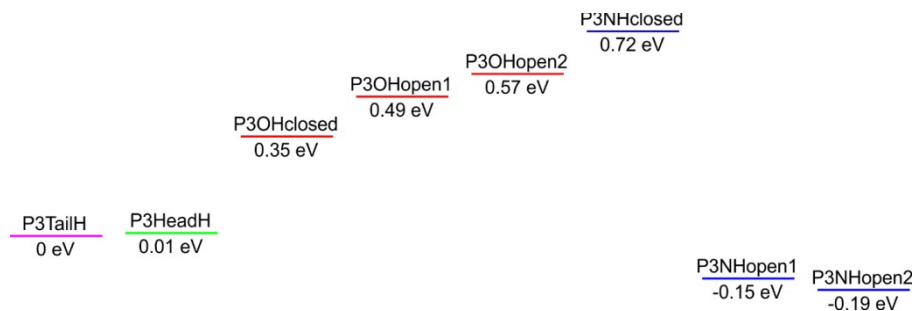


Figure S9. Relative Gibbs free energy of representative protonation state of **P3** in acidic environments.

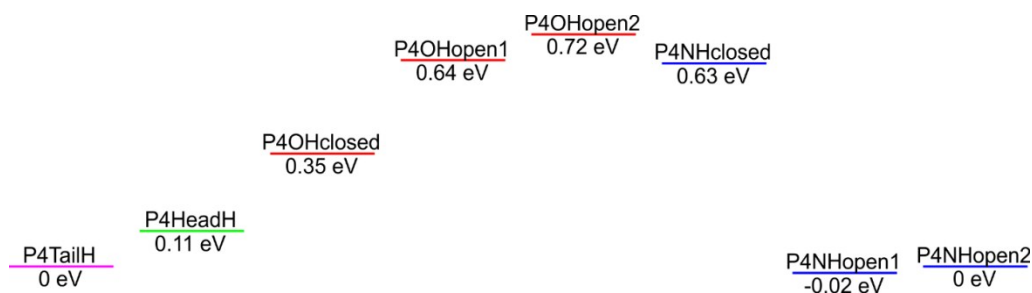


Figure S10. Relative Gibbs free energy of representative protonation state of **P4** in acidic environments.

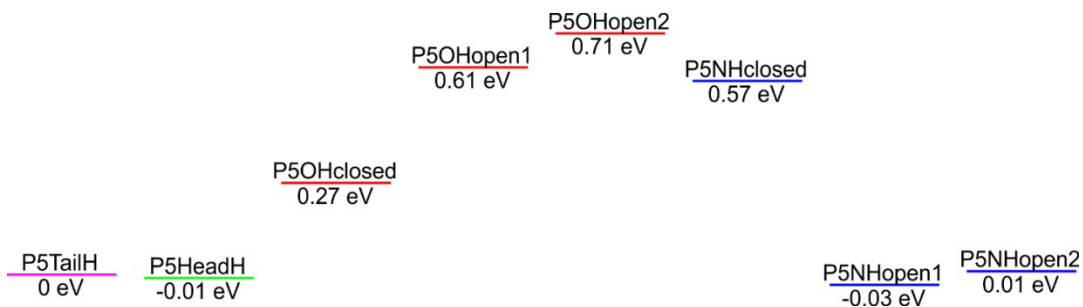


Figure S11. Relative Gibbs free energy of representative protonation state of **P5** in acidic environments.

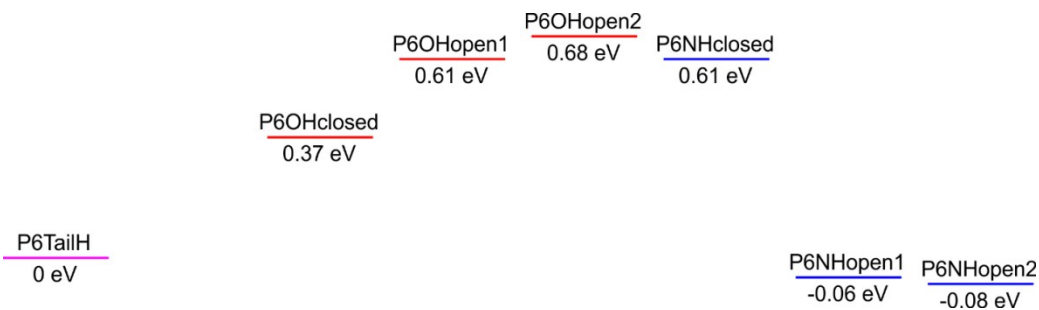


Figure S12. Relative Gibbs free energy of representative protonation state of **P6** in acidic environments.

2.10 Energy barriers during ring-opening reactions

To compute the energy barrier of the ring-opening reactions of rhodamine spiroamides during acid-activation, we first need to establish the reaction path. Based on our analysis, we proposed the following reactions path (Figure S13). We expect that the ring-opening process is the rate-determining step because it is the only step that involves the breaking of chemical bonds. It is noteworthy that the final process of amide rotation may or may not occur, which is subjected to the relative stability of **PX-NHopen1** and **PX-NHopen2**.

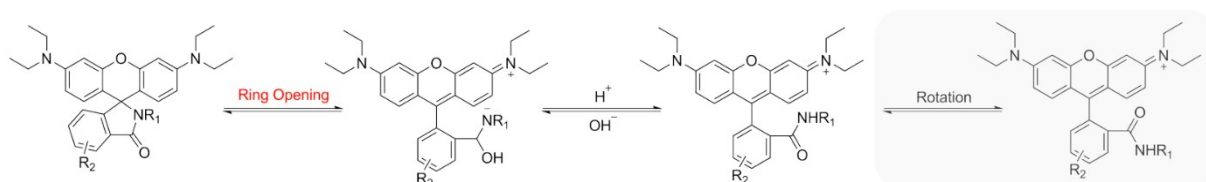


Figure S13. The ring-opening process of rhodamine spiroamides during acid-activation, as proposed by us.

We continued to compute the energy barrier during the ring-opening process for **P1-P6** (Table S5; Figures S14-S19). Our results show that **P4** and **P5** exhibit the highest energy barriers during the ring-opening process (Figure 2f). These large barriers are attributed to the “locking” effect of the intramolecular hydrogen bonds with the amide groups in **P4** and **P5**.

Among **P1-P3** and **P6** (which do not possess intramolecular hydrogen bonds), **P6** demonstrates the highest energy barriers (Table S5). This is due to relatively strong CH...O interactions around the amide group in **P6** (Figure S5).

Table S5. Relative Gibbs free energy (eV) of lactams, zwitterions and the associated transition states (TS) of **P1-P6**.^a

Compound	Lactam	Transition State (TS)	Zwitterion
P1	0.00	1.27	1.12
P2	0.00	1.32	1.19
P3	0.00	1.22	1.06
P4	0.00	1.36	1.21
P5	0.00	1.36	1.17
P6	0.00	1.35	1.21

^a Lactams are set as references in the calculations of relative Gibbs free energy of **PX**, where **X** = **1-6**.

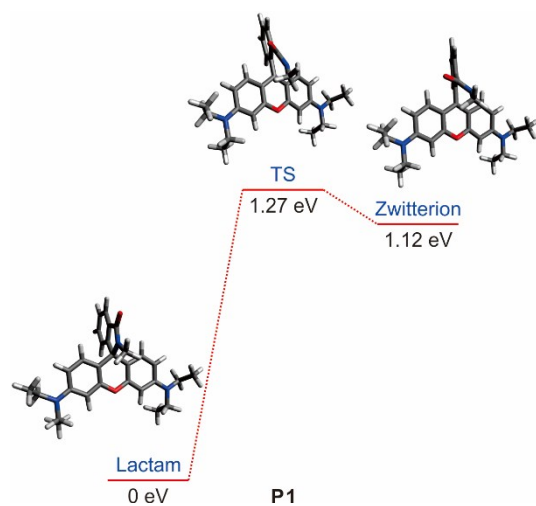


Figure S14. Optimized molecular structures and relative Gibbs free energy of the lactam, transition state, zwitterion of **P1** in water.

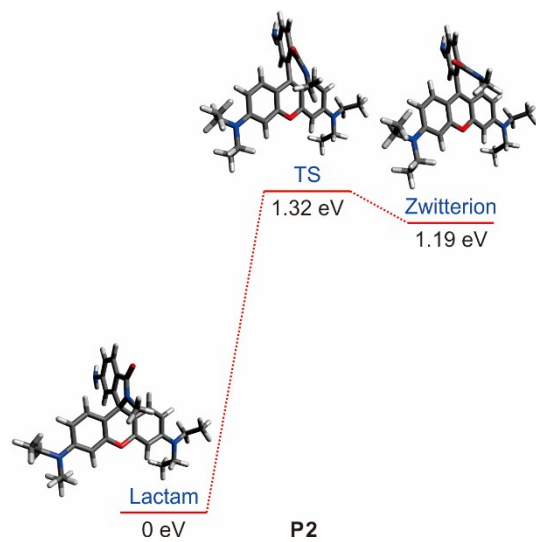


Figure S15. Optimized molecular structures and relative Gibbs free energy of the lactam, transition state, zwitterion of **P2** in water.

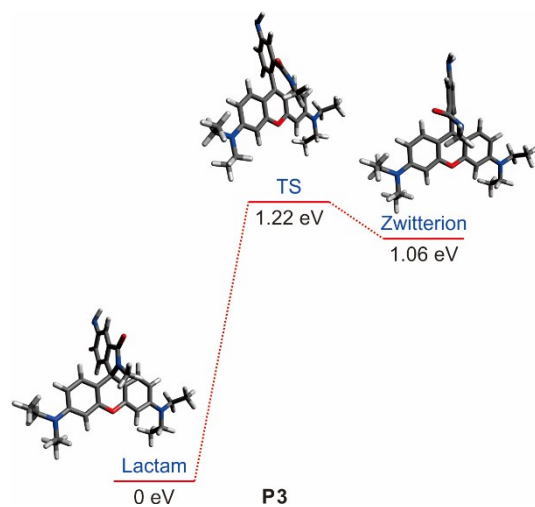


Figure S16. Optimized molecular structures and relative Gibbs free energy of the lactam, transition state, zwitterion of **P3** in water.

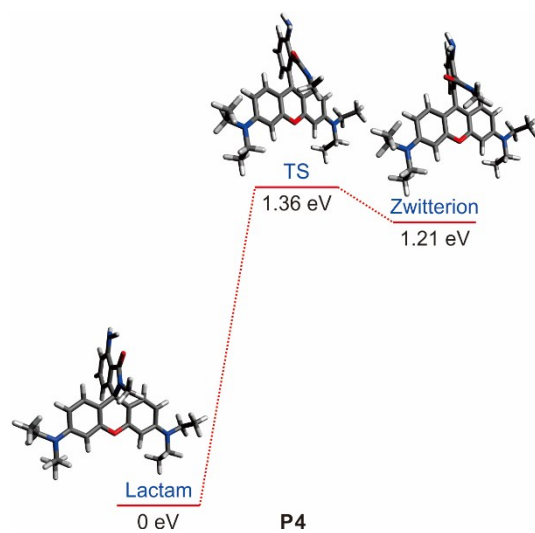


Figure S17. Optimized molecular structures and relative Gibbs free energy of the lactam, transition state, zwitterion of **P4** in water.

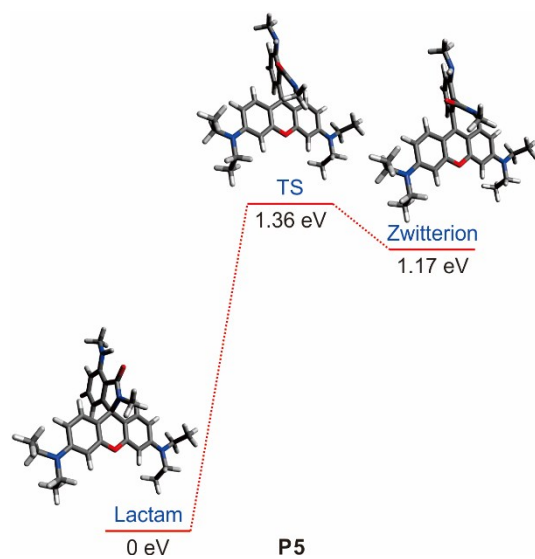


Figure S18. Optimized molecular structures and relative Gibbs free energy of the lactam, transition state, zwitterion of **P5** in water.

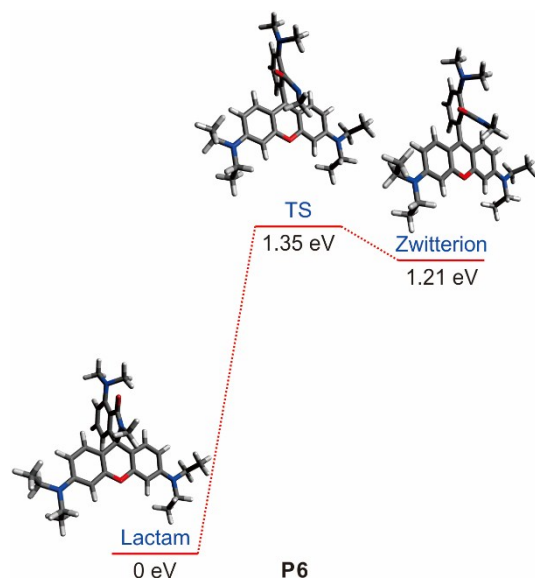


Figure S19. Optimized molecular structures and relative Gibbs free energy of the lactam, transition state, zwitterion of **P6** in water.

2.11 UV-vis absorption and PL spectra of P9 and P10 in different pH PBS buffer solution

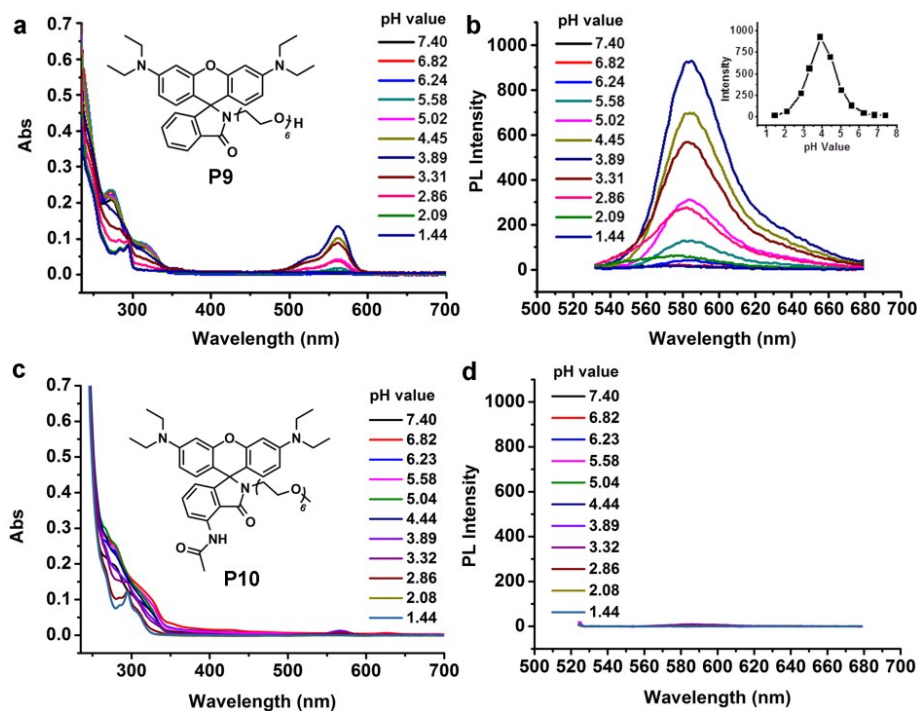
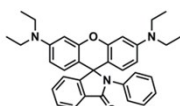


Figure S20. a,c) UV-vis absorption and b,d) PL spectra of **P9** (10 μ M) and **P10** (10 μ M) in PBS buffer solution with different pH values. Excited wavelength: 520 nm. Insets of a,c): corresponding chemical structures of **P9** and **P10**. Insets of b): the peak emission intensity of **P9** as a function of pH.

2.12 Switching properties of rhodamine spirolactams determined by laser flash photolysis

Table S6. Switching properties of rhodamine spirolactams determined by laser flash photolysis.

Compounds	τ	τ	τ	τ
	in dioxane	in CH_2Cl_2	in DMSO/ H_2O (v/v, 1/2)	in DMSO/ H_2O (v/v, 1/19)
P1	62.5 ns	-	-	-
P7	59.7 ns	-	-	-
P11	31.5 ns	-	26.7 ns	-
 N-phenyl-rhodaminelactame	200 ms	-	-	-
P18	-	-	46 ns	105 ns

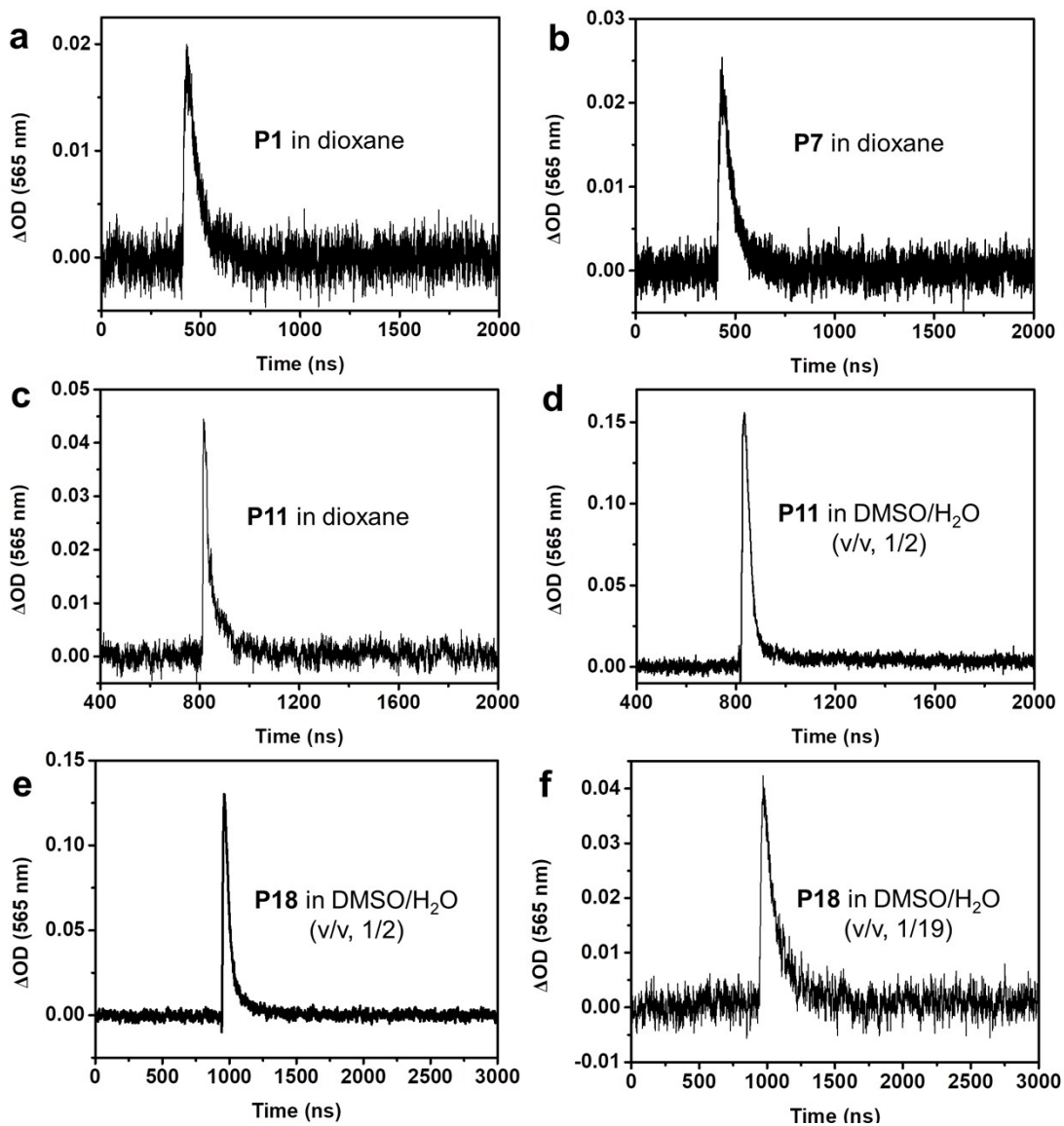


Figure S21. Laser flash photolysis of rhodamine derivatives. Transient absorption decay curves of **P1**, **P7** and **P11** after 266 nm laser pulsing (30 mJ/pulse), and **P18** after 355 nm laser pulsing (60 mJ/pulse) in different solvent at room temperature.

2.13 CLSM images of MCF-7 cells stained with P12 and P13 and taken at different culture time

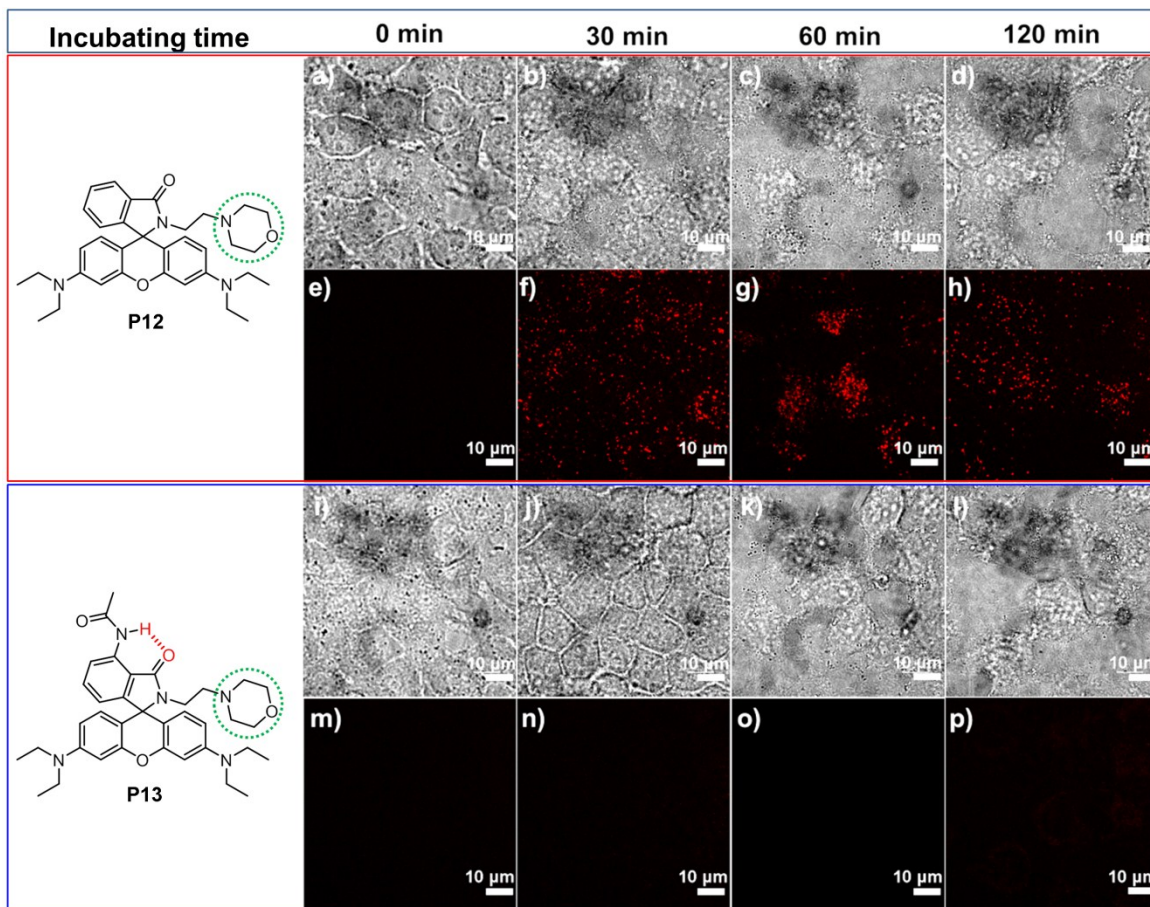


Figure S22. CLSM images of MCF-7 cells stained with **P12** (10 μ M) and **P13** (10 μ M) and taken with different culture time (0-120 min). (**a-d, i-l**) Bright-field. (**e-h, m-p**) Red channel. Excitation wavelength: 545 nm, emission collection window: 580–653 nm.

2.14 Time-dependent change of the peak absorbance of the open isomer of P1 and P7 in CH₂Cl₂ solution under and then after 254 nm UV irradiations were removed.

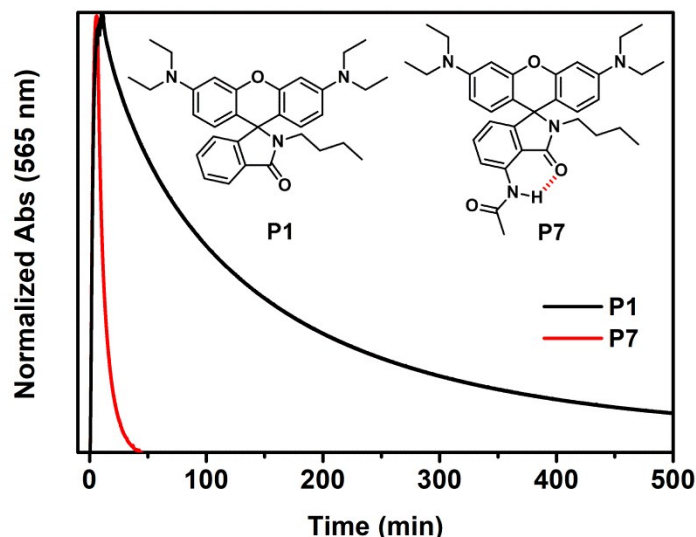


Figure S23. Time-dependent change of the peak absorbance of the open isomer of **P1** and **P7** in CH₂Cl₂ solution (1×10^{-5} M, monitored at 565 nm), under and then after 254 nm UV irradiations were removed.

2.15 Calculated UV-vis absorption spectrum and frontier molecular orbitals of P16 in aqueous solution

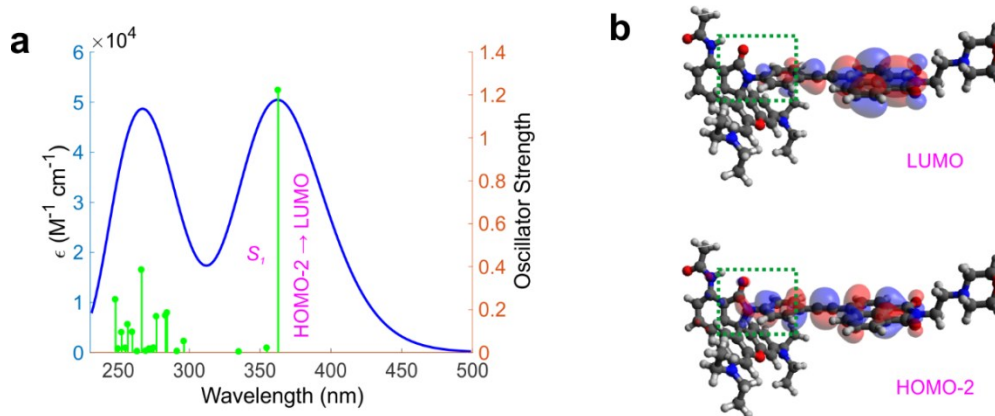


Figure S24. (a) Calculated UV-vis absorption spectrum of **P17** (in the lactam configuration) in aqueous solution. (b) HOMO-2 and LUMO of **P17** (in the lactam configuration); the first absorption band of **P17** is dominated by the transition from HOMO-2 to LUMO.

Notes: Our calculations show that laser irradiations in the first absorption band of **P17** photoexcite the chromophore attached with the lactam nitrogen in **P17** (Figure S24). This photoexcitation, dominated by a HOMO-2→LUMO transition, induces a substantial charge transfer away from the spirocyclic moiety (Figure S24b; highlighted in green boxes). Consequently, the resulted charge transfer effectively raises the electron-withdrawing strength of the spirocyclic moiety and facilitates the ring-opening reactions in **P17** to form charge-separated zwitterion.

2.16 Single molecule properties of P17 at optimal laser power density

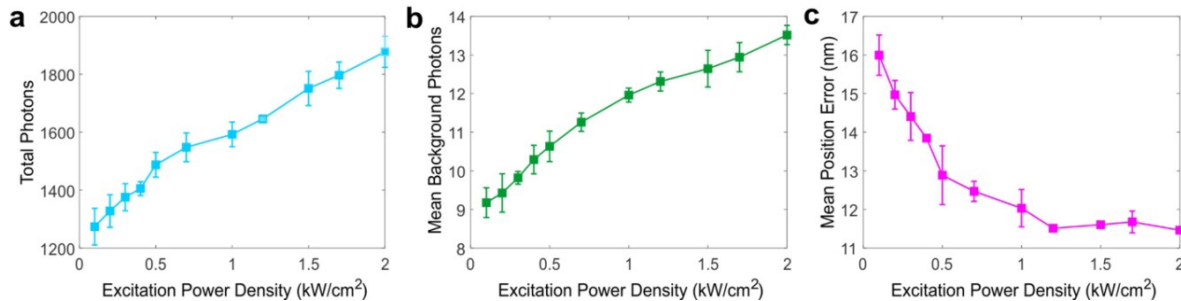
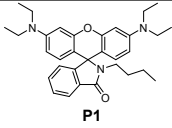
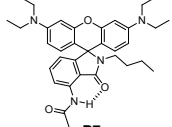
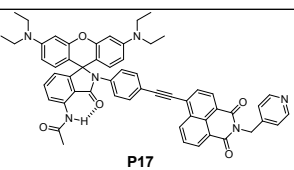
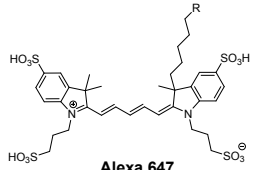


Figure S25. Single molecule properties of **P17** at various excitation laser power densities: **(a)** distribution of total photons, **(b)** background photons, and **(c)** position error.

2.17 Comparative analyses of various aspects of our best perform rhodamine spirolactams (P17 and P7) with common P1 and the Alexa 647.

Table S7. Comparative analyses of various aspects of our best perform rhodamine spirolactams (**P17** and **P7**) with common **P1** and the Alexa 647.

compounds	fluorescence quantum yield (Φ_F)	photoactivation light wavelength/excitation light wavelength	photons per single molecule per frame	total photons	mean background photons	localization positions	acid-sensitivity	other additives (thiols and antioxidant)
 P1	0.38% ^b	≤ 375 nm/561 nm	— ^a	— ^a	— ^a	— ^a	acid-sensitive	not required
 P7	0.36% ^b	≤ 375 nm/561 nm	— ^a	— ^a	— ^a	— ^a	acid-resistant	not required
 P17	— ^b	405nm (60 W/m ²)/561 nm (1.2 KW/m ²)	1293.0 \pm 71.5	1645.7 \pm 10.4	12.3 \pm 0.2	11.5 \pm 0.1 nm	acid-resistant	not required
 Alexa 647	0.33 ^b	405nm (60 W/m ²)/640 nm (1.2 KW/m ²) ^c	2600.3 \pm 228.9	14097.7 \pm 1261.3	7.7 \pm 0.6	8.1 \pm 0.5 nm	acid-resistant	required

^aWe cannot measure these properties because of the absence of a rare UV laser (≤ 375 nm).

^b Φ_F of the ring-open form of **P1** and **P7** were measure in CH₂Cl₂/CH₃OH (9/1, v/v) because of their poor water solubility, while Φ_F of Alexa 647 in PBS is obtained from the dye manufacturer when known. However, we cannot measure the Φ_F of **P17** as it is difficult to obtain its ring-open isomer after adding acid.

^cAlexa 647-labeled proteins were adsorbed on coverglass and illuminated with two lasers at 405 nm (60 W/m²) and 640 (1.2 KW/m²), to photoactivate and excite its fluorescence.

2.18 Pearson Correlation Coefficients for CLSM images of MCF-7 cells stained with LTG and P12 or P13

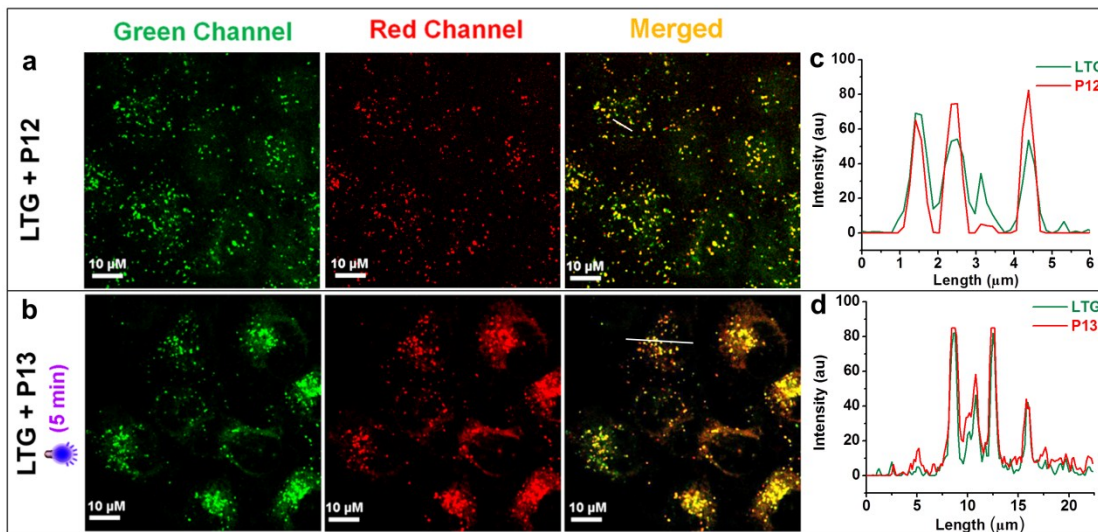
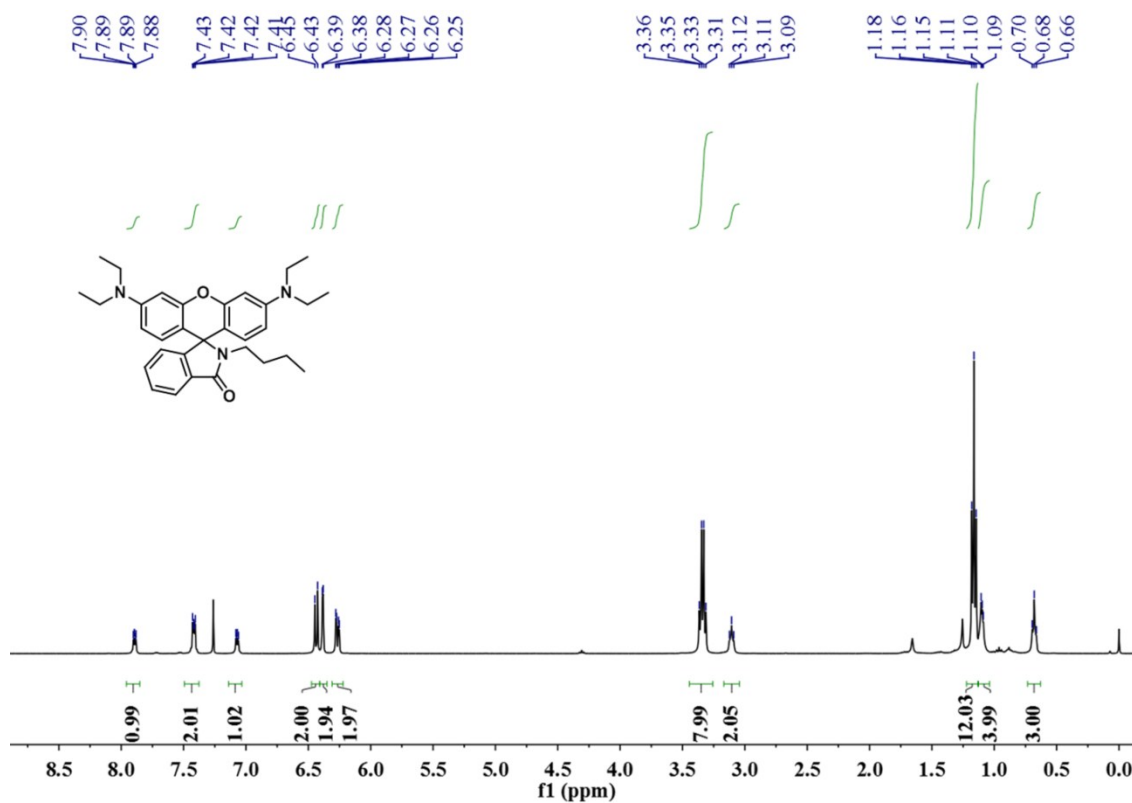


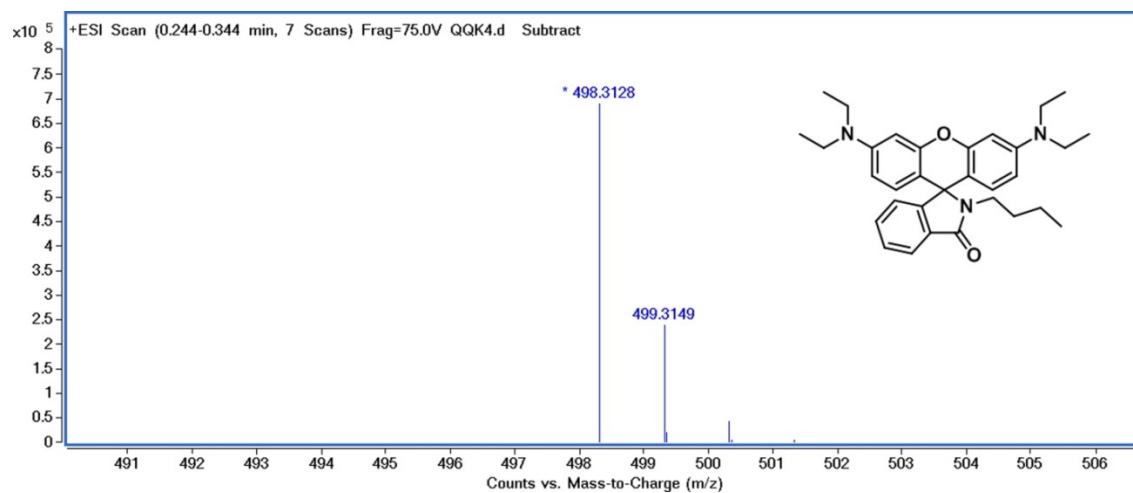
Figure S26. Colocalization confocal images of MCF-7 cells stained with LTG (0.1 μM) and a) **P12** (10 μM) or b) **P13** (10 μM); green channel: excitation at 488 nm, emission collected from 500 to 550 nm; red channel: excitation at 561 nm, emission collected from 580 to 653 nm. c,d) Corresponding intensity profile of regions of interest (cross-sectional analysis along the white line).

Notes: As can be seen from the **Figure S26**, the intensity profiles of the linear regions of interest across MCF-7 cells stained with LTG and **P12** or **P13** display close synchrony. The high Pearson coefficients are 0.905 (LTG with **P12**) and 0.925 (LTG with **P13** activated by UV light for 5 mins), respectively.

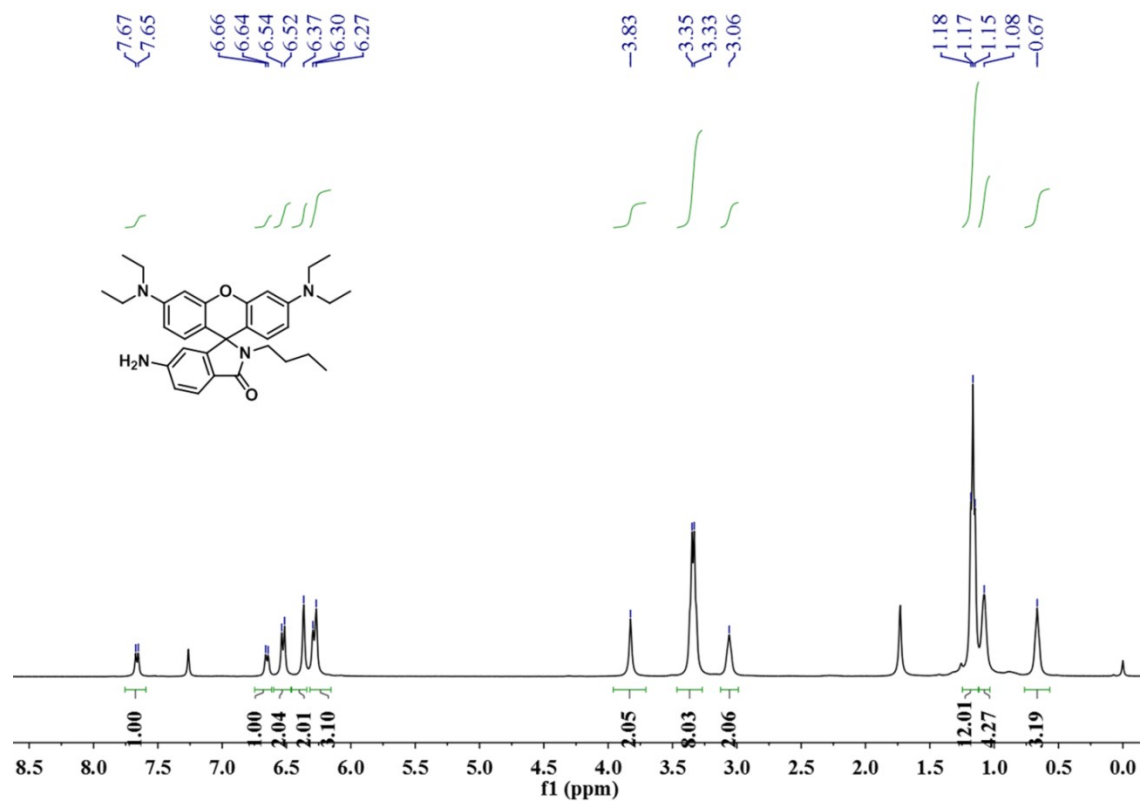
3. ^1H NMR, ^{13}C NMR and MS spectra of the compounds



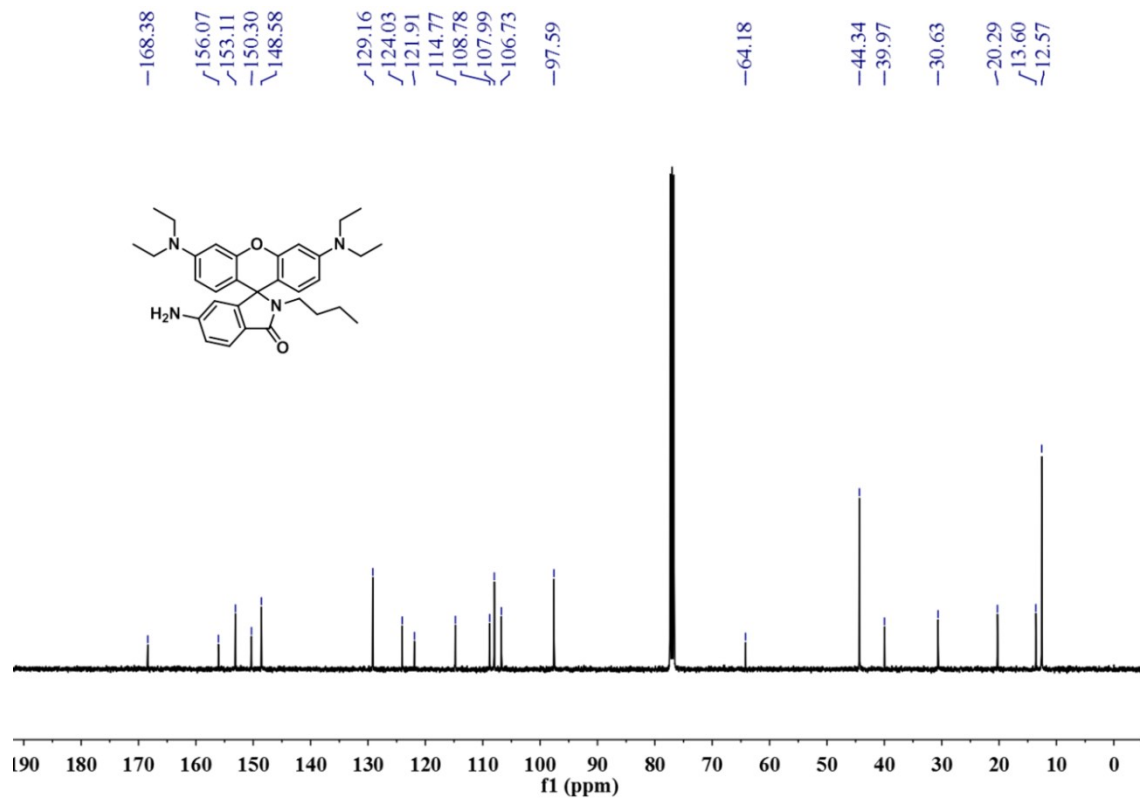
^1H NMR spectrum of **P1** in CDCl_3 .



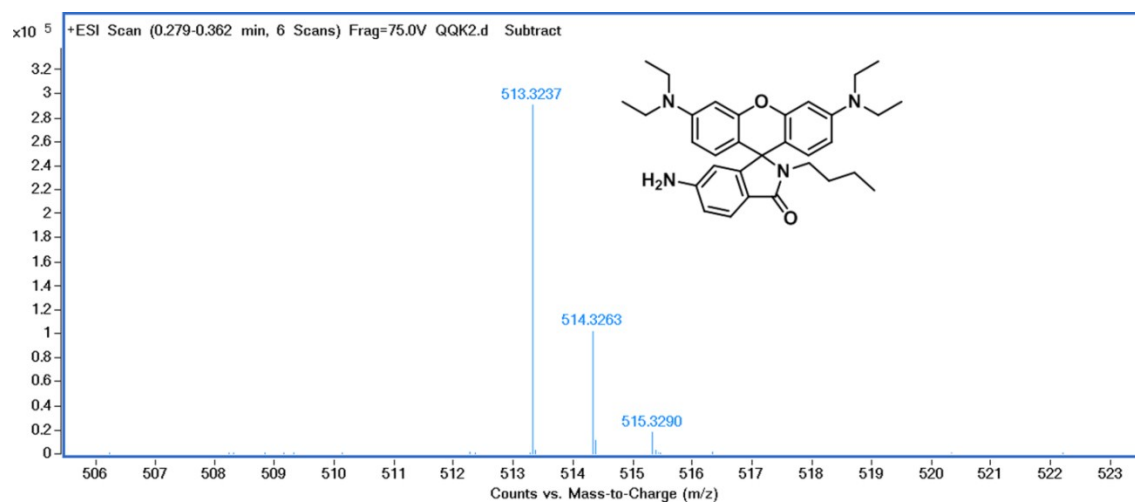
HRMS (ESI) of **P1**.



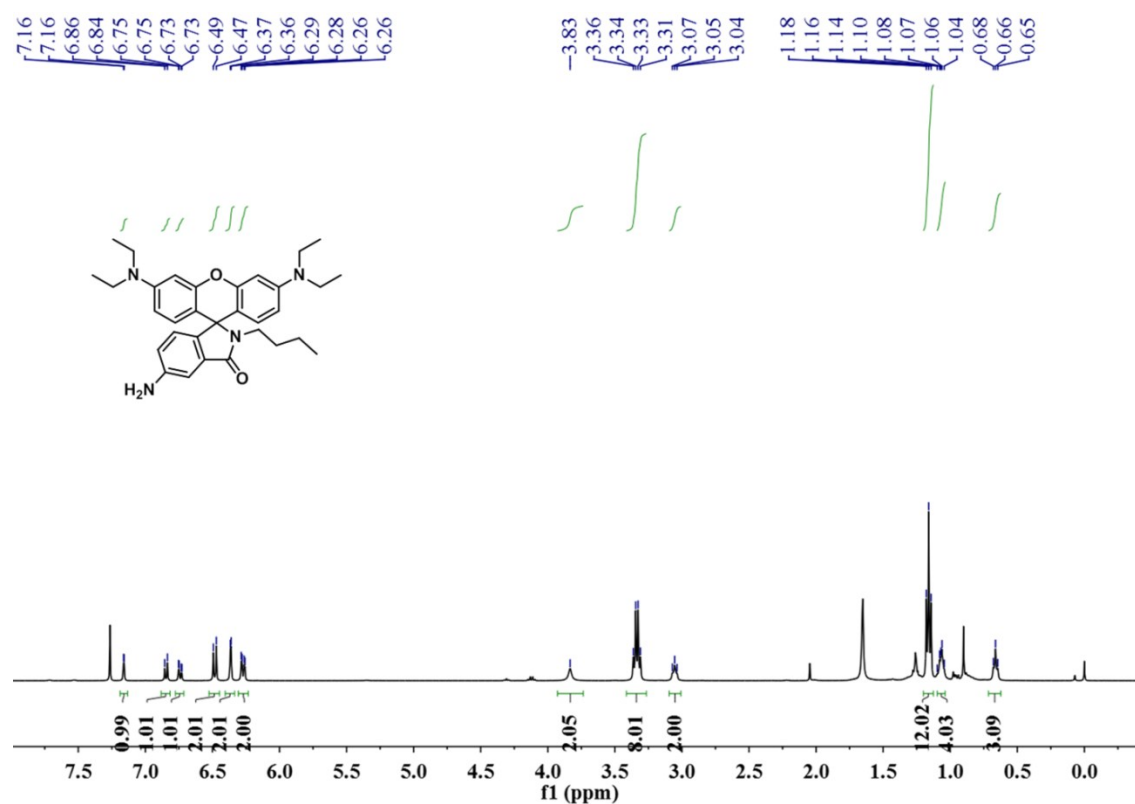
¹H NMR spectrum of P2 in CDCl₃.



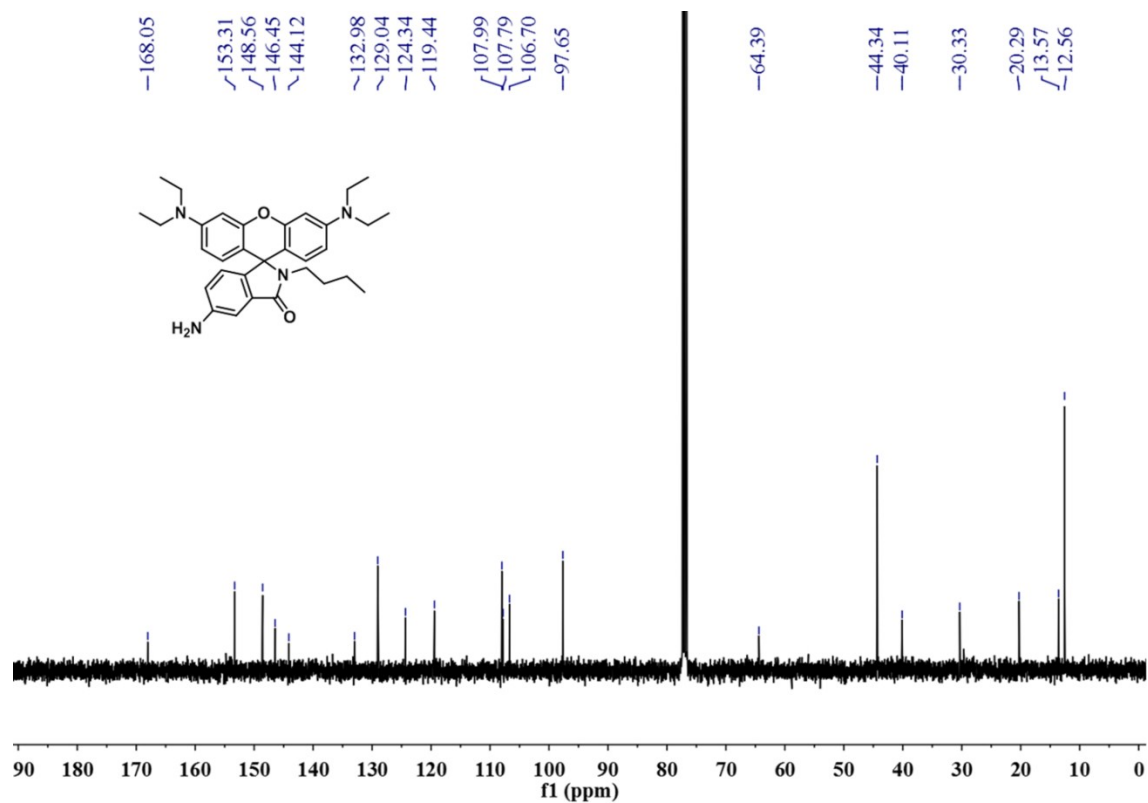
¹³C NMR spectrum of P2 in CDCl₃.



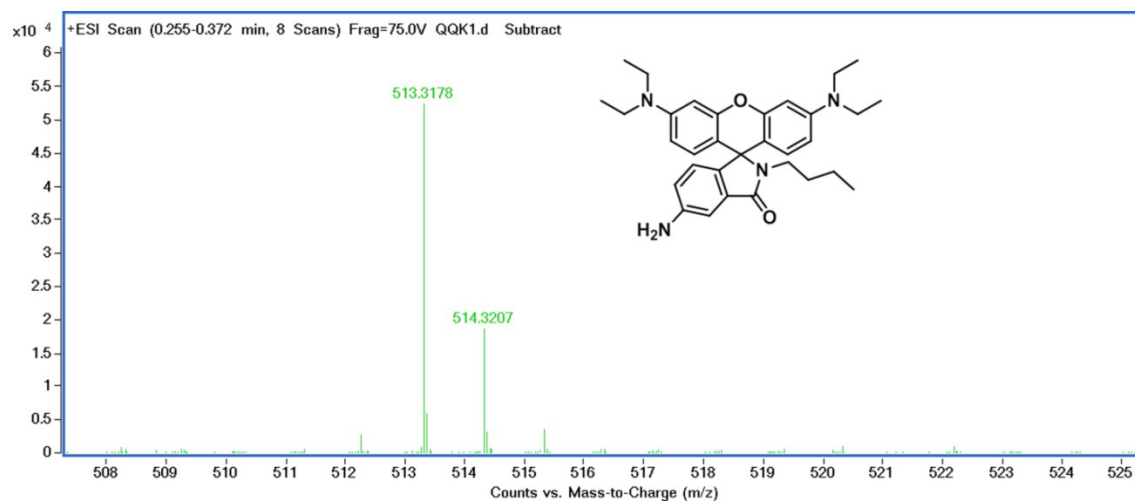
HRMS (ESI) of P2.



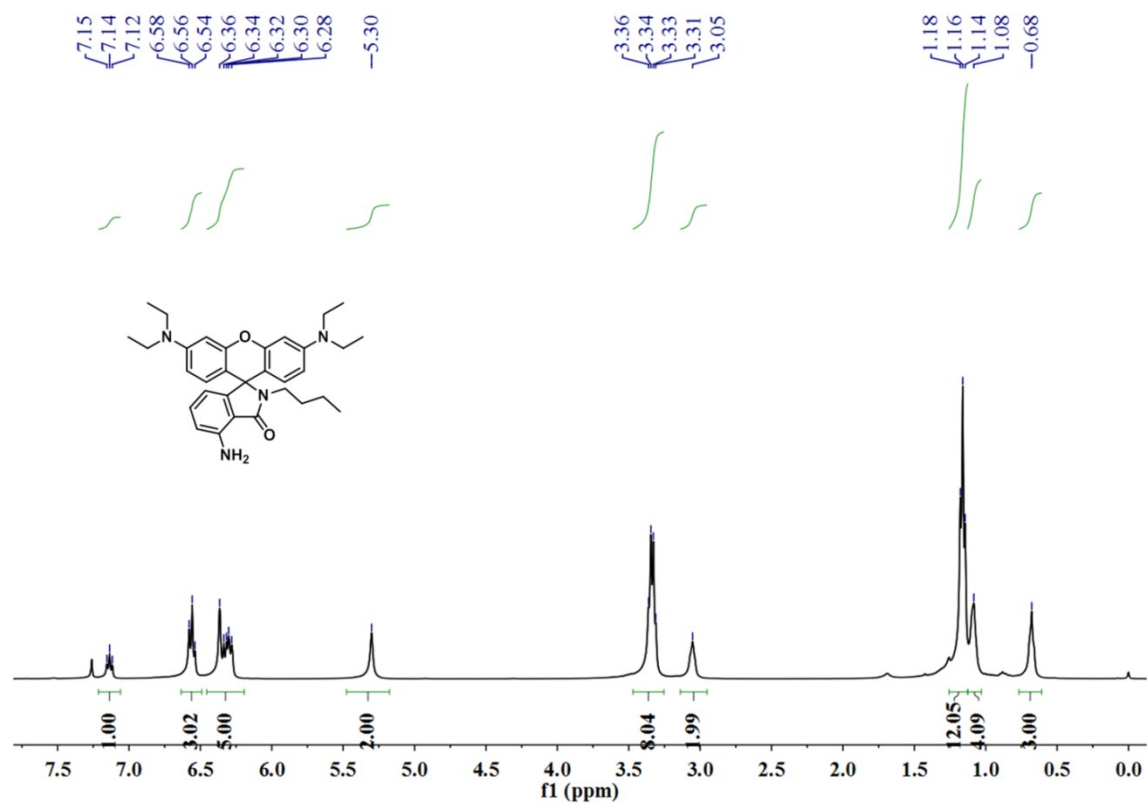
¹H NMR spectrum of P3 in CDCl₃.



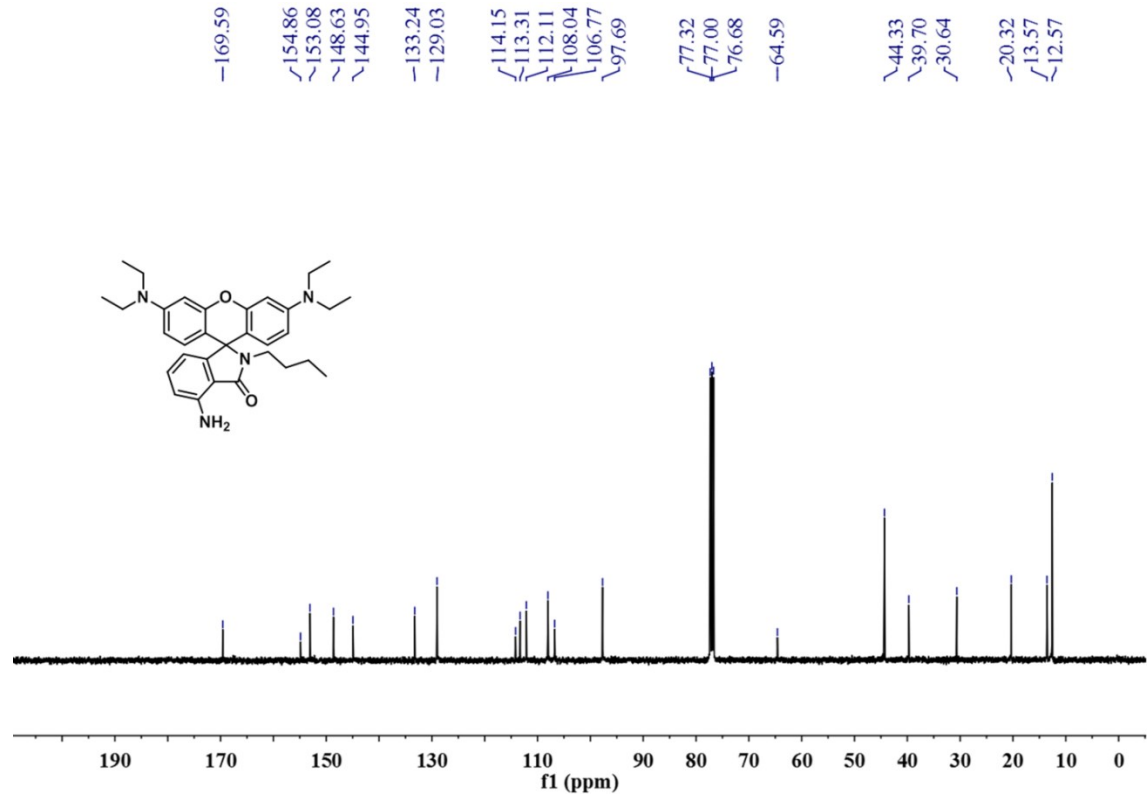
¹³C NMR spectrum of P3 in CDCl₃.



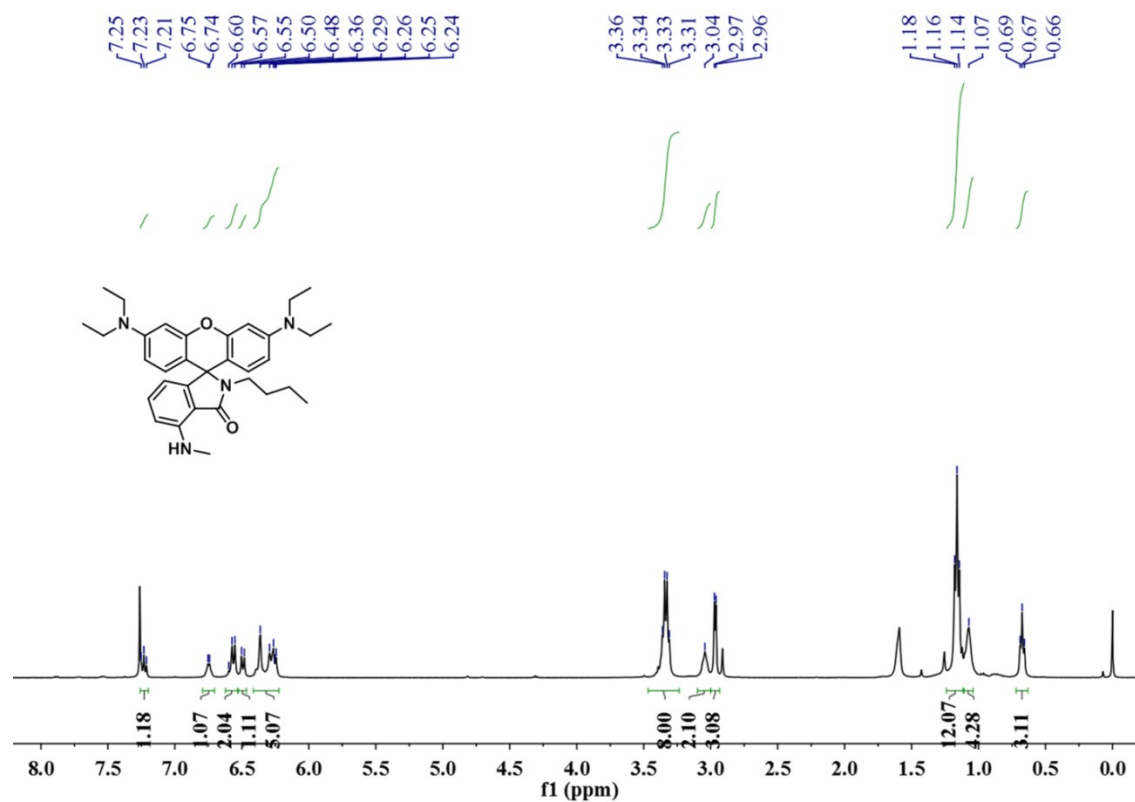
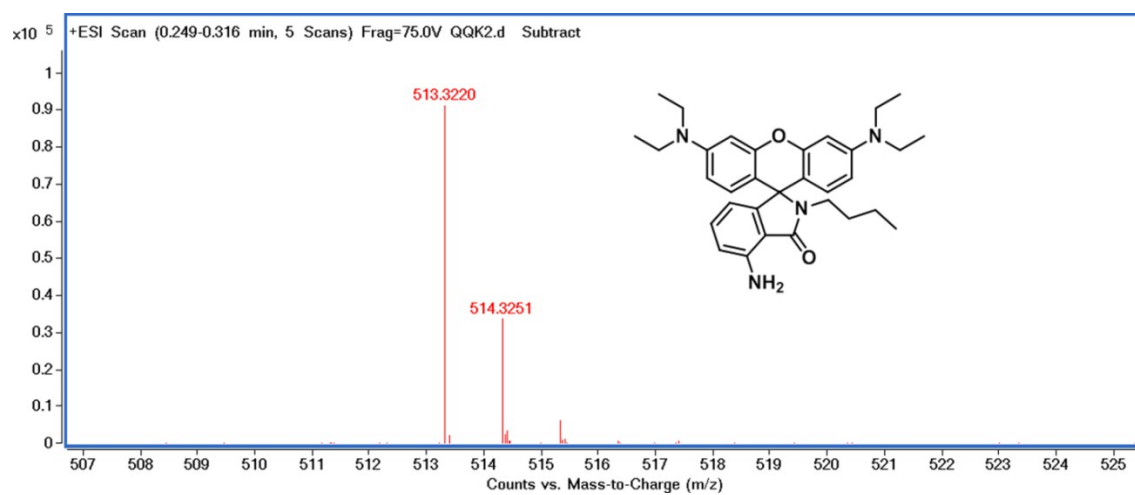
HRMS (ESI) of P3.

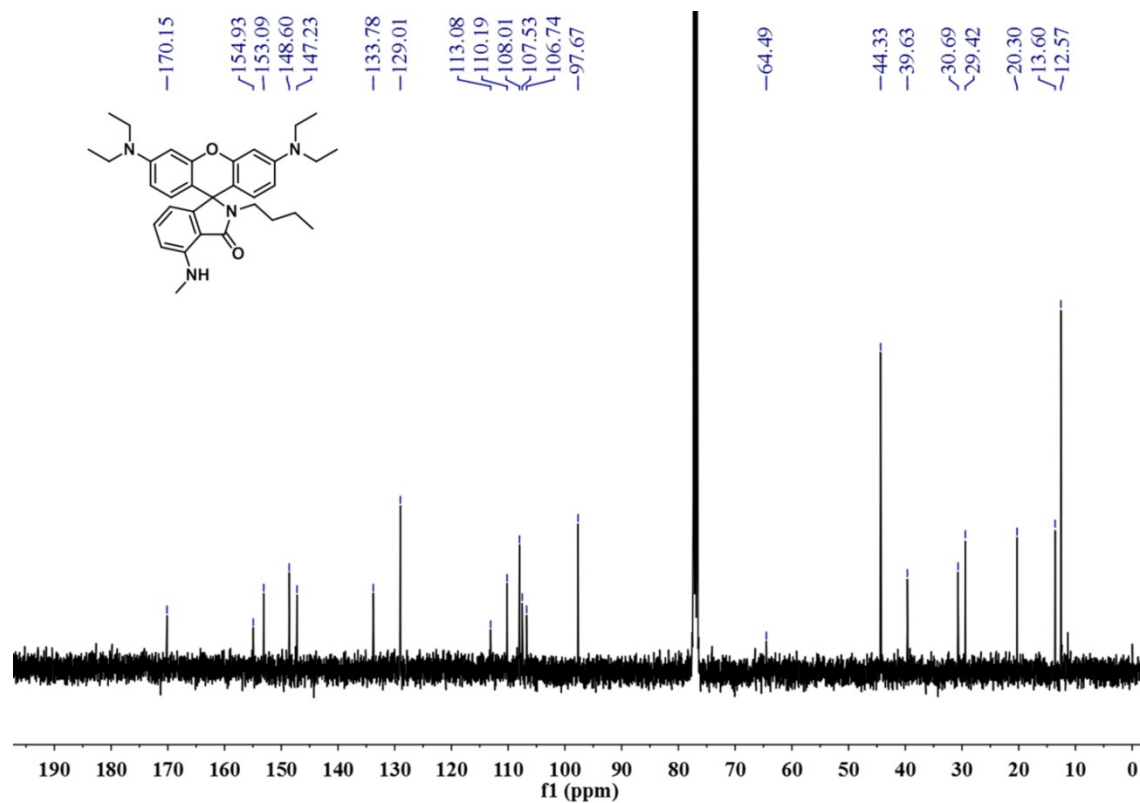


¹H NMR spectrum of **P4** in CDCl₃.

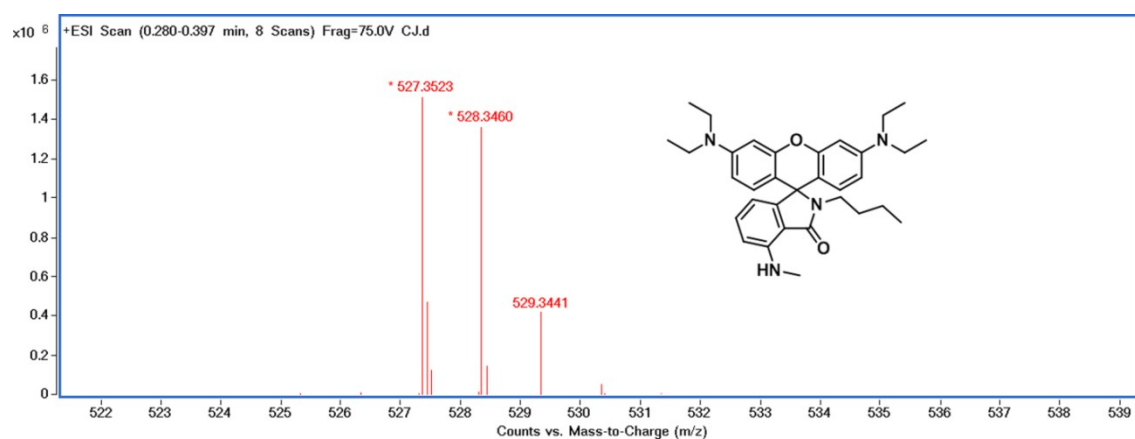


¹³C NMR spectrum of **P4** in CDCl₃.

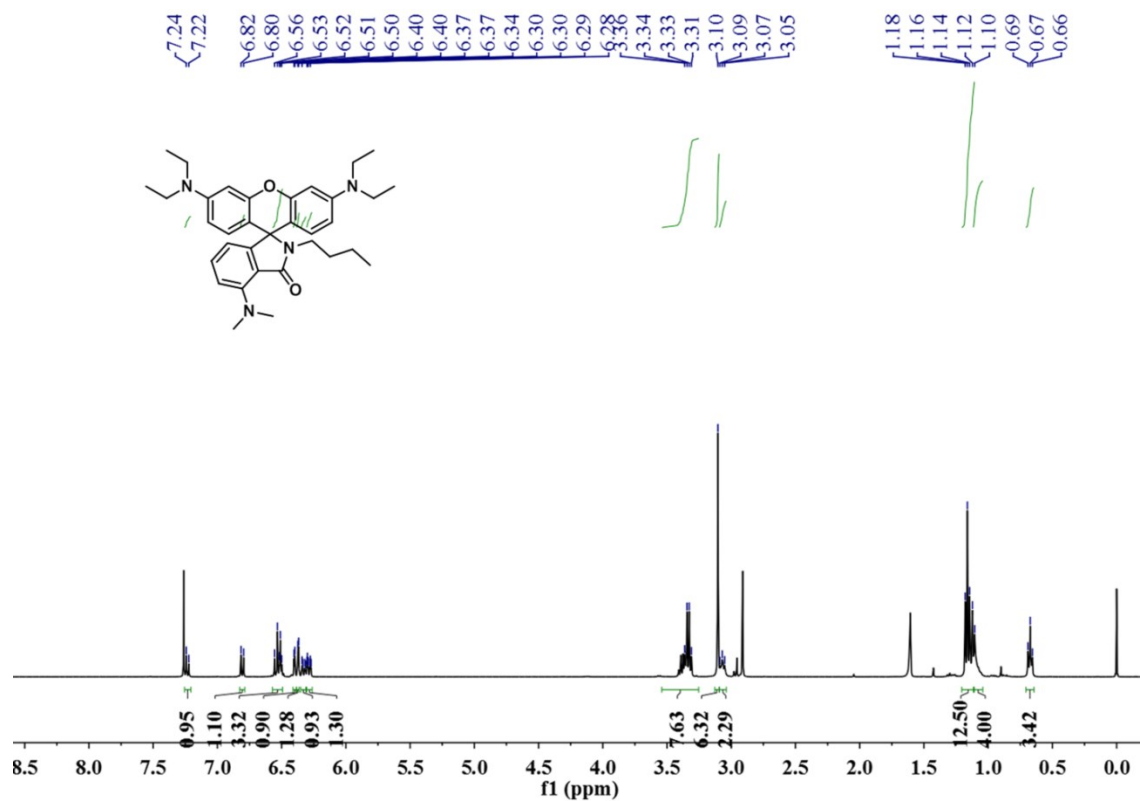




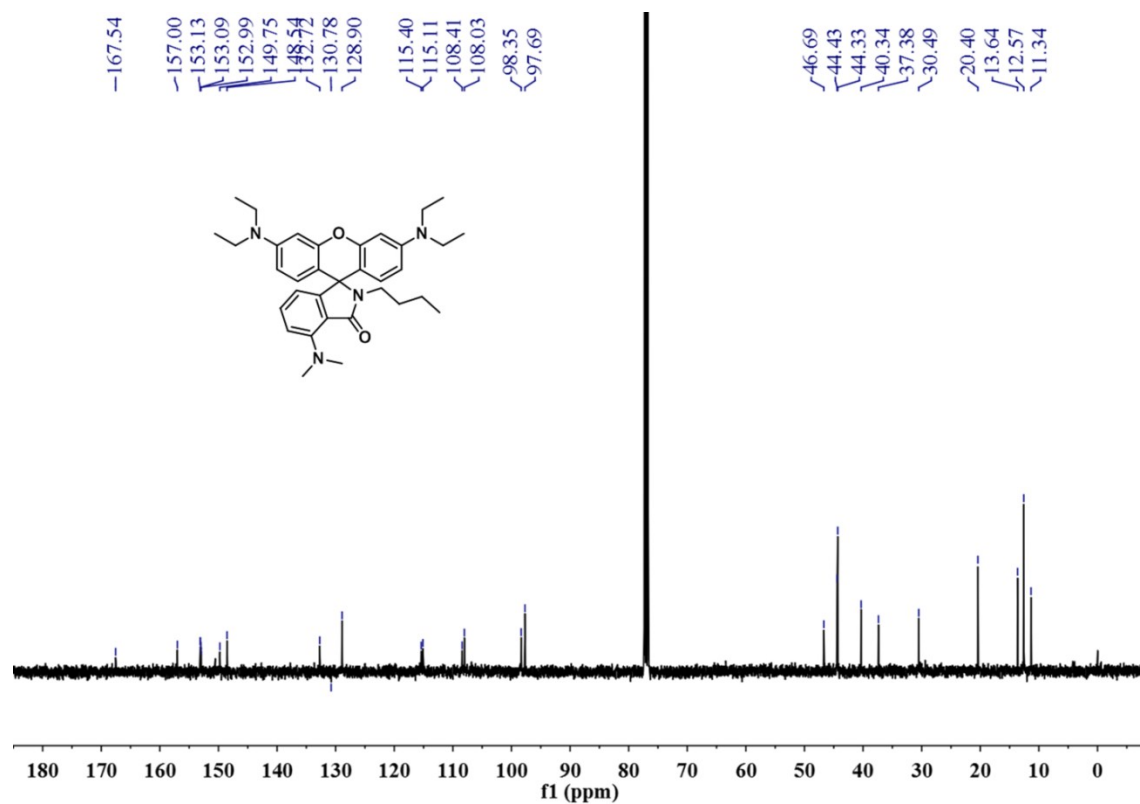
^{13}C NMR spectrum of **P5** in CDCl_3 .



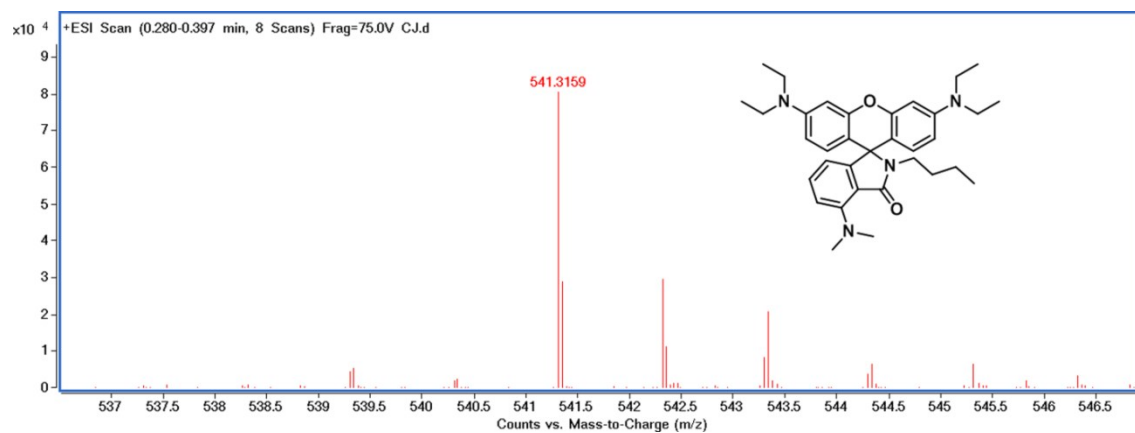
HRMS (ESI) of **P5**.



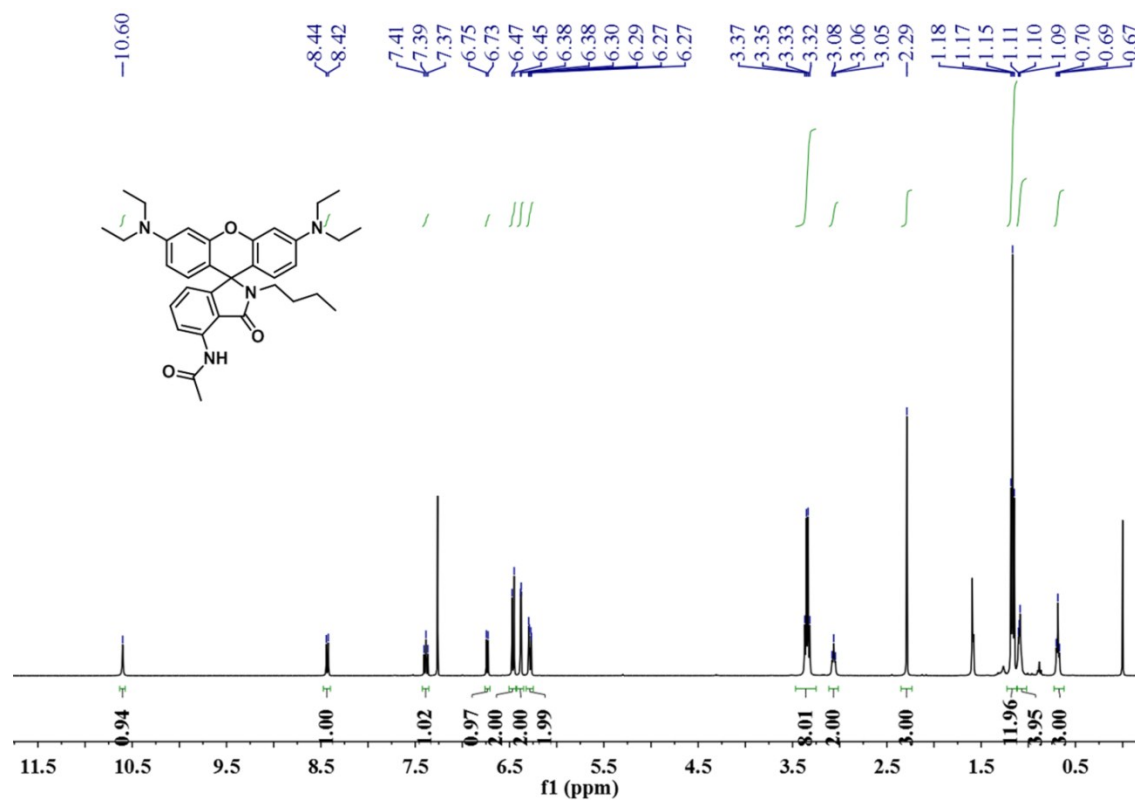
¹H NMR spectrum of **P6** in CDCl₃.



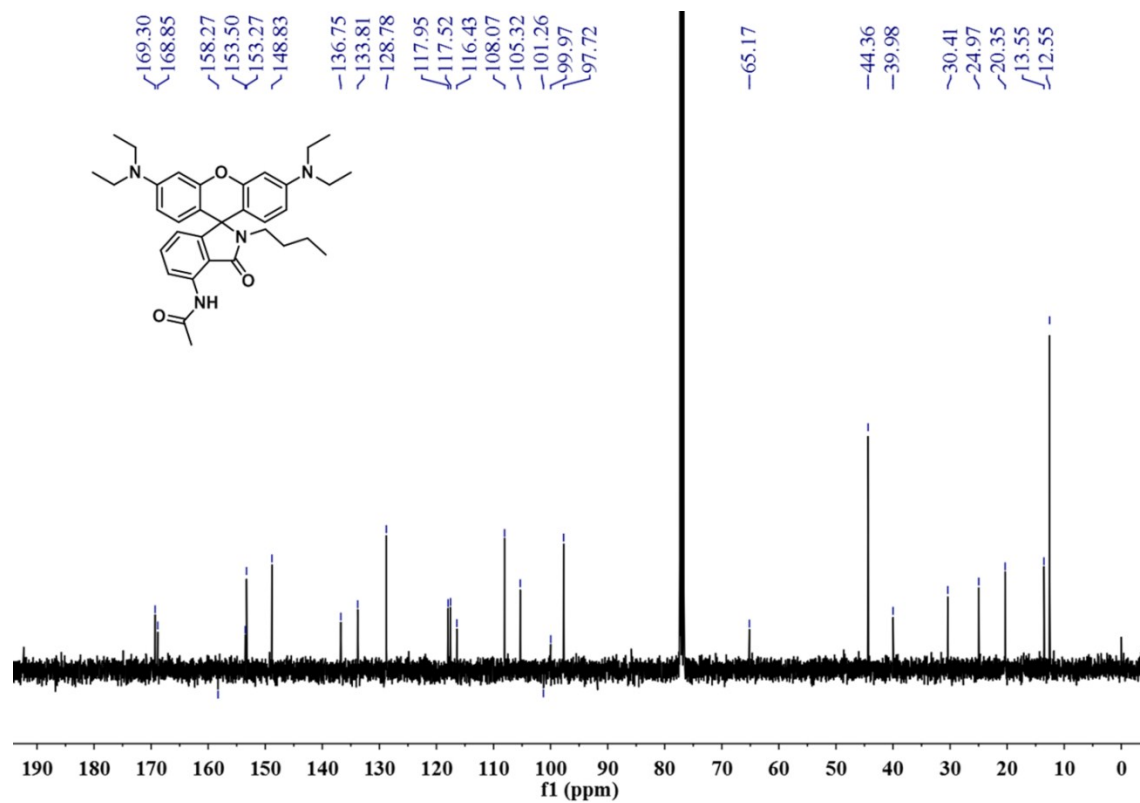
¹³C NMR spectrum of **P6** in CDCl₃.



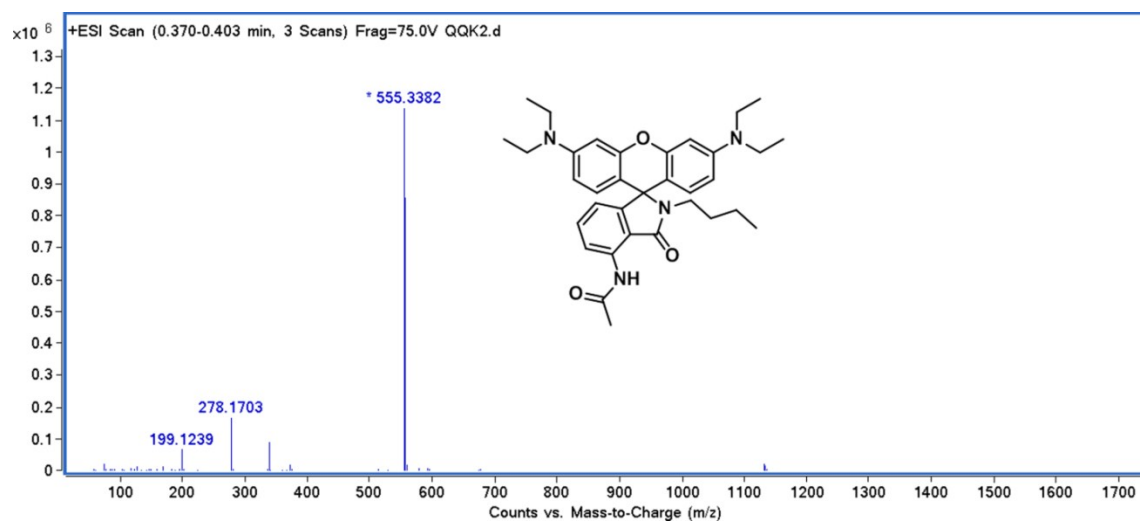
HRMS (ESI) of **P6**.



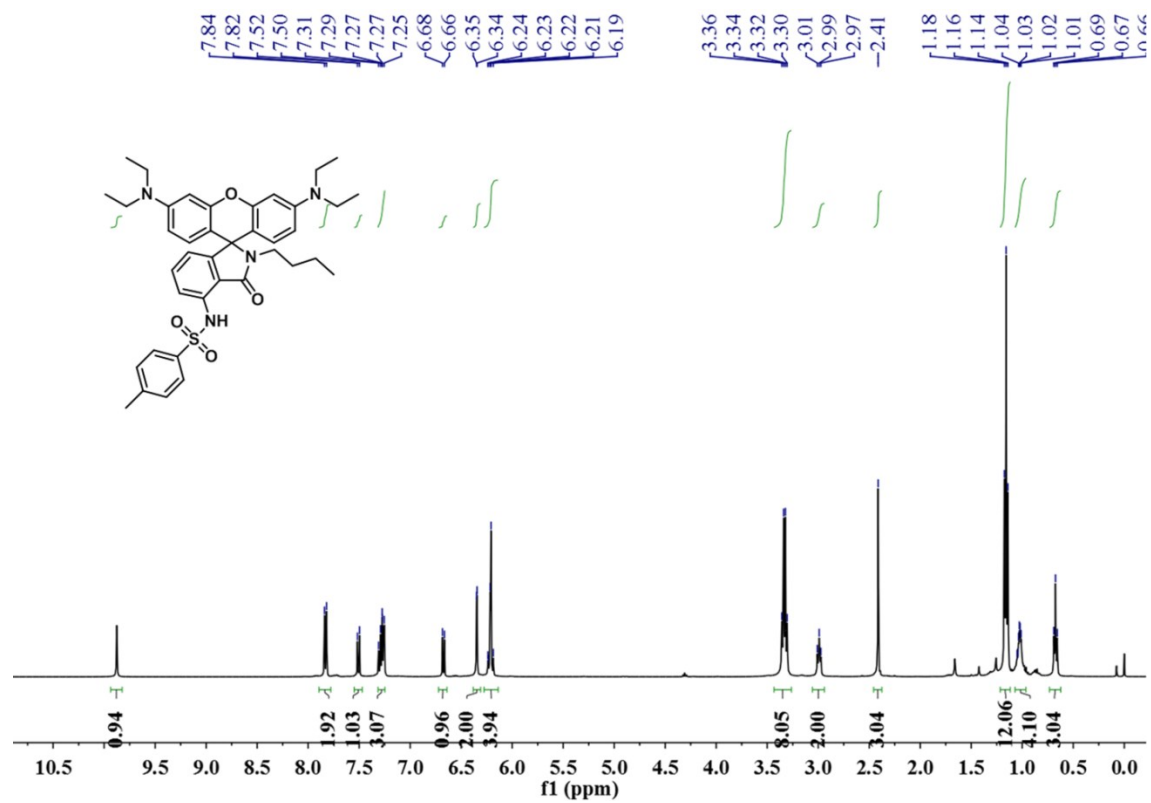
^1H NMR spectrum of **P7** in CDCl_3 .



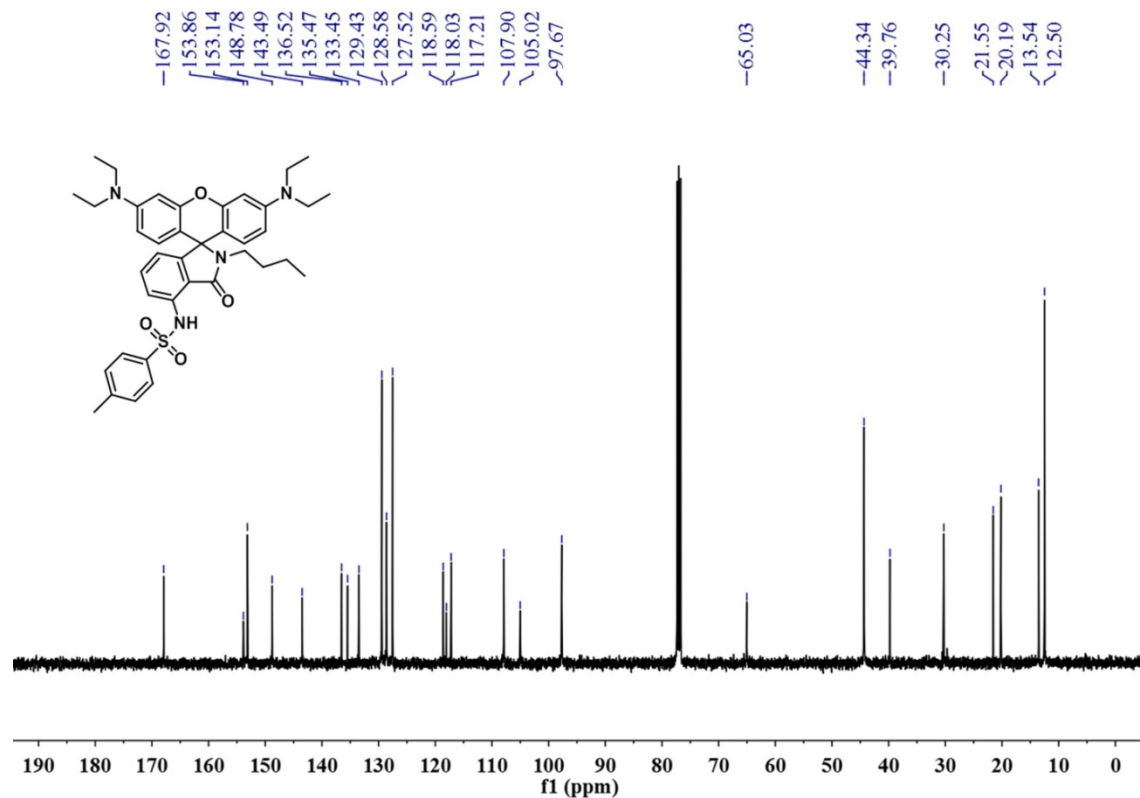
¹³C NMR spectrum of P7 in CDCl₃.



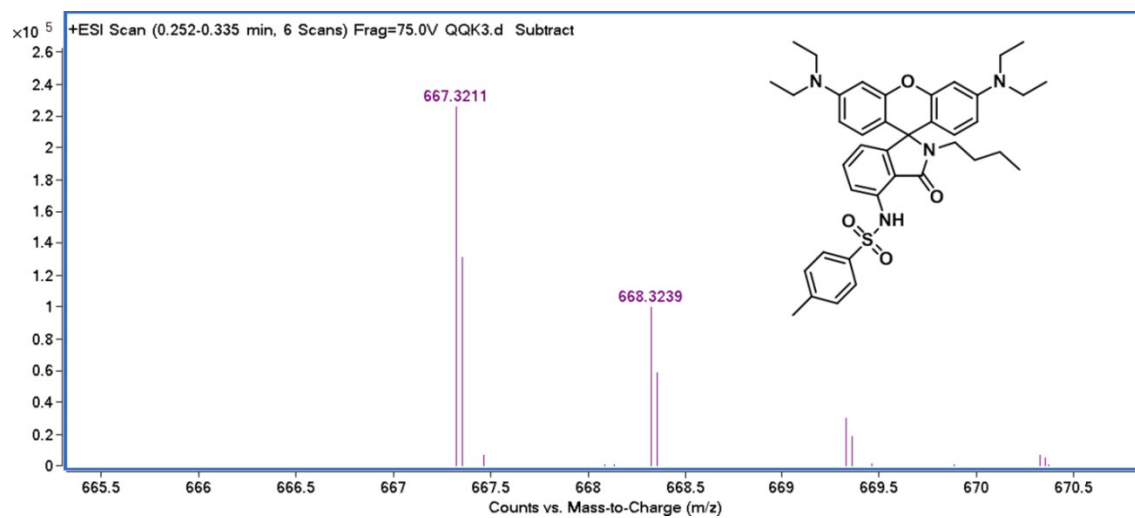
HRMS (ESI) of P7.



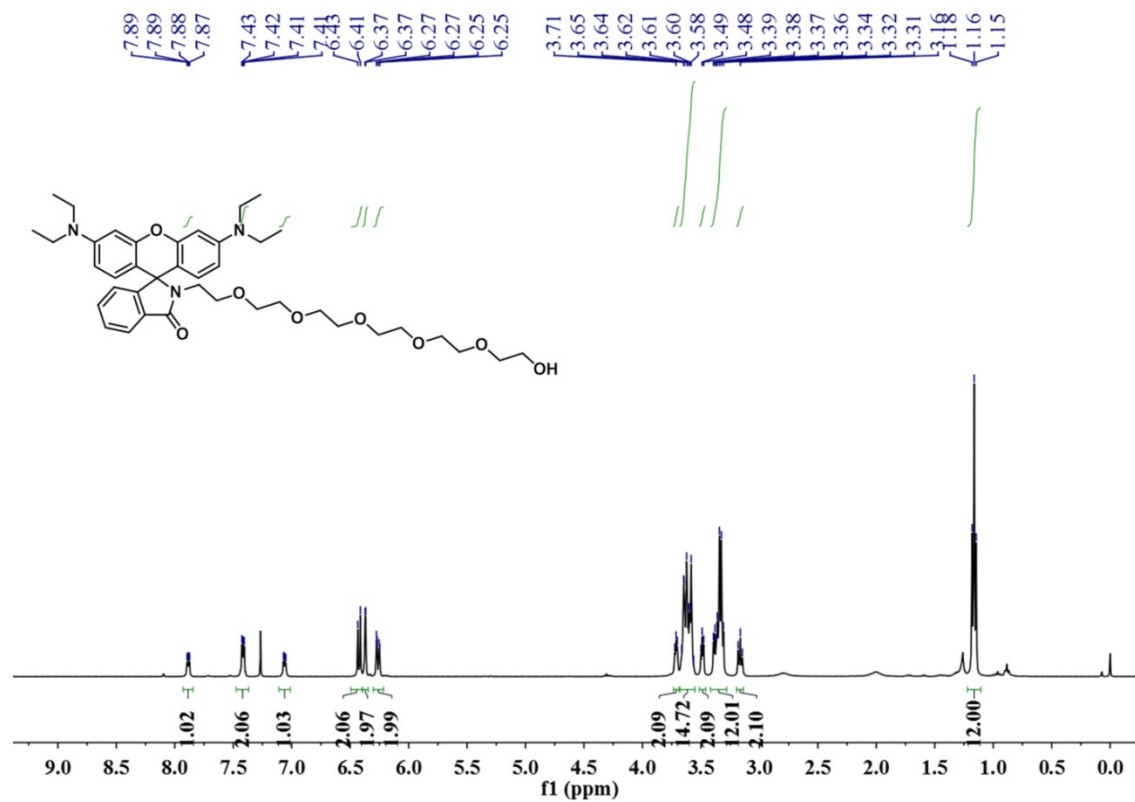
¹H NMR spectrum of P8 in CDCl₃.



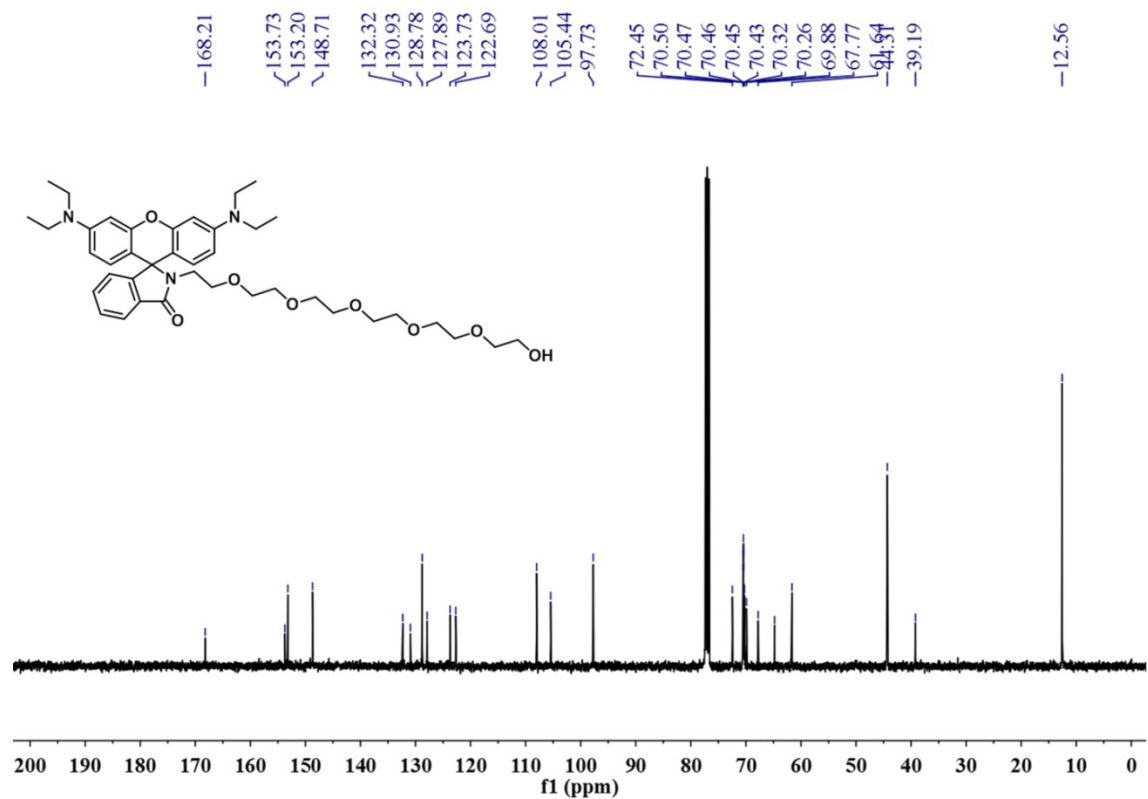
¹³C NMR spectrum of P8 in CDCl₃.



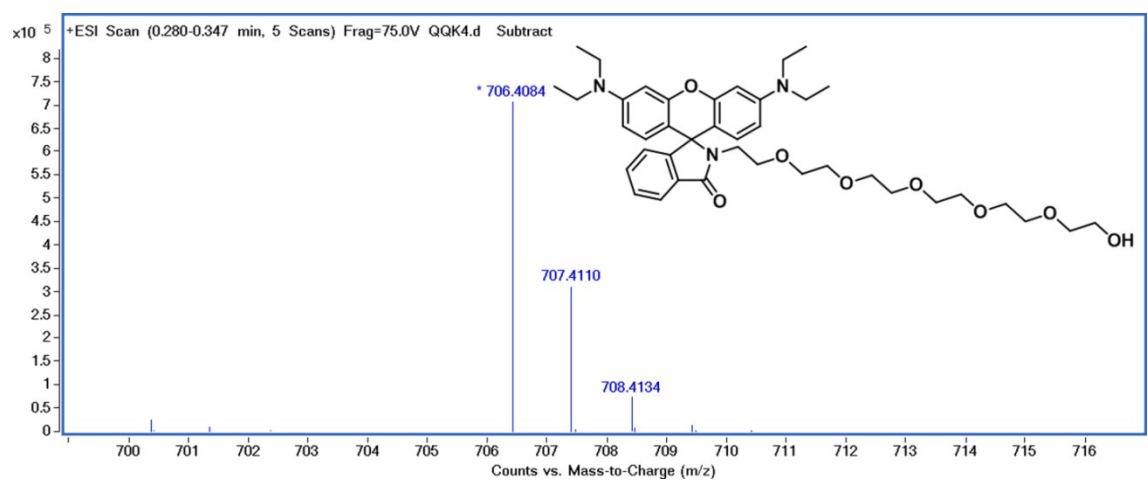
HRMS (ESI) of **P8**.



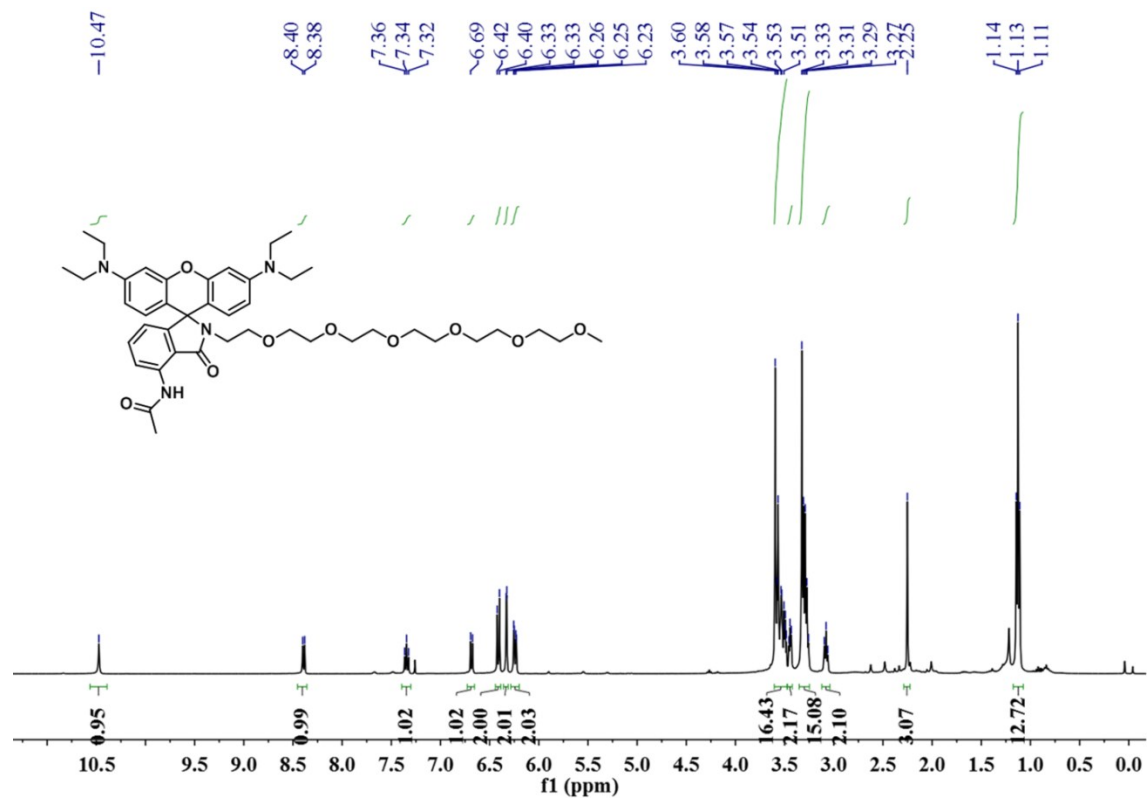
^1H NMR spectrum of **P9** in CDCl_3 .



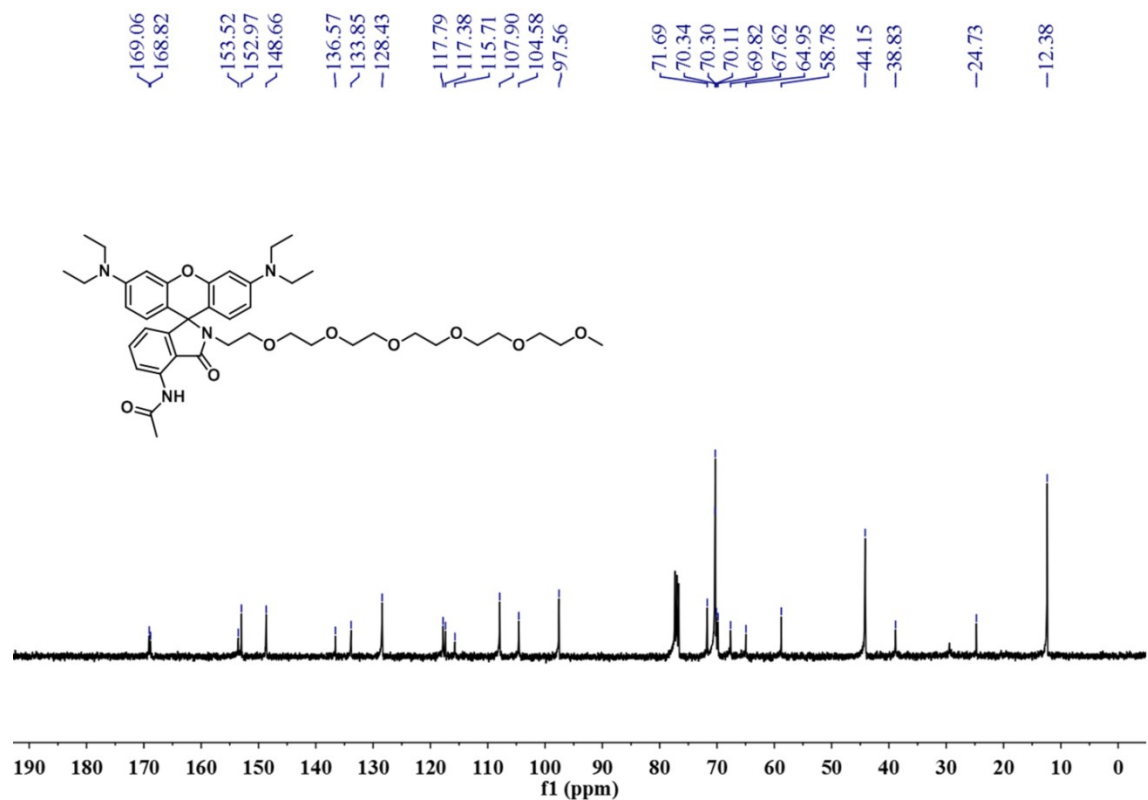
^{13}C NMR spectrum of **P9** in CDCl_3 .



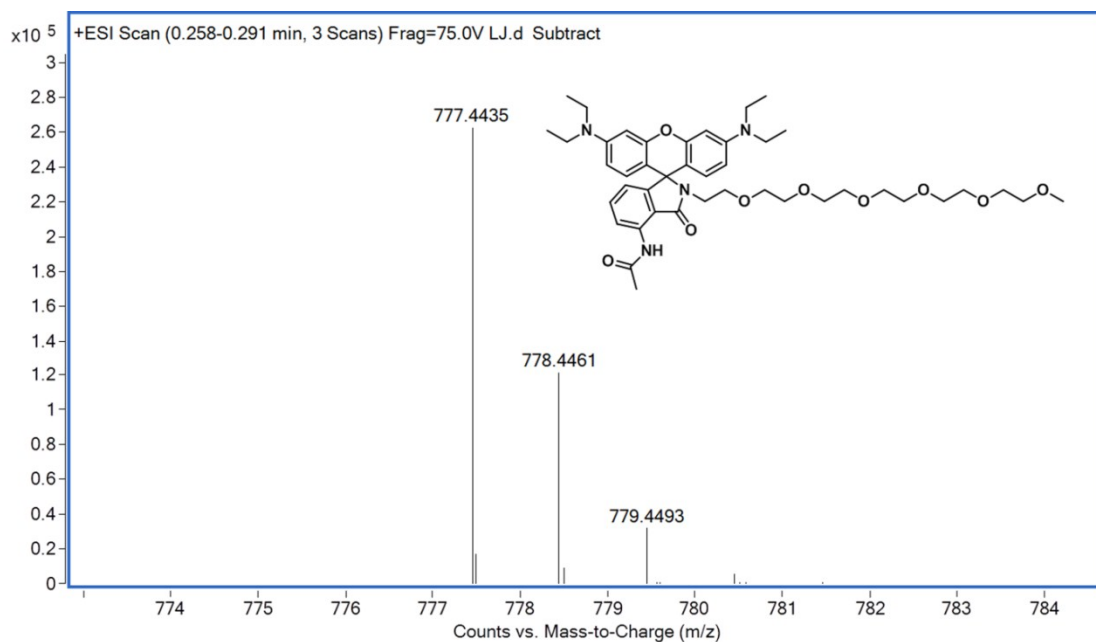
HRMS (ESI) of **P9**.



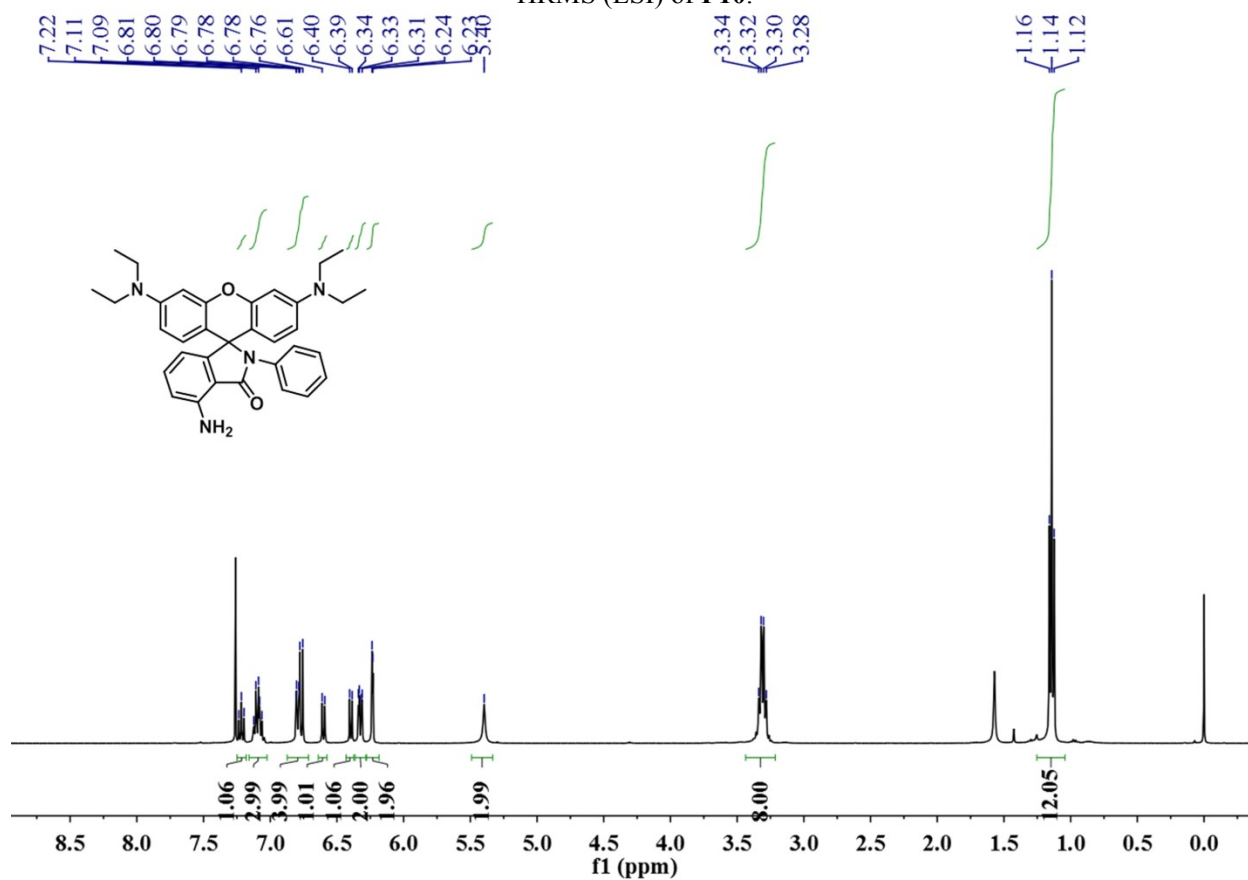
¹H NMR spectrum of **P10** in CDCl₃.



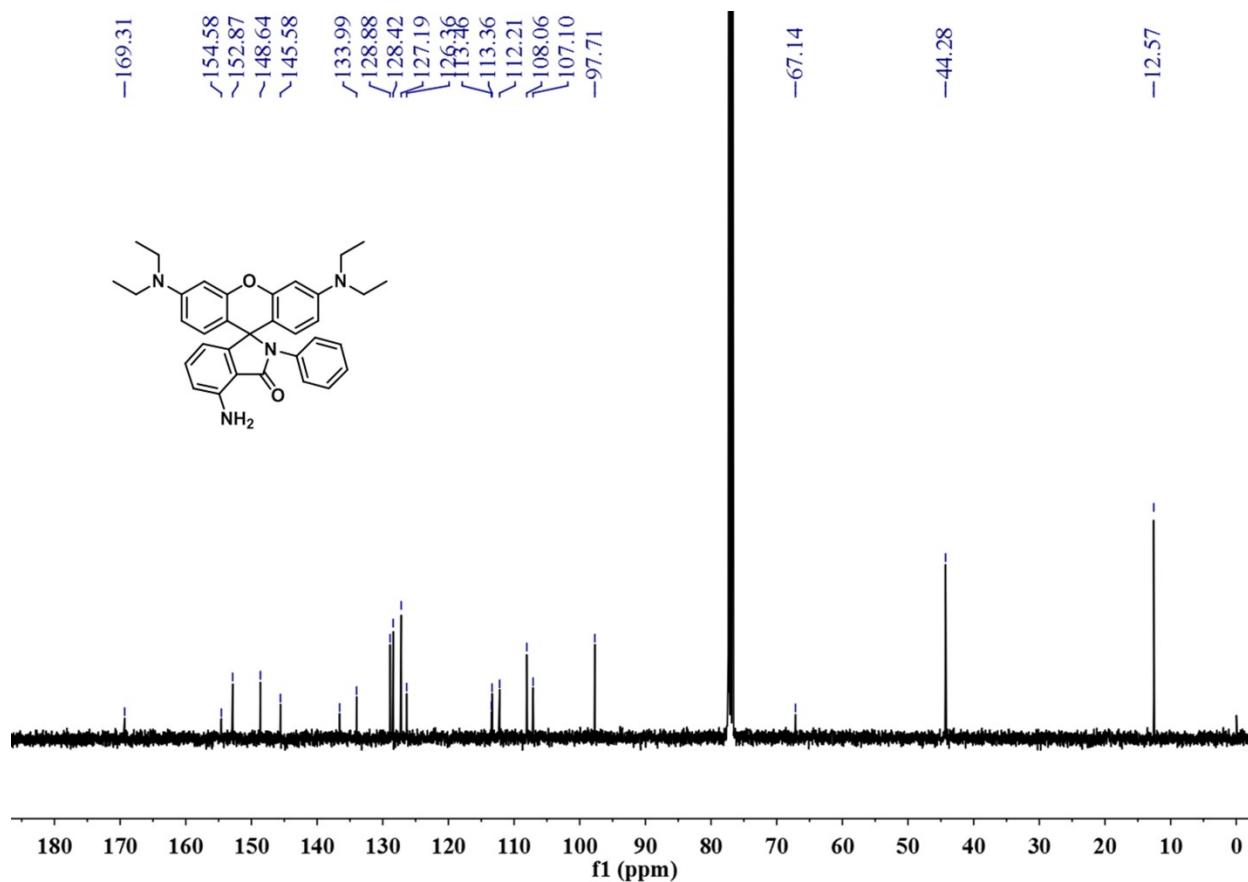
¹³C NMR spectrum of **P10** in CDCl₃.



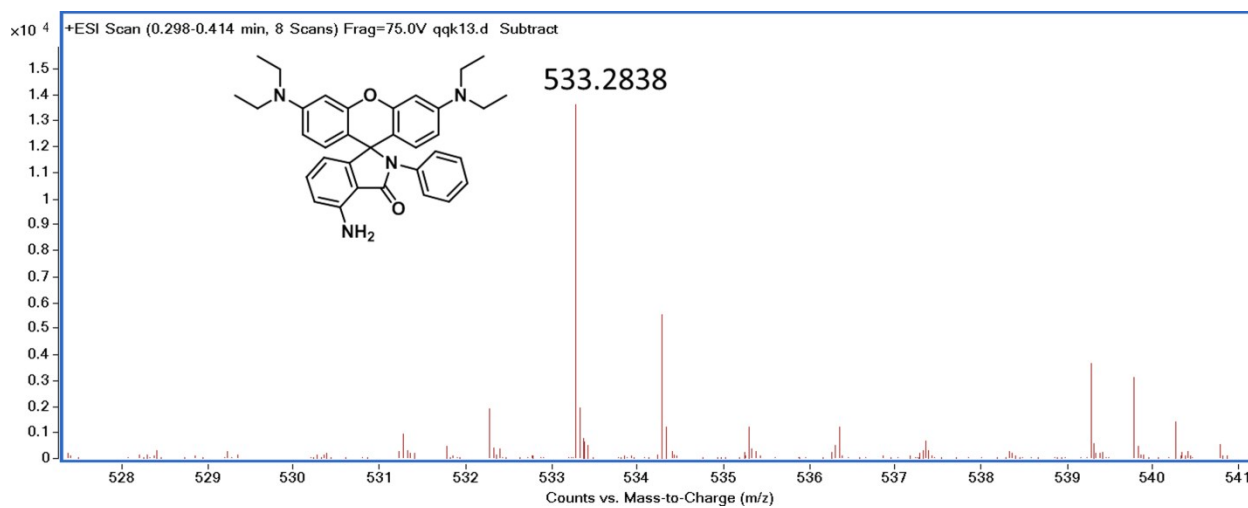
HRMS (ESI) of **P10**.



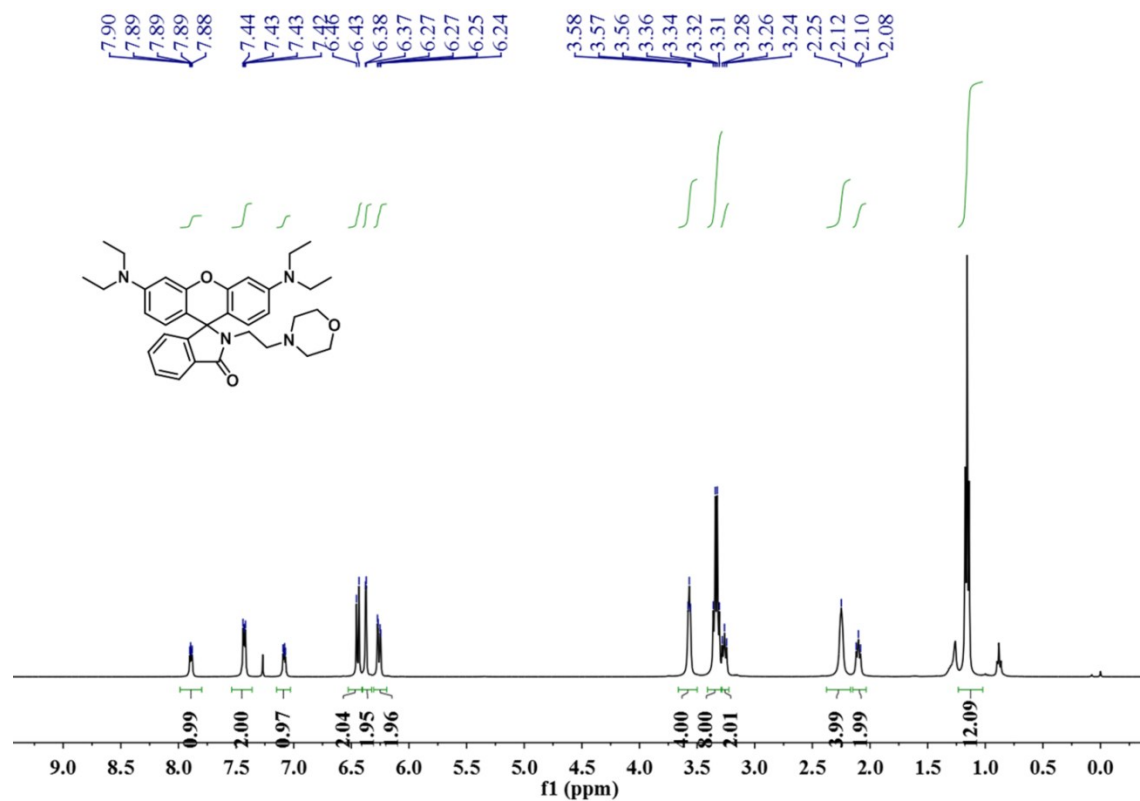
^1H NMR spectrum of **P11** in CDCl_3 .



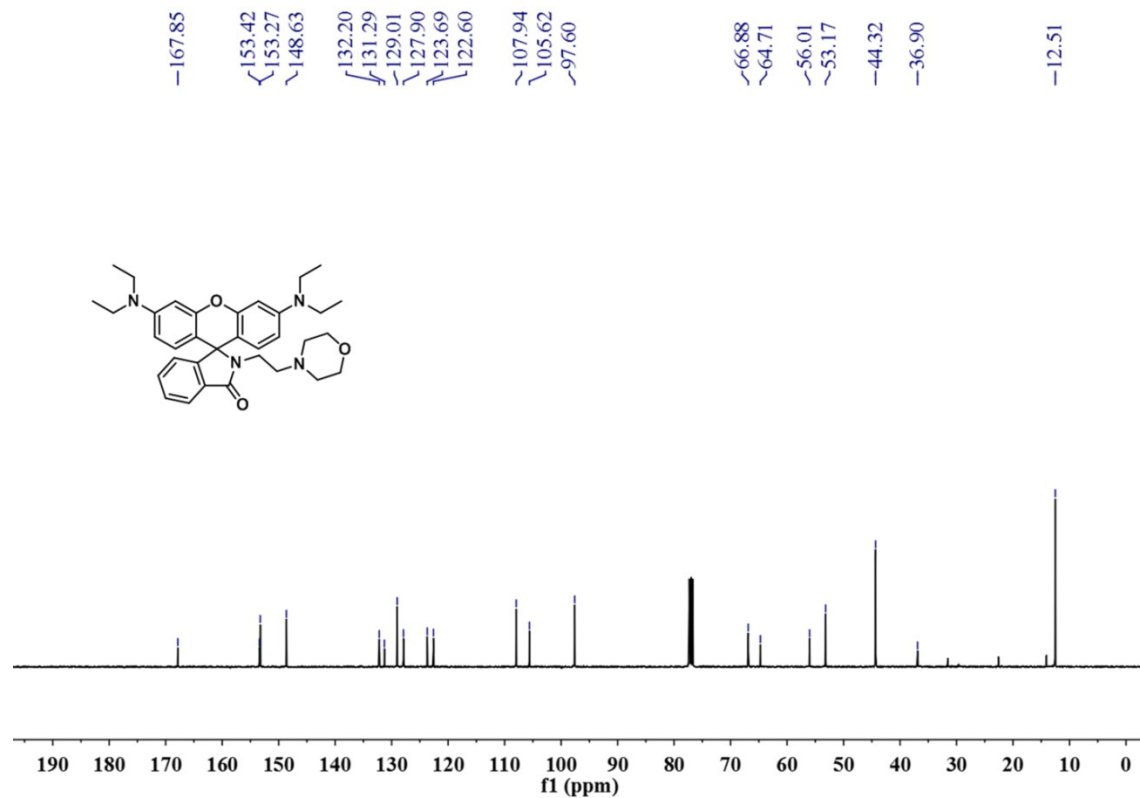
^{13}C NMR spectrum of **P11** in CDCl_3 .



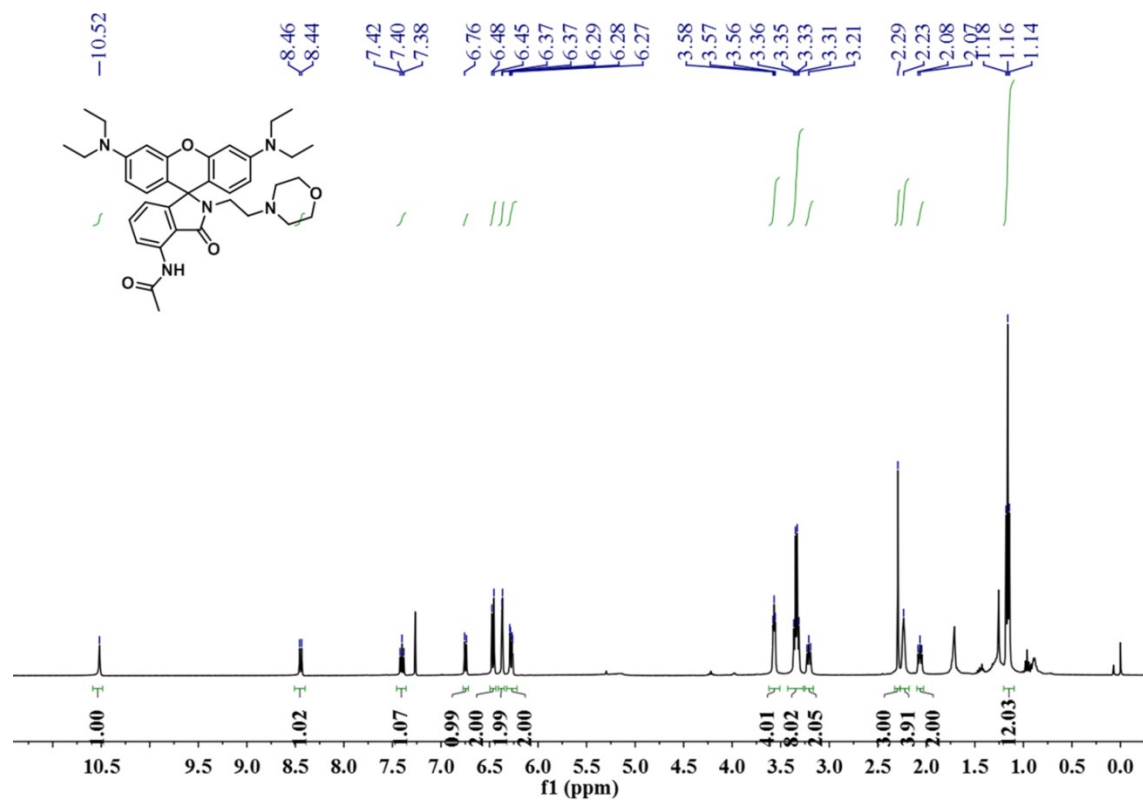
HRMS (ESI) of **P11**.



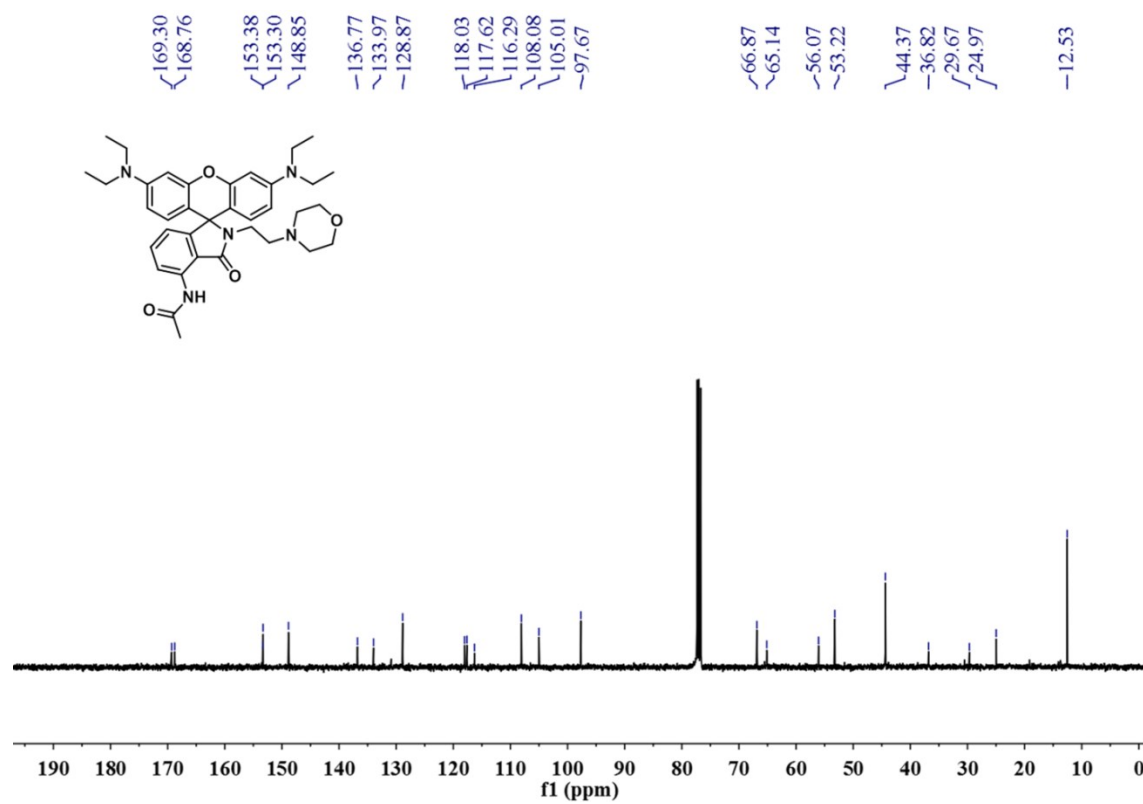
¹H NMR spectrum of **P12** in CDCl₃.



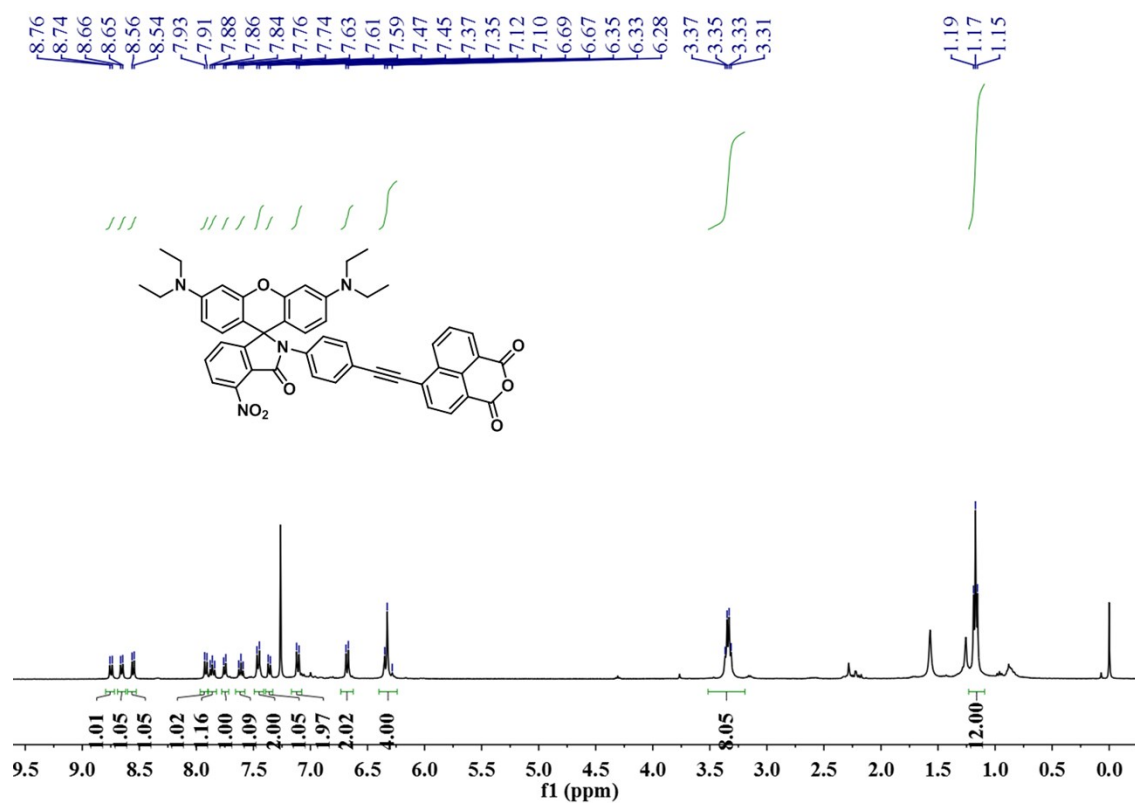
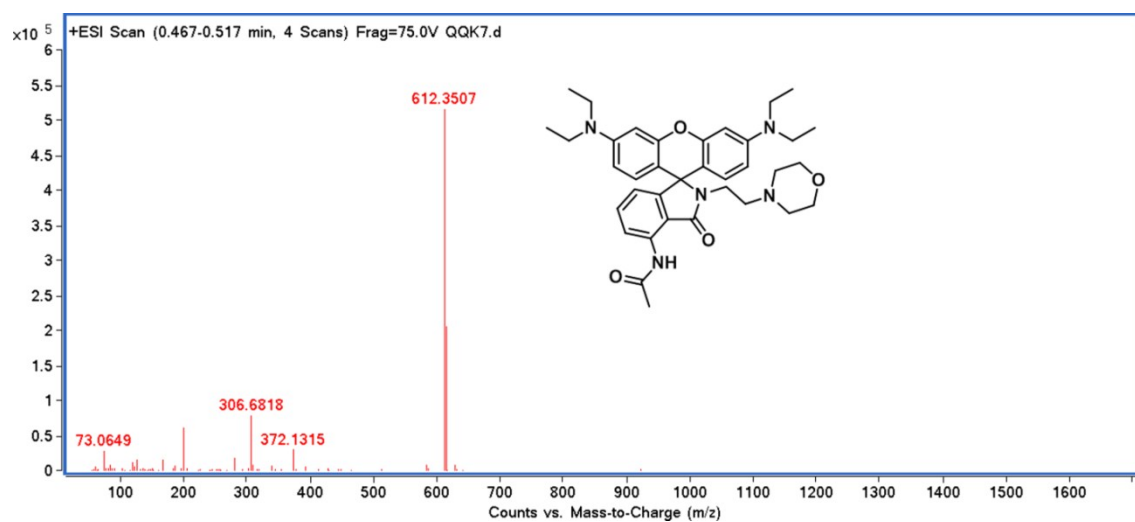
¹³C NMR spectrum of **P12** in CDCl₃.

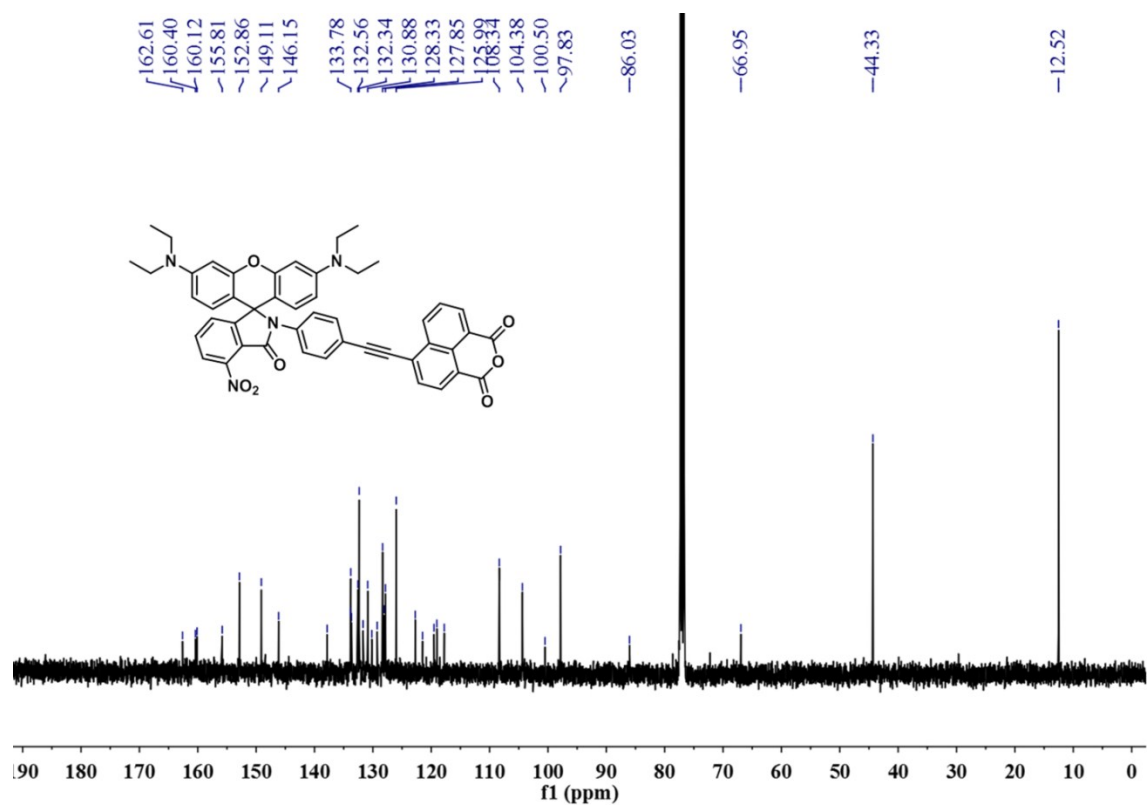


¹H NMR spectrum of **P13** in CDCl₃.

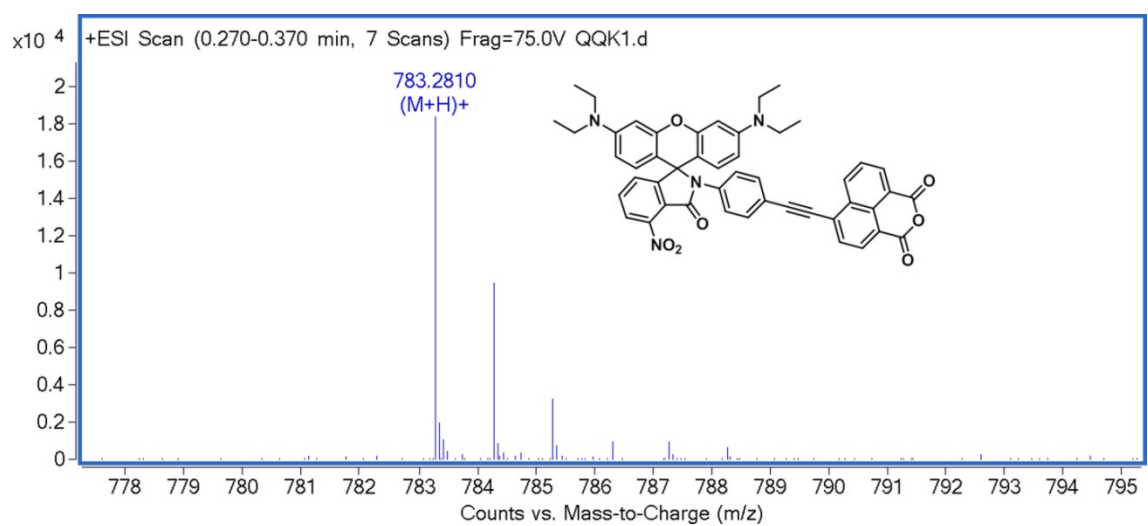


¹³C NMR spectrum of **P13** in CDCl₃.

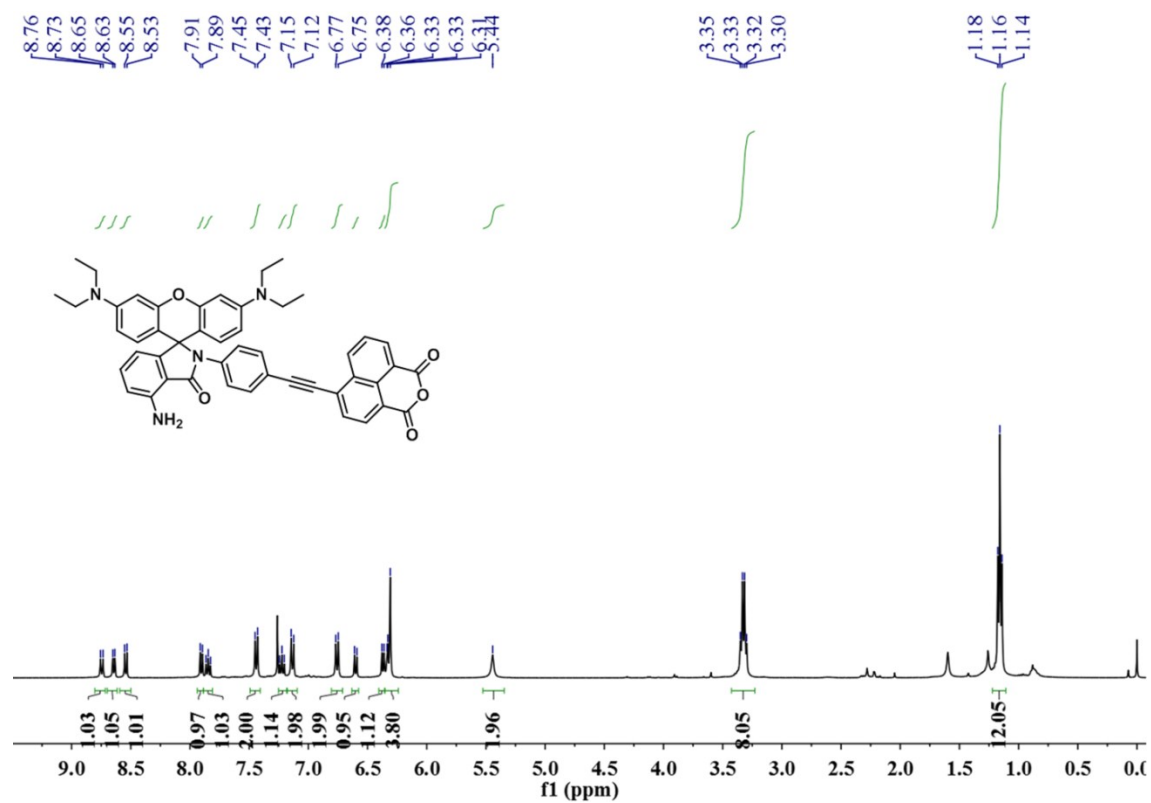




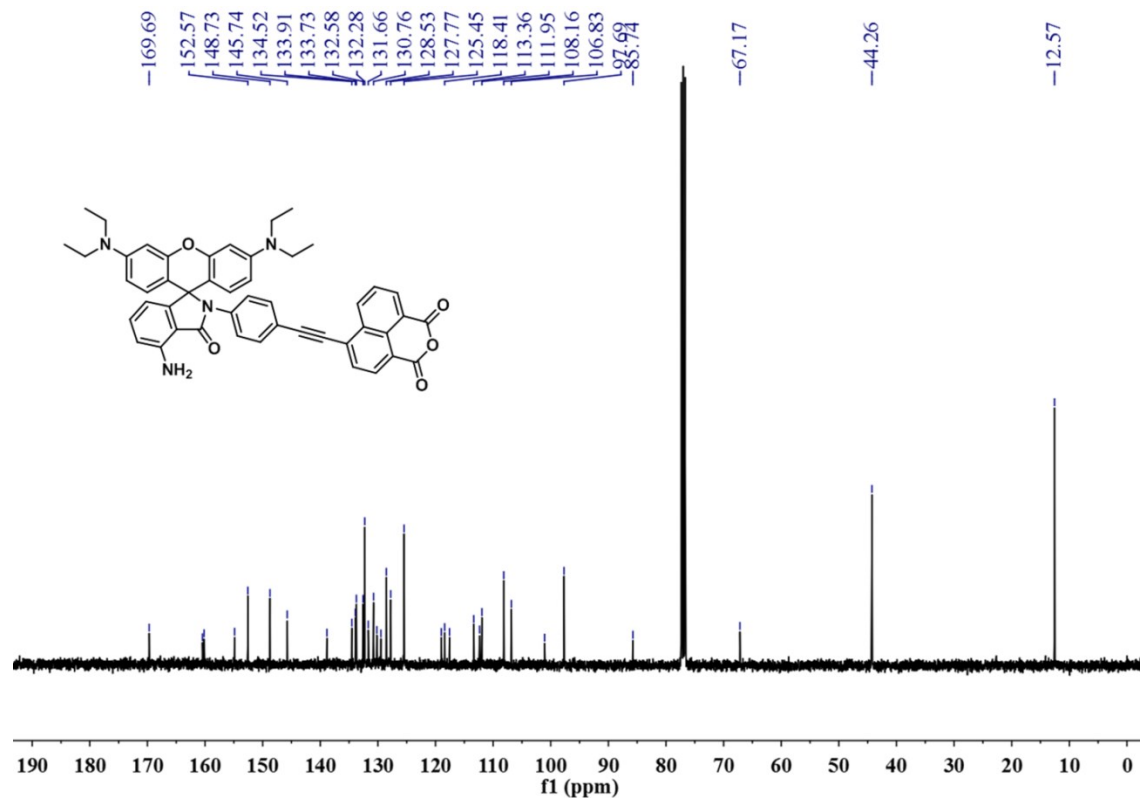
¹³C NMR spectrum of **P14** in CDCl₃.



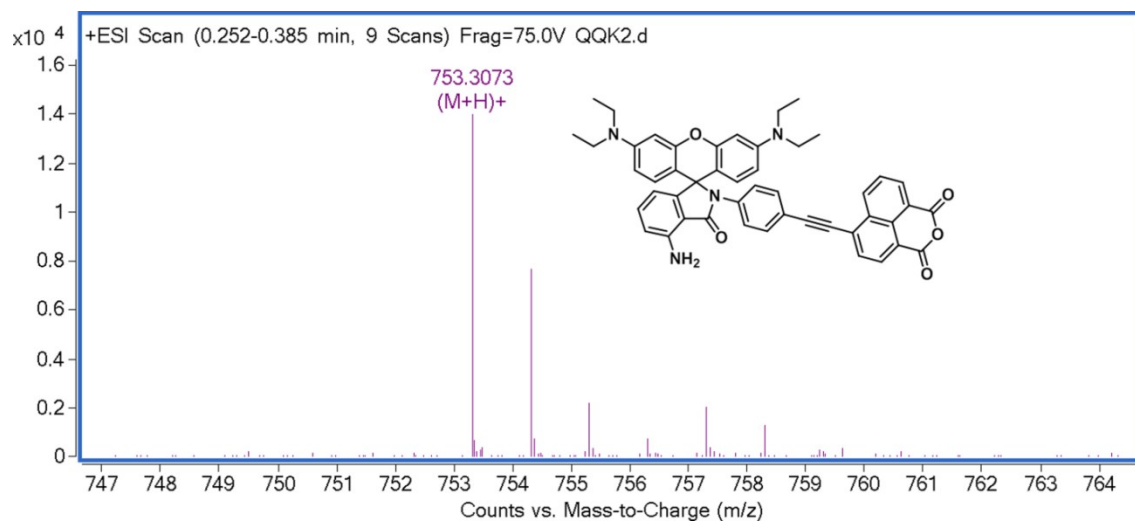
HRMS (ESI) of **P14**.



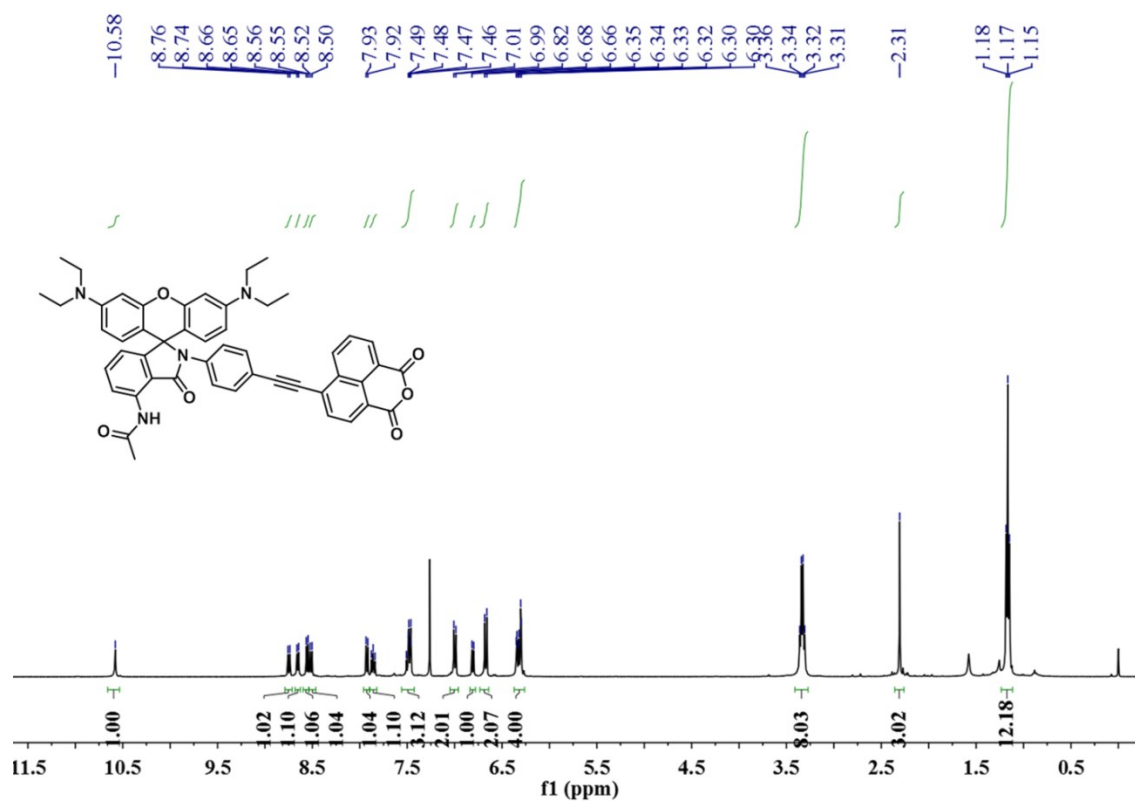
¹H NMR spectrum of P15 in CDCl₃.



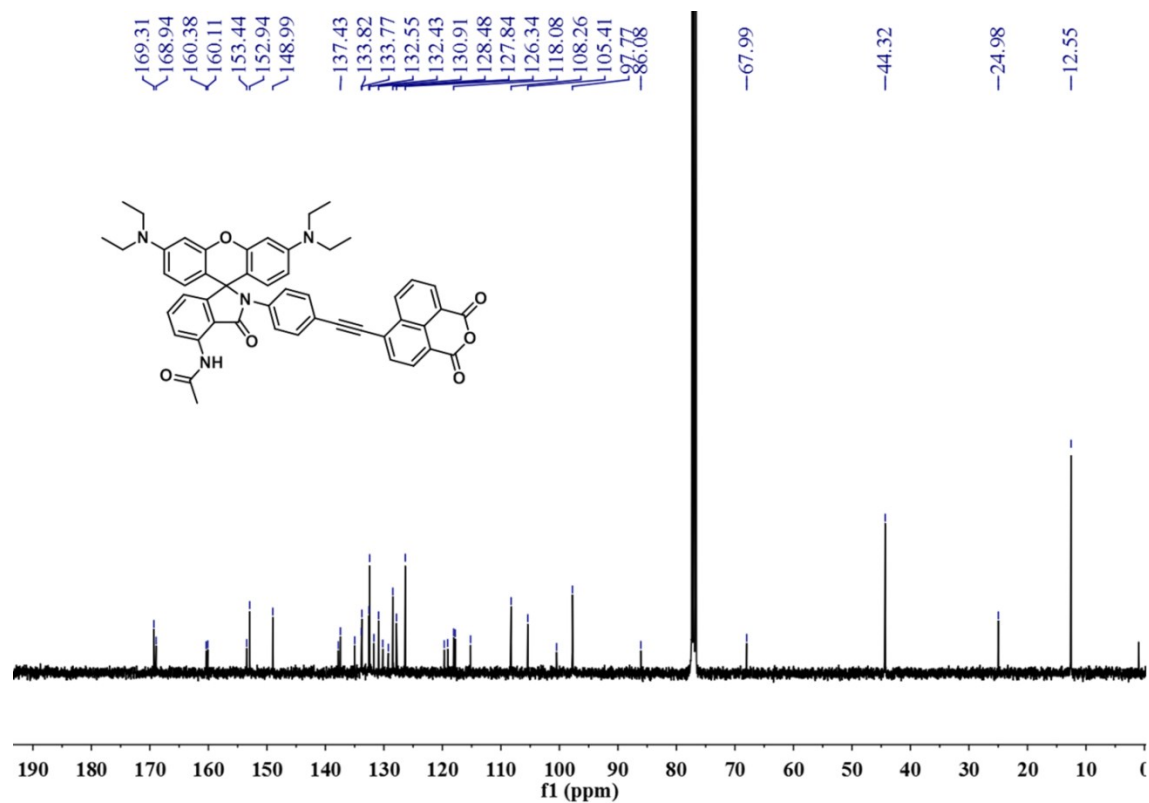
¹³C NMR spectrum of P15 in CDCl₃.



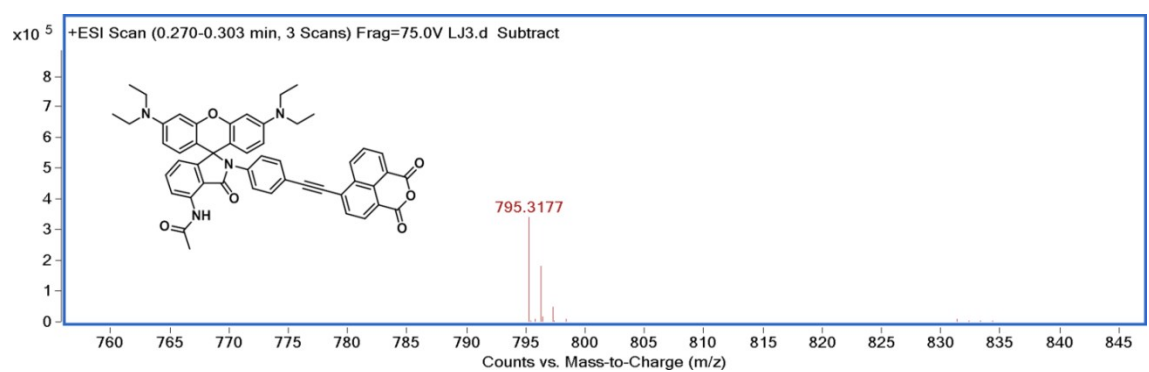
HRMS (ESI) of **P15**.



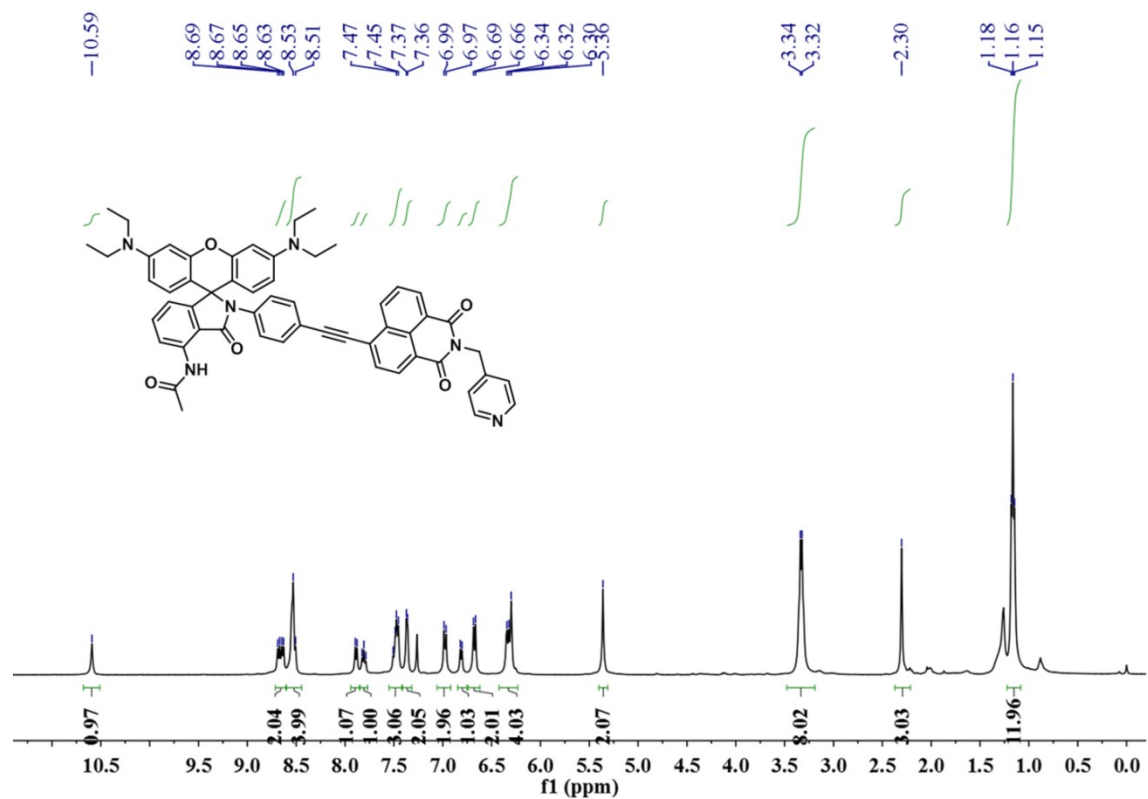
¹H NMR spectrum of **P16** in CDCl₃.



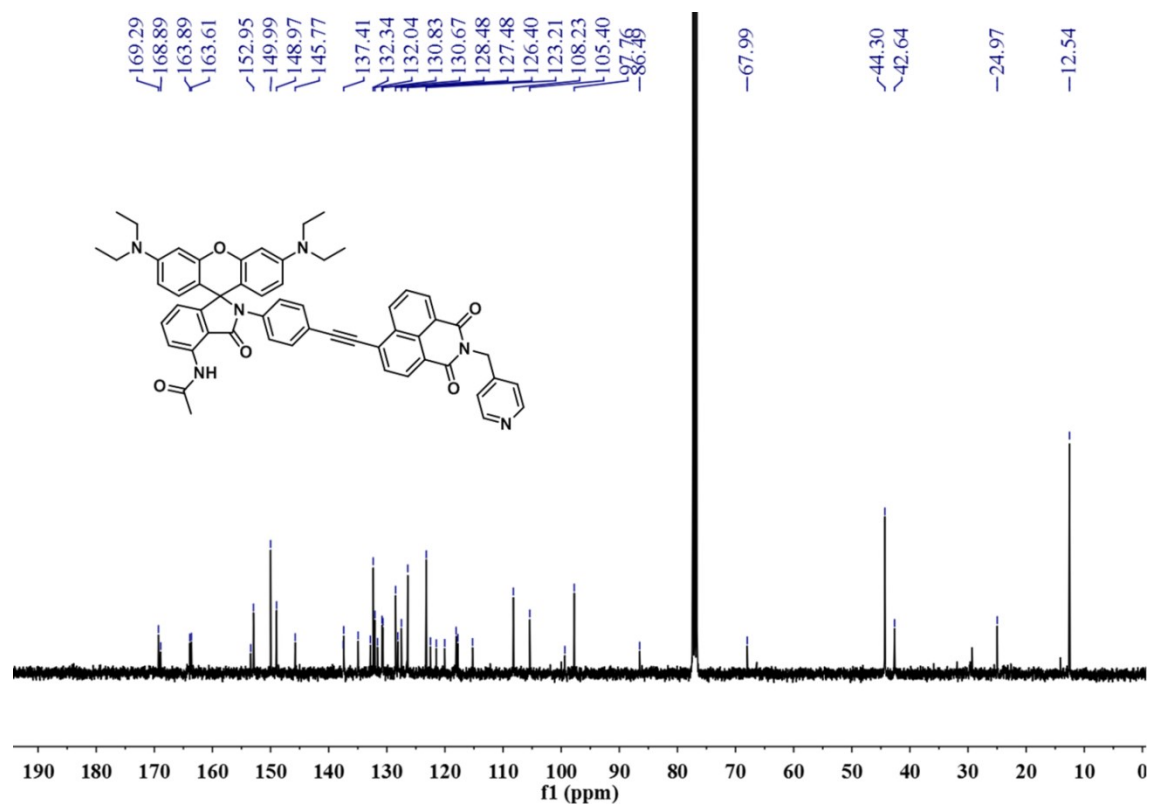
^{13}C NMR spectrum of **P16** in CDCl_3 .



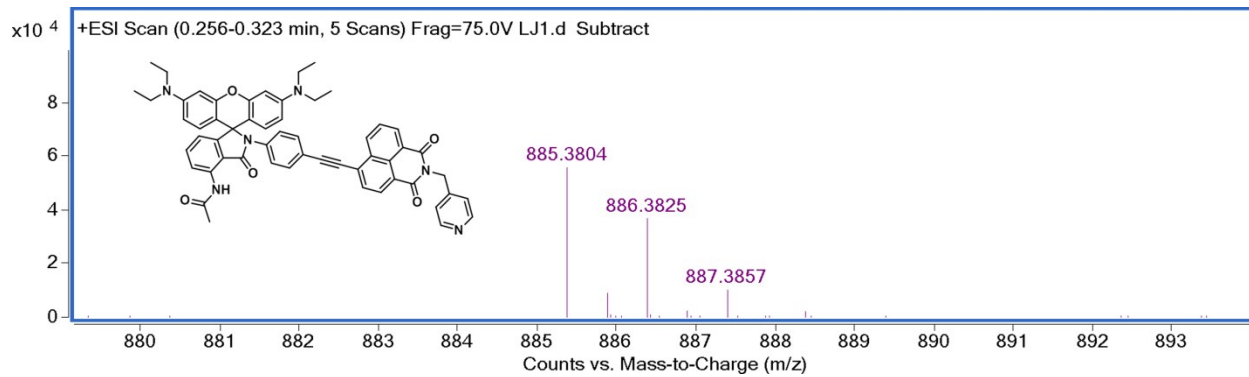
HRMS (ESI) of **P16**.



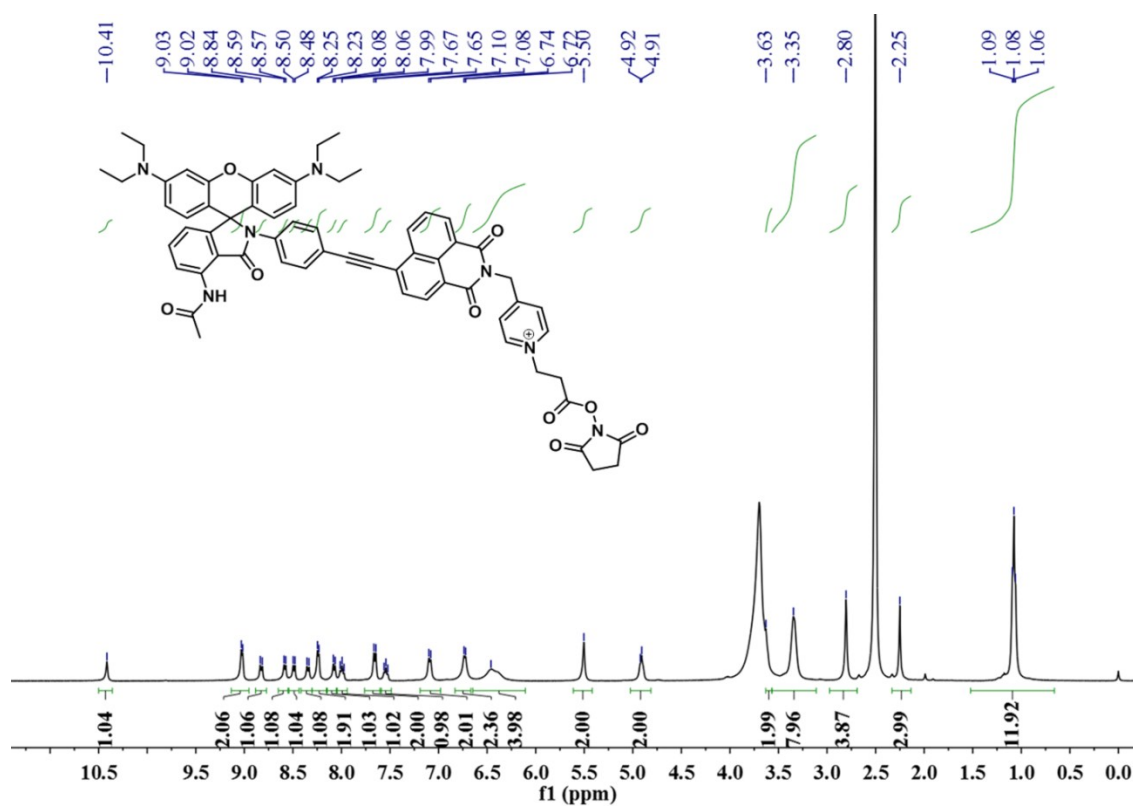
¹H NMR spectrum of **P17** in CDCl₃.



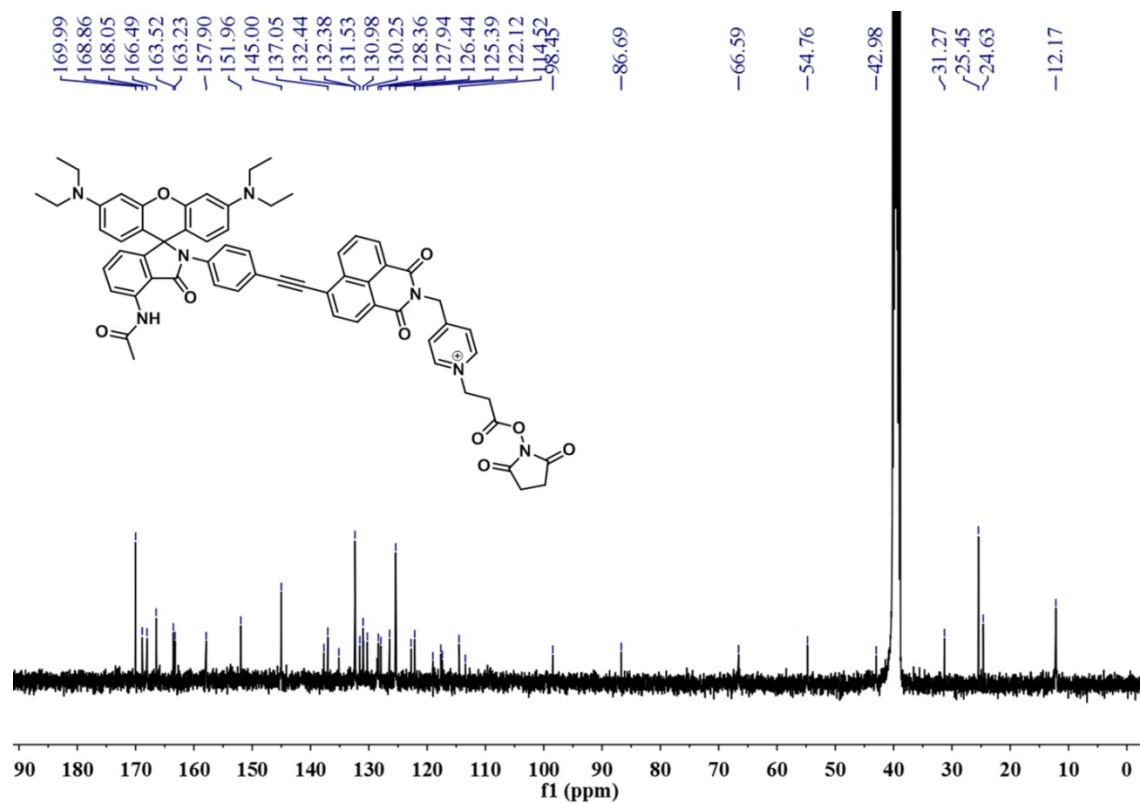
¹³C NMR spectrum of **P17** in CDCl₃.



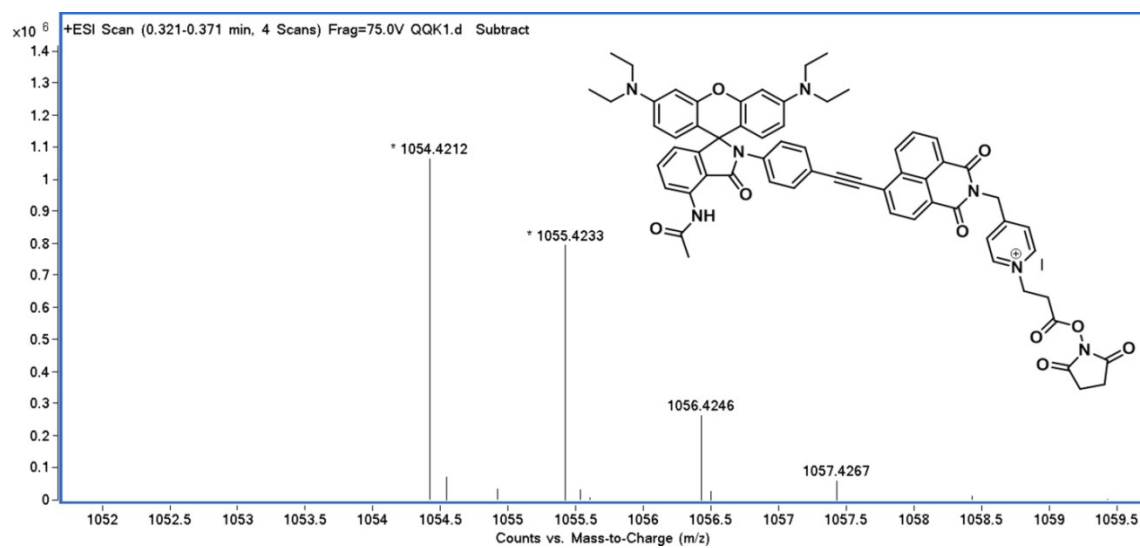
HRMS (ESI) of **P17**.



¹H NMR spectrum of **P18** in DMSO-*d*₆.



¹³C NMR spectrum of **P18** in DMSO-*d*₆.



HRMS (ESI) of **P18**.

4. References.

1. Zhang, I.; Wang, Y.; Wan, C.; Xing, Z.; Li, W.; Li, M.; Zhang, S. X. *RSC Adv.* **2015**, *5*, 66416-66419.
2. Frisch, M. J.; Trucks, G. W.; Schlegel, H. B.; Scuseria, G. E.; Robb, M. A.; Cheeseman, J. R.; Scalmani, G.; Barone, V.; Petersson, G. A.; Nakatsuji, H.; Li, X.; Caricato, M.; Marenich, A. V.; Bloino, J.; Janesko, B. G.; Gomperts, R.; Mennucci, B.; Hratchian, H. P.; Ortiz, J. V.; Izmaylov, A. F.; Sonnenberg, J. L.; Williams; Ding, F.; Lipparini, F.; Egidi, F.; Goings, J.; Peng, B.; Petrone, A.; Henderson, T.; Ranasinghe, D.; Zakrzewski, V. G.; Gao, J.; Rega, N.; Zheng, G.; Liang, W.; Hada, M.; Ehara, M.; Toyota, K.; Fukuda, R.; Hasegawa, J.; Ishida, M.; Nakajima, T.; Honda, Y.; Kitao, O.; Nakai, H.; Vreven, T.; Throssell, K.; Montgomery Jr., J. A.; Peralta, J. E.; Ogliaro, F.; Bearpark, M. J.; Heyd, J. J.; Brothers, E. N.; Kudin, K. N.; Staroverov, V. N.; Keith, T. A.; Kobayashi, R.; Normand, J.; Raghavachari, K.; Rendell, A. P.; Burant, J. C.; Iyengar, S. S.; Tomasi, J.; Cossi, M.; Millam, J. M.; Klene, M.; Adamo, C.; Cammi, R.; Ochterski, J. W.; Martin, R. L.; Morokuma, K.; Farkas, O.; Foresman, J. B.; Fox, D. J. *Gaussian 16*, Wallingford, CT, 2016.
3. Zhao, Y.; Truhlar, D. G. *Theor. Chem. Acc.* **2008**, *120*, 215-241.
4. Marenich, A. V.; Cramer, C. J.; Truhlar, D. G. *J. Phys. Chem. B* **2009**, *113*, 6378-6396.
5. Cui, X.; Zhao, J.; Lou, Z.; Li, S.; Wu, H.; Han, K. L. *J. Org. Chem.* **2015**, *80*, 568-581.
6. Shen, S. L.; Chen, X. P.; Zhang, X. F.; Miao, J. Y.; Zhao, B. X. *J. Mater. Chem. B* **2015**, *3*, 919-925.
7. Brown, R. C.; Li, Z.; Rutter, A. J.; Mu, X.; Weeks, O. H.; Smith, K.; Weeks, I. *Org. Biomol. Chem.* **2009**, *7*, 386-394.